Zoological Journal of the Linnean Society, 2021, **XX**, 1–44. With 20 figures.

Total evidence phylogenetic analysis reveals polyphyly of *Anostomoides* and uncovers an unexpectedly ancient genus of Anostomidae fishes (Characiformes)

BRIAN L. SIDLAUSKAS[1,†], FERNANDO M. ASSEGA[2,†], BRUNO F. MELO[3], CLAUDIO OLIVEIRA[3] and JOSÉ L.O. BIRINDELLI[2,*]

[1]*Department of Fisheries and Wildlife, Oregon State University, 104 Nash Hall, Corvallis, OR 97331, USA*
[2]*Programa de Pós-Graduação em Ciências Biológicas, Universidade Estadual de Londrina, Centro de Ciencias Biologicas, Universidade Estadual de Londrina, Rodovia Celso Garcia Cid, Campus Universitário, 86057-970, Londrina, PR, Brazil*
[3]*Departamento de Biologia Estrutural e Funcional, Instituto de Biociências, Universidade Estadual Paulista, R. Prof. Dr. Antonio C. W. Zanin, 250, Rubião Jr, 18618–689, Botucatu, SP, Brazil*

Received 18 June 2020; revised 8 January 2021; accepted for publication 28 February 2021

The nearly 150 species of Anostomidae comprise one of the most diverse and taxonomically dynamic families of Neotropical freshwater fishes. A recent revision of the enigmatic and poorly diagnosed genus *Anostomoides* demonstrated that it contains two valid species, each with complicated taxonomic histories; however, that study did not address their phylogenetic placement. Herein, we integrate molecular and morphological data to demonstrate their distant evolutionary relationship, and thus the polyphyly of *Anostomoides*. While we reconstruct one of the species in a previously hypothesized placement within a clade also containing *Laemolyta*, *Rhytiodus* and *Schizodon*, the other represents a morphologically and genetically distinctive lineage that diverged early in the history of the family. We describe and illustrate the osteology of this remarkable species, discuss the evolutionary implications of its unique suite of features, and use those characteristics to diagnose a new genus that evolved independently of all other known members of the family for approximately 37 Myr.

ADDITIONAL KEYWORDS: Anostomoidea – fishes – molecular – morphology – Neotropics – osteology – phylogeny – South America – taxonomy – total evidence.

INTRODUCTION

The nearly 150 species of anostomid fishes comprise one of the most diverse components of the Characiformes (Nelson *et al.*, 2016; Ramirez *et al.*, 2017), which itself contains about a third of all Neotropical fish species (Fricke *et al.*, 2020). Members of the family demonstrate vibrant and strikingly different colour patterns (Fig. 1; Géry, 1977; Sidlauskas & Vari, 2012), range from southern Central America to Argentina (Garavello & Britski, 2003; Sidlauskas & Birindelli, 2017) and vary greatly in skeletal anatomy and other aspects of morphology (Sidlauskas, 2007; Sidlauskas & Vari, 2008). This attracted the interest of dozens of scientists throughout the history of ichthyology. The family name is derived from the Greek words *ano* (upturned) and *stoma* (mouth), chosen to characterize the first member of the family known to science, *Salmo anostomus* Linnaeus, 1758. That species has a conspicuously upturned mouth and was soon placed in its own genus, *Anostomus* Scopoli, 1777, in recognition of its obvious differences from the Northern Hemisphere salmonids. The subsequent descriptions of several terminal-mouthed species in the genus *Leporinus* Agassiz, 1829 (Bloch, 1794; Müller & Troschel, 1844) revealed wide variation in mouth position and colour pattern among anostomid species, which Valenciennes summarized shortly thereafter (*in* Cuvier & Valenciennes, 1850).

*Corresponding author: E–mail: josebirindelli@uel.br
†These authors contributed equally.
[Version of record, published online 7 June 2021; http://zoobank.org/urn:lsid:zoobank.org:pub:A7A88AB9-DF88-49AE-8678-681A5F21CE27]

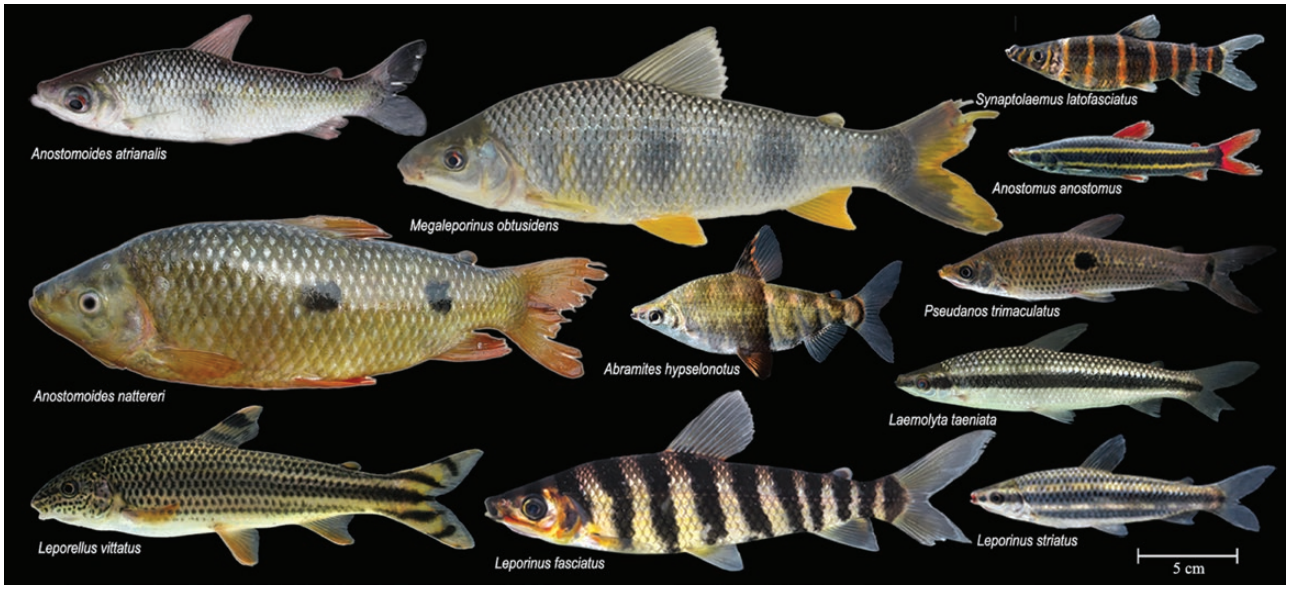

Figure 1. Diversity of the Anostomidae exemplified by some of its species, and including both valid species of *Anostomoides*. All specimens photographed live.

Taxonomic work on the family has since accelerated (Steindachner, 1875; Borodin, 1929; Myers, 1950; Winterbottom, 1980; Santos & Jégu, 1987; Garavello, 1990; Britski, 1997; Sidlauskas & Santos, 2005; Birindelli & Britski, 2009; Burns *et al.*, 2017), and the past two decades have seen particular activity in anostomid systematics, with an average of two species being described or re-described each year. Despite this activity, much about the taxonomy and phylogeny of the 15 currently recognized anostomid genera remains to be discovered.

Perhaps because of the ambiguity of its original description, *Anostomoides* Pellegrin, 1909 has long stood as one of the most enigmatic anostomid genera. Between 1885 and 1886, Jean Chaffanjon and his team collected three specimens from the Orinoco River in Venezuela possessing slightly upturned mouths. Pellegrin (1909) considered these to be intermediate between *Leporinus* and *Anostomus* and described the genus *Anostomoides* to contain his new species: *Anostomoides atrianalis* Pellegrin, 1909 (Fig. 1). Just three years later, Eigenmann (1912) described similar specimens collected at Crab Falls in the Essequibo River, Guyana, under the name *Schizodontopsis laticeps* Eigenmann, 1912. Borodin (1931) recognized the similarity between Pellegrin's and Eigenmann's specimens and considered *Anostomoides* to be a subgenus of *Schizodontopsis* Garman, 1890, while Myers (1950) pointed out that insufficient information existed to evaluate the validity of *Anostomoides*. In keeping with Jordan (1920)'s designation of *Anostomus proximus* Garman, 1890 as the type species for *Schizodontopsis*, Géry (1974) recognized *Schizodontopsis* as a synonym of *Laemolyta* Cope, 1872, a genus with an upturned jaw and distinctive incisiform dentary teeth clearly present also in Garman's species. However, Géry simultaneously transferred Eigenmann's species to *Anostomoides*, citing the possession of 'teeth like certain leporins' and 'mouth upturned like in the subgenus *Laemolyta*'. Since *Laemolyta* was then considered to be a subgenus of *Anostomus*, it is clear that Géry considered *Anostomoides* to be a transitional genus between the extremes of *Leporinus* and *Anostomus*. The concept persisted, and several decades later Santos & Zuanon (2006) followed it when they described *Anostomoides passionis* Santos & Zuanon, 2006, an apparently endemic species from the rapids of the Xingú River in Brazil with a slightly upturned mouth.

The first comprehensive phylogeny for the Anostomidae appeared to confirm Pellegrin and Géry's intuition. Using primarily osteological data, Sidlauskas & Vari (2008) reconstructed *Anostomoides* as sister to a large clade containing *Laemolyta*, *Anostomoides atrianalis* and various other genera with slightly or distinctly upturned mouths, with that entire assemblage embedded within a paraphyletic *Leporinus* (Fig. 2A). That paper also proposed several potential synapomorphies for *Anostomoides*, such as a fenestra on the lateral wing of the lateral ethmoid, biscupid symphyseal teeth of the premaxilla, and possession of three branchiostegal rays rather than the four possessed by most anostomids. However, those authors were only able to examine skeletal material of

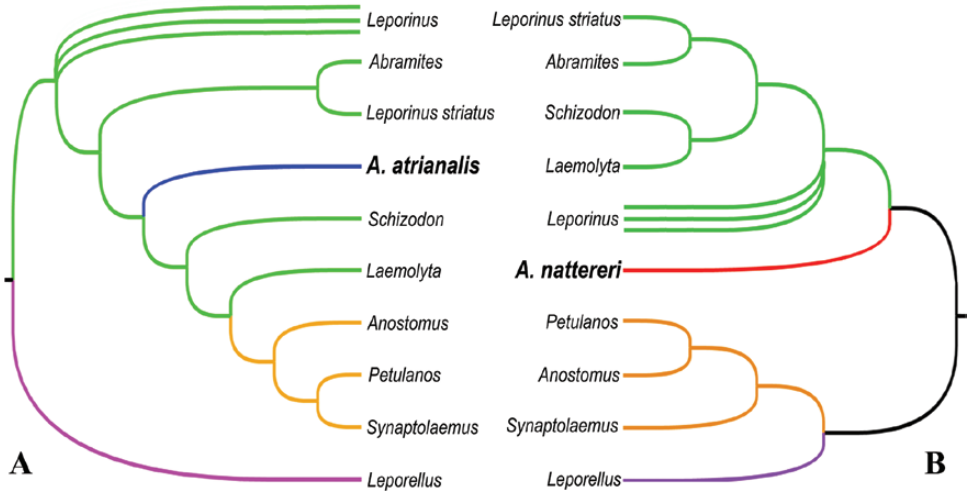

Figure 2. Hypotheses of the phylogenetic relationships of the two valid species of *Anostomoides*. A, cladogram based on 158 morphological characters (modified from Sidlauskas & Vari, 2008). B, cladogram based on data from 1051 exons (modified from Betancur-R *et al.*, 2018).

two small specimens of *Anostomoides*, one from Peru and one from Venezuela, which were nearly identical in morphology. As such, the authors could not determine whether these putative synapomorphies characterized the entire genus, or just a single species inhabiting the Amazon and Orinoco.

A recent taxonomic revision of the genus (Assega & Birindelli, 2019) recognized Pellegrin's and Eigenmann's species as identical, and thus synonymized *Anostomus laticeps* (Eigenmann, 1912) with *A. atrianalis*. Both of the specimens in Sidlauskas & Vari's (2008) morphological phylogeny belong to that species. Assega & Birindelli also demonstrated that *A. passionis* is a junior synonym of *Leporinus nattereri* Steindachner, 1876, long known only from its poorly preserved type series at Harvard's Museum of Comparative Zoology and Vienna's Naturhistorisches Museum. They transferred Steindachner's species to *Anostomoides* accordingly, but did not examine its internal anatomy.

Nearly concurrent with that taxonomic revision, a phylogenomic study of the Characiformes (Betancur-R *et al.*, 2018) reconstructed *Anostomoides nattereri* (listed as *A. passionis*) in a position not nested deeply within *Leporinus* or near *Laemolyta*, but rather diverging at one of the earliest cladogenetic events in the family (Fig. 2B). Recent molecular analyses of the Anostomidae (Ramirez *et al.*, 2016, 2017) recovered topologies similar to that of Betancur-R *et al.* (2018), but did not include *Anostomoides*. A subsequent multi-locus phylogeny for all Characiformes (Burns & Sidlauskas, 2019) placed *Anostomoides atrianalis* (listed as *A. laticeps*) in a clade also including *Laemolyta*, *Rhytiodus* Kner, 1858 and *Schizodon* Agassiz in Spix & Agassiz, 1829. That position is similar to the morphological reconstruction of *Anostomoides atrianalis'* affinities, and yet nowhere near the position for *Anostomoides nattereri* reconstructed by Betancur-R *et al.* (2018) using phylogenomics. Thus, the results to date support different placements for the two species of *Anostomoides*; however, no study has included both species, nor has any study integrated molecular and morphological data of these taxa. As such, the monophyly of the genus remains untested, and its context within the larger picture of anostomid evolution remains unclear.

This present contribution fills that knowledge gap by collecting molecular and morphological data for both putative species of *Anostomoides*, integrating those data with previously published matrices, analysing those partitions separately and simultaneously in a total evidence framework, time-calibrating the resulting phylogeny and reconstructing the evolutionary history of salient morphological characters. The results strongly indicate polyphyly for the current concept of *Anostomoides*, with *A. atrianalis* deeply nested within *Leporinus* and closely related to *Laemolyta*, *Rhytiodus* and *Schizodon* as originally hypothesized on the basis of morphology (Sidlauskas & Vari, 2008), and *A. nattereri* diverging from all other anostomids early in the diversification of the family, as also suggested by phylogenomic analysis (Betancur-R *et al.*, 2018). Because this latter species represents the sole known species within a highly divergent lineage, and because its internal anatomy has never been documented, study of its morphology has the potential to clarify initial patterns of morphological diversification within the Anostomidae. Accordingly,

we describe and illustrate its osteology and diagnose it formally as the sixteenth known genus in this remarkable family of fishes.

MATERIAL AND METHODS

Taxon sampling

In broad strokes, we integrated new data on both nominal species of *Anostomoides* with a previously published morphological data matrix (Sidlauskas & Vari, 2008) and GenBank sequences for six commonly sequenced loci in characiform systematics. Much of the prior genetic data have been used to infer previous hypotheses of anostomid or anostomoid phylogeny (Ramirez *et al.*, 2017; Melo *et al.*, 2018; Burns & Sidlauskas, 2019; and others). Taxon sampling in the molecular partition prioritized sequences of the same species present in the morphological partition, but also included representatives of a few genetically distinctive lineages for which morphological data were not available. The final matrix includes 55 anostomid species and 11 outgroup species, most of which are represented in both data partitions.

In assembling the morphological data, we removed a few taxa from Sidlauskas & Vari's (2008) matrix, updated identifications based on insights not available at the time of original publication and added one extinct species. We excluded *Pseudanos irinae* Winterbottom, 1980 because it is a junior synonym of *Pseudanos trimaculatus* (Kner, 1858) (Birindelli *et al.*, 2012), a species already included in the analyses. *Leporinus maculatus* J. P. Müller & Troschel, 1844 is used instead of *Leporinus pellegrini* Steindachner, 1910 because the latter is a likely synonym of the former (Géry *et al.*, 1988; Mol *et al.*, 2012). Based on our re-examination, the specimen listed by Sidlauskas & Vari (2008) as *Leporinus* cf. *moralesi* Fowler, 1942 is a juvenile of *Leporinus taeniatus* Lütken, 1875, and hence we updated the identification. The extinct species †*Leporinus scalabrinii* (Ameghino, 1898) was included, with coding of morphological characters from the single known fossil provided by Bogan *et al.* (2012).

Leporellus Lütken, 1875 requires taxonomic revision, and species identification in that genus are tentative. Even though it is currently impossible to distinguish specimens of *Leporellus pictus* (Kner, 1858) and *Leporellus vittatus* (Valenciennes, 1850) based on morphological features, the type localities for those nominal species are distant, and the specimens examined by Sidlauskas & Vari (2008) span a wide geographic range. Following the Sidlauskas & Vari (2008) paper, we identified specimens from the upper Paraná basin as *L. pictus* and specimens from the Amazon and Orinoco basins as *L. vittatus*.

Eight species represented in the molecular data set lack corresponding morphological data. Five of these represent *Megaleporinus* J. L. Ramírez, Birindelli & Galetti, 2017, a recently described (Ramirez *et al.*, 2017) genus not sampled by Sidlauskas & Vari (2008). Two others, *Hypomasticus copelandii* (Steindachner, 1875) and *Hypomasticus steindachneri* (Eigenmann, 1907), represent species recently transferred to *Hypomasticus* Borodin, 1929 (Birindelli *et al.*, 2020). We also added *Leporinus lacustris* Amaral Campos, 1945 to increase representation within the diverse and complex genus *Leporinus*.

Outgroup selection largely follows Sidlauskas & Vari (2008) and includes two or three representatives of the three most closely related families (Chilodontidae, Curimatidae and Prochilodontidae), one representative each of two other related families (Hemiodontidae and Parodontidae) and one species of *Brycon* J. P. Müller & Troschel, 1844 (Bryconidae), a more distantly related genus whose osteology has been studied and described exhaustively (Weitzman, 1962). Recent phylogenetic (Burns & Sidlauskas, 2019) and phylogenomic studies (Betancur-R *et al.*, 2018) have confirmed these interfamilial relationships. The distant outgroups in the Citharinidae and Distichodontidae examined by Sidlauskas & Vari (2008) were removed, because some recent phylogenomic studies suggested that these taxa may not belong to the Characiformes (Chakrabarty *et al.*, 2017; Faircloth *et al.*, 2020). Based on preliminary analyses with and without these taxa, the removal of these three species did not impact phylogenetic relationships within the Anostomidae.

Molecular data were unavailable for four of the outgroup species used in Sidlauskas & Vari (2008) and herein. For these taxa, we combined the existing morphological data with sequence data from a congener, this forming a chimaera representing a genus-level taxon. The taxon *Curimatopsis* Steindachner, 1876 unites molecular data from *Curimatopsis myersi* Vari, 1982 with morphological data from *Curimatopsis microlepis* C. H. Eigenmann & R. S. Eigenmann, 1889. *Hemiodus* J. P. Müller, 1842 unites molecular data from *H. unimaculatus* (Bloch, 1794) with morphological data from *H. ocellatus* (Vari, 1982). *Parodon* Valenciennes in Cuvier & Valenciennes, 1850 combines molecular data from *Parodon nasus* Kner, 1859 with the morphology of *Pa. suborbitalis* Valenciennes, 1850, and *Prochilodus* Agassiz in Spix & Agassiz, 1829 links molecular data from *Prochilodus nigricans* Spix & Agassiz, 1829 with morphological data from *Prochilodus rubrotaeniatus* Jardine, 1841. This decision allowed us to avoid the difficult inferential situation in which either the morphological or molecular data partitions were missing entirely for key outgroup taxa.

Morphological data

Morphological data included the character matrix of Sidlauskas & Vari (2008), plus data from the extinct species †*Leporinus scalabrinii* (Bogan *et al.*, 2012) and new data from examination of several skeletons of both nominal species of *Anostomoides* (Table 1). Large skeletons (*A. nattereri:* MZUSP 110595, *N* = 3, 230–242 mm SL, Amazon basin; *A. atrianalis*: MZUSP 67269, *N* = 2, 218–225 mm SL, Amazon basin) were prepared as dry skeletons following Bemis *et al.* (2004). These include two specimens of *A. atrianalis* much larger than those investigated by Sidlauskas & Vari (2008). Additional small specimens (*A. nattereri*: MZUEL 20445, *N* = 1, 86.1 mm SL, Orinoco basin; MZUSP 5429, *N* = 1, 141 mm SL, Amazon basin; *A. atrianalis:* INPA 15193, *N* = 1, 122 mm SL, Amazon basin; MZUEL 20017, 112.2 mm SL, Orinoco basin) were cleared and double stained (cs) following Taylor & Van Dyke (1985). Skeletons were dissected using the technique described by Weitzman (1974), which is itself a slight modification of Ridewood's (1904) method. Osteological investigation revealed several unusual or intermediate morphologies in *Anostomoides nattereri* that required non-trivial coding decisions, one new polymorphism in *A. atrianalis*, and numerous differences between the species. These are detailed in the results.

Osteological nomenclature follows Weitzman (1962), with updated terms as suggested by the Teleost Anatomy Ontology (Dahdul *et al.*, 2010), available at http://bioportal.bioontology.org/ontologies/TAO. Museum abbreviations follow Sabaj (2019). Externally visible characteristics (mainly related to coloration) were coded via examination of the many alcohol-preserved specimens listed in Assega & Birindelli (2019).

The final morphological data matrix includes 158 characters coded for 46 living ingroup taxa, one extinct ingroup taxon and 11 outgroup taxa. Inapplicable characters were coded as '-', such as in the case of characters encoding the morphology of structures absent in a particular species. Missing data, such as in the case of the extinct †*Leporinus scalabrinii* [known from a single fossil specimen missing its postcranium, MACN A-9889 (Bogan *et al.*, 2012)] were coded as '?'. Polymorphic characters were coded as such in the matrix. The data matrix was assembled in Mesquite v.3.61 (Maddison & Maddison, 2017) and is available online from the MorphoBank website (project number 3894).

Table 1. Character states for 158 morphological characters coded for *Anostomoides nattereri*. Characters are based on Sidlauskas & Vari (2008)

Species	Morphological character states
Anostomoides nattereri	1000101(12)00001000111000100 00000413(01)040(01)00111?1101 10010000000111000 10??0011001 00000011001010110121000 10000 11110001000001000000000 01001 11011010010100011111000010

Molecular data

The molecular data set includes the mitochondrial genes cytochrome oxidase *c* subunit I (*COI*, 630 bp), cytochrome *b* (*Cytb*, 1005 bp) and 16S rRNA (16S, 599 bp), and the nuclear genes *myosin heavy chain 6 gene* (*Myh6*, 750 bp), *recombination activating gene 1* (*Rag1*, 1317 bp) and *recombination activating gene 2* (*Rag2*, 1020 bp). These are by far the most frequently sequenced genes in characiform systematics and have been included in many recent Sanger-based studies of characiform phylogeny (Oliveira *et al.*, 2011; Ramirez *et al.*, 2017; Melo *et al.*, 2018; Burns & Sidlauskas, 2019; and others).

We newly sequenced molecular data for two specimens of *Anostomoides atrianalis* (AUM 53813, Caura River, Orinoco basin; UFRO-I 8702, Aripuanã River, Amazon basin) and three specimens of *A. nattereri* (INPA 40009, INPA 40840, MZUSP 110595, all from the Xingú River, Amazon basin). DNA extractions from muscle or fins were carried out using a DNeasy Tissue Kit (Qiagen Inc.) following the manufacturer's instructions. We amplified (or attempted to amplify) partial sequences of the aforementioned six genes. Primer sequences were obtained from the literature (Palumbi, 1996; Lovejoy & Collette, 2001; Li *et al.*, 2007; Melo *et al.*, 2011; Abe *et al.*, 2013). We used 12.5 µL as a total volume with 9.075 µL double-distilled water, 1.25 µL 5× reaction buffer, 0.375 $MgCl_2$, 0.25 µL dNTP mix at 8 mM, 0.25 µL of each primer at 10 µM, 0.05 µL Platinum Taq DNA polymerase enzyme (Invitrogen; www.invitrogen.com) and 1.0 µL genomic DNA (10–50 ng). PCR parameters consisted of an initial denaturation (4 min at 95 °C) followed by 28–30 cycles of chain denaturation (30 s at 95 °C), primer hybridization (30–60 s at 52–54 °C) and nucleotide extension (30–60 s at 72 °C). Fragments were visualized using 1% agarose gel and the PCR products were cleaned using ExoSAP. Sequencing followed using dye terminators (BigDye Terminator v.3.1 Cycle Sequencing Ready Reaction Kit, Applied Biosystems) and purified through ethanol precipitation. Samples were sequenced on an ABI 3130 Genetic Analyzer (Applied Biosystems) at the Universidade Estadual Paulista Júlio de Mesquita Filho, Botucatu, Brazil.

From GenBank, we obtained DNA sequences of the specimen of *Anostomoides atrianalis* (FMNH 123875, Nanay River, Amazonas basin) examined by Burns & Sidlauskas (2019), 38 other species of Anostomidae and 11 outgroup species. In order to diminish the amount of missing data, in cases when molecular data from a single specimen were not available for all six markers, sequence data from more than one specimen of the same species were combined, similar to the approach taken by Arce *et al.* (2017), Kealy & Beck (2017) and Mirande (2018). When sequences from multiple individuals were available for a locus, we chose the individual that minimized missing data. Table 2 includes a complete list of catalogue and GenBank accession numbers for the molecular samples.

Gene sequences were aligned using Clustal Omega (Madeira *et al.*, 2019) using the website https://www.ebi.ac.uk/Tools/msa/clustalo/. Loop regions were retained in the 16S alignment, with the resulting gaps coded as missing data using the '?' symbol. Aligned sequences were transferred to Mesquite v.3.61 (Maddison & Maddison, 2017), where highly variable and saturated regions with poor phylogenetic signal at the ends of the sequences were trimmed. Gene trees for each alignment were generated in MrBayes v.3.2.7a (Ronquist *et al.*, 2012) to check for and remove contaminated sequences (those identical to a species in another genus, or those clustering a species in a wildly different placement from its congeners). Sequences were then concatenated in Geneious v.11.1.2 (Kearse *et al.*, 2012) to form a molecular matrix containing 5309 bp and 55 terminals spanning three individuals of *Anostomoides atrianalis*, three of *A. nattereri*, 38 other species of Anostomidae and 11 outgroup species, and which was then used in an initial topological inference without time calibration (see Supporting Information, matrix also available in the MorphoBank website as project 3894). For the final time-calibrated analysis only the single specimen of each species of *Anostomoides* with the most complete data was included in the matrix (FMNH 123875, MZUSP 110595). Earlier exploratory analyses used alternative specimens to ensure that specimen choice did not affect the resulting topology substantially.

Phylogenetic analyses and time calibration

Phylogenetic relationships and divergence times among 55 species of Anostomidae and 11 outgroup species were investigated in a combined molecular and morphological analysis in BEAST v.2.6.2 (Bouckaert *et al.*, 2014), using the CladeAge package (Matschiner *et al.*, 2017; Barido-Sottani *et al.*, 2018). Models of nucleotide evolution were estimated via the bModelTest package (Bouckaert & Drummond, 2017). The Mk model (Lewis, 2001) was used for the morphological data set, assuming equal rates of character change. We used the birth-death tree prior and a relaxed lognormal clock model, setting the net diversification rate between 0.041 and 0.081 and turnover rate between 0.001 and 0.37, as recommended by Santini *et al.* (2009). The sampling rate varied between 0.0066 and 0.01806, as suggested by Foote & Miller (2007) [see also Matschiner *et al.* (2017)]. All other parameters were left as default. PartitionFinder v.1.1.1 (Lanfear *et al.*, 2012) was implemented to select the best partitioning scheme for the molecular matrix using the corrected Akaike Information Criterion (AICc). The analysis was rooted on *Brycon falcatus* J. P. Müller & Troschel, 1844, a representative of the distant outgroup Bryconidae.

We patterned tip- and node-based fossil calibrations on a set of fossils also used in two recent studies of characiform phylogeny (Burns & Sidlauskas, 2019; Kolmann *et al.*, 2020). We calibrated the age of the clade including all terminals except *Brycon falcatus* (equivalent to the tree root) using †*Tiupampichthys intermedius* Gayet & Jégu, 2003, an extinct species of Erythrinoidea from the Cretaceous-Palaeogene boundary of Bolivia (approximately 66.5 to 60 Mya), and isolated pacu-like fossil teeth from the lower and basal middle El Molino Formation in Bolivia (Gayet *et al.*, 1991; Dahdul, 2010), which date to the Late Cretaceous between 72 and 64 Mya (Gayet *et al.*, 1991: fig. 1). All of these fossils fit in the crown clade defined by our extant sample of species. We therefore set the minimum on the first fossil occurrence in the clade at 60 Mya and the maximum at 72 Mya.

We use Cenozoic fossil teeth exceedingly similar to the dentition of modern *Hypomasticus*, *Leporellus*, *Leporinus* and *Megaleporinus* (Antoine *et al.*, 2016), to calibrate the crown clade of the Anostomidae. The dentition in this family is highly distinctive and unlike that found in any closely related families, which are edentulous (Curimatidae), bear numerous tiny teeth (Prochilodontidae, Chilodontidae) or have broad, chisel-like teeth optimized for scraping algae (Parodontidae). Although there is some possibility that the fossil teeth are from a stem anostomid, based on their close match to the distinctive modern morphology we posit that they better calibrate the crown of the family than its stem. Although there is no precise date estimation for the fossils, they originate in a stratigraphic section of the Cenozoic deposit in the Contamana area of Peru (Antoine *et al.*, 2016: fig. 3). Based on the age of the stratum, the fossils must be slightly older than 26.63 Mya and are likely much younger than 41.05 Mya. We placed a minimum age on the first fossil occurrence of the Anostomidae at 26.63 Mya, and maximum of 41.05 Mya. We calibrated the minimum age of the split between *Curimata inornata* Vari, 1989 and *Potamorhina laticeps* (Valenciennes, 1850) using

Table 2. Voucher information and GenBank accession numbers for specimens included in the analyses

Species	*COI*	*Cytb*	*RAG1*	*RAG2*	*Myh6*	16S
Abramites hypselonotus	KF568968 (UFRO-I 8234)	KF569011 (UFRO-I 8234)	KF569054 (UFRO-I 8234)	KF569097 (UFRO-I 8234)	MW929623 (AUM 53813)	MK208260 (ANSP 178126)
Anostomoides atrianalis	MT427907 (AUM 53813)	MW929618 (AUM 53813)	-	MW929622 (AUM 53813)	MW929623 (AUM 53813)	-
Anostomoides atrianalis	MT427906 (FMNH 123875)	MK214000 (FMNH 123875)	MW929620 (FMNH 123875)	MK208235 (FMNH 123875)	MK208226 (FMNH 123875)	MK208250 (FMNH 123875)
Anostomoides atrianalis	MT427905 (UFRO-I 8702)	MW929619 (UFRO-I 8702)	MW929621 (UFRO-I 8702)	-	-	-
Anostomoides nattereri	MW929624 (MZUSP 110595)	-	-	-	-	-
Anostomoides nattereri	MW929625 (INPA 40009)	-	-	-	-	-
Anostomoides nattereri	MW929626 (INPA 40840)	-	-	-	-	-
Anostomus anostomus	-	AY791352 (AMNH 233421)	-	-	-	AY787954 (AMNH 233421)
Anostomus ternetzi	KF568970 (MZUSP 113996)	KF569013 (MZUSP 113996)	KF569056 (MZUSP 113996)	KF569099 (MZUSP 113996)	KF569142 (MZUSP 113996)	HQ171317 (LBP 4375)
Brycon falcatus	-	KF780016 (LBP 6878)	KF780090 (LBP 6878)	KF780123 (LBP 6878)	KF780051 (LBP 6878)	-
Caenotropus maculosus	KF562410 (MHNG 2717.052)	KF562441 (ANSP 189156)	KF562489 (ANSP 189156)	-	KF562465 (MHNG 2717.052)	-
Caenotropus mestomorgmatos	KF562412 (ANSP 180516)	KF562442 (ANSP 180516)	KF562490 (ANSP 180516)	KX086991 (ANSP 180516)	KF562466 (ANSP 180516)	KF562384 (ANSP 180516)
Chilodus punctatus	EU185612 (LBP 2713)	KF562460 (LBP 15541)	KF562509 (LBP 15541)	HQ289405 (LBP 4090)	KF562483 (LBP 15541)	EU181604 (LBP 2713)
Curimata inornata	MH537235 (LBP 13842)	MH537451 (USNM 402471)	MH542764 (USNM 402471)	MH542848 (USNM 402471)	MH537570 (USNM 402471)	-
Curimatopsis myersi	KU519362 (LBP 14006)	MH537430 (LBP 14006)	MH542738 (LBP 14006)	MH542834 (LBP 14006)	MH537550 (LBP 14006)	-
Gnathodolus bidens	-	MK213997 (AUM 53991)	-	MK208232 (AUM 53991)	MK208229 (AUM 53991)	MK208247 (AUM 53991)
Hemiodus unimaculatus	KX086790 (OS 18345)	KX086807 (OS 18345)	KX086968 (OS 18345)	KX086980 (OS 18345)	KX 086916 (OS 18345)	KX087042 (OS 18345)
Hypomasticus copelandii	KF568978 (MCNI 459)	KF569021 (MCNI 459)	KF569064 (MCNI 459)	KF569107 (MCNI 459)	KF569150 (MCNI 459)	-
Hypomasticus megalepis	KX020571 (MZUEL 10200)	KX020574 (MZUEL 10200)	KX020580 (MZUEL 10200)	KX020583 (MZUEL 10200)	KX020577 (MZUEL 10200)	MK208253 (USNM 402921)

Table 2. Continued

Species	*COI*	*Cytb*	*RAG1*	*RAG2*	*Myh6*	16S
Hypomasticus mormyrops	KX020572 (MZUEL 8022)	KX020575 (MZUEL 8022)	KX020581 (MZUEL 8022)	KX020584 (MZUEL 8022)	KX020578 (MZUEL 8022)	-
Hypomasticus pachycheilus	KF568973 (UFRO-I 2156)	KF569016 (UFRO-I 2156)	KF569059 (UFRO-I 2156)	KF569102 (UFRO-I 2156)	KF569145 (UFRO-I 2156)	-
Hypomasticus steindachneri	KF568994 (MCNIP 379)	KF569037 (MCNIP 379)	KF569080 (MCNIP 379)	KF569123 (MCNIP 379)	KF569166 (MCNIP 379)	EU181599 (LBP 2380)
Laemolyta garmani	KP864686 (MUSM 47361)	KP864704 (MUSM 47361)	KP864710 (MUSM 47361)	KP864722 (MUSM 47361)	KP864716 (MUSM 47361)	-
Laemolyta proxima	KP864691 (UFRO-I 14043)	KP864705 (UFRO-I 14043)	KP864711 (UFRO-I 14043)	KP864723 (UFRO-I 14043)	KP864717 (UFRO-I 14043)	MK208251 (ANSP 180323)
Laemolyta taeniata	KP864698 (UFRO-I 7897)	KP864707 (UFRO-I 9073)	KP864713 (UFRO-I 9073)	KP864726 (UFRO-I 8004)	KP864719 (UFRO-I 9073)	-
Leporellus vittatus	KF568980 (MZUSP 113987)	KF569023 (MZUSP 113987)	KF569066 (MZUSP 113987)	KF569109 (MZUSP 113987)	KF569152 (MZUSP 113987)	-
Leporellus pictus	GU701640 (LBP 11255)	-	-	-	-	-
Leporinus agassizi	MF664283 (MUSM 47362)	MF664300 (MUSM 47362)	MF664330 (MUSM 47362)	MK208236 (OS 18369)	MK208225 (OS 18369)	MK208252 (OS 18369)
Leporinus fasciatus	KF568981 (UFRO-I 3343)	KF569024 (UFRO-I 3343)	KF569067 (UFRO-I 3343)	KF569110 (UFRO-I 3343)	KF569153 (UFRO-I 3343)	HQ171321 (LBP 4459)
Leporinus friderici	KF568982 (MZUSP 113983)	KF569025 (MZUSP 113983)	KF569068 (MZUSP 113983)	KF569111 (MZUSP 113983)	KF569154 (MZUSP 113983)	EU181602 (LBP 3179)
Leporinus jatuncochi	MF285873 (OS 18325)	KY524557 (OS 18325)	KY524516 (OS 18325)	KY524528 (OS 18325)	KY524502 (OS 18325)	MF285869 (OS 18325)
Leporinus lacustris	KF568985 (MZUSP 113991)	KF569028 (MZUSP 113991)	KF569071 (MZUSP 113991)	KF569114 (MZUSP 113991)	KF569157 (MZUSP 113991)	EU181638 (LBP 2340)
Leporinus striatus	KF568995 (MZUSP 113986)	KF569038 (MZUSP 113986)	KF569081 (MZUSP 113986)	KF569124 (MZUSP 113986)	KF569167 (MZUSP 113986)	EU181636 (LBP 2736)
Leporinus taeniatus	EU185597 (LBP 261)	EU182989 (LBP 329)	KF569082 (MCP 44097)	KF569125 (MCP 44097)	KF569168 (MCP 44097)	EU181632 (LBP 329)
Leporinus tigrinus	KF568997 (GEPEMA 5514)	KF569040 (GEPEMA 5514)	KF569083 (GEPEMA 5514)	KF569126 (GEPEMA 5514)	KF569169 (GEPEMA 5514)	-
Megaleporinus elongatus	KU134853 (MCNIP 375)	KU134871 (MCNIP 375)	KU134907 (MCNIP 375)	KU134925 (MCNIP 375)	KU134889 (MCNIP 375)	-
Megaleporinus macrocephalus	KU134856 (MZUSP 118667)	KU134874 (MZUSP 118667)	KU134910 (MZUSP 118667)	KU134928 (MZUSP 118667)	KU134892 (MZUSP 118667)	GU078466 (LAGENPE 143)
Megaleporinus muyscorum	KU134857 (ICNMHN 19074)	KU134875 (ICNMHN 19074)	KU134911 (ICNMHN 19074)	KU134929 (ICNMHN 19074)	KU134893 (ICNMHN 19074)	-
Megaleporinus obtusidens	KU134859 (MCP 25476)	KU134877 (MCP 25476)	KU134913 (MCP 25476)	KU134931 (MCP 25476)	KU134895 (MCP 25476)	KT362316 (LBP 5669)
Megaleporinus trifasciatus	KU134865 (MUSM 47351)	KU134883 (MUSM 47351)	KU134919 (MUSM 47351)	KU134937 (MUSM 47351)	KU134901 (MUSM 47351)	-

Table 2. Continued

Species	*COI*	*Cytb*	*RAG1*	*RAG2*	*Myh6*	16S
Parodon nasus	GU701588 (LBP 20440)	HQ289714 (LBP 1135)	HQ289328 (LBP 1135)	HQ289521 (LBP 1135)	HQ289137 (LBP 1135)	HQ171429 (LBP 1135)
Petulanos plicatus	-	MK214003 (AUM 44717)	-	MK208240 (AUM 44717)	MK208224 (AUM 44717)	MK208255 (AUM 44717)
Potamorhina laticeps	MH537301 (LBP 6133)	MH537393 (LBP 6133)	MH542706 (LBP 6133)	MH542811 (LBP 6133)	MH537516 (LBP 6133)	-
Prochilodus nigricans	MH068834 (LBP12865)	KX086836 (LBP12865)	KX086955 (LBP12865)	KX087014 (LBP12865)	KX086902 (LBP12865)	AY788075 (AMNH 233305)
Pseudanos gracilis	-	MK213999 (ANSP 180320)	-	MK208234 (ANSP 180320)	MK208227 (ANSP 180320)	MK208249 (ANSP 180320)
Pseudanos trimaculatus	KF569003 (UFRO-I 14970)	KF569046 (UFRO-I 14970)	KF569089 (UFRO-I 14970)	KF569132 (UFRO-I 14970)	KF569175 (UFRO-I 14970)	-
Pseudanos winterbottomi	-	MK213996 (AUM 39855)		MK208231 (AUM 39855)	MK208230 (AUM 39855)	MK208246 (AUM 39855)
Rhytiodus lauzannei	KF569005 (UFRO-I 6840)	KF569048 (UFRO-I 6840)	KF569091 (UFRO-I 6840)	KF569134 (UFRO-I 6840)	KF569177 (UFRO-I 6840)	MK208259 (LBP 4239)
Rhytiodus microlepis	KF569004 (UFRO-I 18647)	KF569047 (UFRO-I 18647)	KF569090 (UFRO-I 18647)	KF569133 (UFRO-I 18647)	KF569176 (UFRO-I 18647)	-
Semaprochilodus insignis	MH991707 (INPA 57619)	KX086851 (OS 18380)	KX086973 (ANSP 180205)	KX087032 (LBP 1692)	HQ129006 (-)	-
Schizodon knerii	HQ600859 (MNICP 1339)	MK214006 (LBP 11334)	KF569095 (-)	KF569138 (-)	MK208221 (LBP 11334)	MK208258 (LBP 11334)
Schizodon nasutus	JN989223 (LBP 21861)	-	-	-	-	-
Schizodon fasciatus	KF569007 (MZUSP 113989)	KF569050 (MZUSP 113989)	KF569093 (MZUSP 113989)	KF569136 (MZUSP 113989)	KF569179 (MZUSP 113989)	HQ171308 (LBP 3994)
Schizodon scotorhabdotus	KF562432 (LBP 3046)	KX086810 (AUM 53654)	KX086971 (AUM 53654)	KX086984 (AUM 53654)	KX086920 (AUM 53654)	KX087047 (AUM 53654)
Schizodon vittatus	KF569010 (-)	MK214005 (LBP 12849)	KF569096 (-)	MK208242 (LBP 12849)	MK208222 (LBP 12849)	MK208257 (LBP12849)

†*Cyphocharax mosesi* Travassos & Santos, 1996, an extinct curimatid from the Tremembé Formation in Brazil estimated to be between 33.9 and 23.0 Myr in age old (Malabarba & Malabarba, 2010). Specifically, we used that date range to bound the minimum and maximum of the first known fossilization within that clade. Because the fossil species †*Leporinus scalabrinii* (Bogan *et al.*, 2012) is actually present in our tree, we used a fixed tip-calibration for this species at 6 Mya based on the estimated minimum age of its originating Ituzaingó Formation (Marshall *et al.*, 1983).

The morphological and molecular matrices were combined in BEAUTI v.2.6.2 and then submitted to a Bayesian inference (BI) analysis with 100 000 000 generations, sampled every 10 000 generations in BEAST v.2.6.2. All other parameters were left as default. We checked that each run had reached stationarity by trace inspection in Tracer v.1.7.1 (Rambaut *et al.*, 2018), removed a 10% burn-in portion and verified stationarity of each run by ensuring that the effective sample size (ESS) values for all or most parameters in each run exceeded 200 (Rambaut *et al.*, 2018). We verified convergence between the runs by ensuring that the 95% posterior densities for the overall likelihood values and the parameter values overlapped substantially, and that ESS values for all parameters still exceeded 200 for the pooled posterior distributions. The posterior distribution of trees were then used to construct a maximum clade credibility (MCC) tree in TreeAnnotator v.1.8.4. The posterior distribution was filtered to find the numbers of trees containing each of several possible placements of *Anostomoides nattereri* using the *is.monophyletic* function from the APE package v.5.3 (Paradis & Schliep, 2019) in R v.3.6.2 (R Core Team, 2019). The full data matrix, analysis script, posterior distribution of trees and maximum clade credibility tree are available from Dryad (accession number(s); Sidlauskas *et al.*, 2021), and also from MorphoBank (project number 3894; http://morphobank.org/permalink/?P3894).

Although we posit that the total evidence approach described above yields the most accurate reconstruction currently possible for this data set, we acknowledge the considerable debate surrounding the appropriateness of model-based analysis of phenotypic data (Wright & Hillis, 2014; Puttick *et al.*, 2017; Goloboff *et al.*, 2018, 2019; Caldas & Schrago, 2019). The debate large revolves around the plausibility of the common evolutionary mechanism of the Mk model (Lewis, 2001) for all morphological characters, which may be unlikely for complex data sets spanning a rich assortment of anatomical systems (Goloboff *et al.*, 2019). If so, parsimony analysis of the morphological partition (with or without implied weighting) may be better able to infer the true underlying topology. However, parsimony analysis may perform poorly for the molecular partition, for which the assumption of a common mechanism is much more reasonable (Steel & Penny, 2000) and wherein certain combinations of long and short branches can cause parsimony to infer an incorrect topology (Felsenstein, 1978). Thus, in choosing to apply parsimony or the Mk model to a combined molecular and morphological data set, one must make a questionable assumption about character evolution in one of the two partitions.

Parsimony analysis bears the additional limitation that it does not estimate branch lengths or divergence times, nor does it yield the time-calibrated phylogenies upon which most phylogenetic comparative methods depend (Garamszegi, 2014; Harmon, 2018). Given that this analysis aimed to infer not only topology but also dates of divergence for the known species of *Anostomoides* and sought a calibrated phylogeny suitable for downstream macroevolutionary inference, model-based inference represented the best (and indeed, the only) path forward. Nevertheless, we note the importance of investigating alternative analytical paradigms, and of evaluating the congruence of the signal in the molecular and morphological data sets. To those ends, we perform a parsimony analysis of the morphological data set in TNT v.1.5 (Goloboff & Catalano, 2016) and infer a concatenated Bayesian topology in MrBayes v.3.2.7a (Ronquist *et al.*, 2012). Details of those analyses appear in the Supporting Information.

Ancestral state reconstruction

We reconstructed the evolutionary history of selected osteological characters using maximum likelihood via the ace command in the APE package v.5.3 (Paradis & Schliep, 2019) and using the Bayesian approach of SIMMAP (Bollback, 2006) as implemented in phytools (Revell, 2012). These model-based methods take advantage of the branch length information resulting from phylogenetic inference in BEAST and offer nuanced estimates of the character states possessed by the ancestral species at internal nodes in cases of ambiguous reconstructions. In choosing characters for reconstruction, we focused on those previously proposed as synapomorphies for *Anostomoides* and those for which the two putative *Anostomoides* species displayed different morphologies. We conducted analyses using the MCC topology, and also on alternative topologies selected randomly from the subsets of the posterior distribution of phylogenies that placed *Anostomoides nattereri* in alternative positions. To remove polytomies from the consensus topology and to focus attention on the character states inferred for the most recent common ancestor (MRCA) of the anostomid crown group, we pruned these phylogenies to include a single representative of each anostomid genus before reconstructing ancestral states.

The final analyses depicted herein involve maximum likelihood reconstructions on the MCC topology. In these reconstructions, we used the Akaike Information Criterion (AIC) to compare the fits of an equal rates model (ER) and a model in which the transition rates between the character states were free to vary [the All Rates Different model (ARD)] using the fitMk command from phytools (Revell, 2012). We did not explore the symmetric (SYM) model, because all of the reconstrued characters were binary, thereby rendering the symmetric model equivalent to the equal rates model. For each character, we used the model with the lowest AIC score to perform separate reconstructions with and without *Anostomoides nattereri* pruned from the phylogenies, thereby exploring the effect of the inclusion of that species on the reconstruction. Visualizations use the dotTree function in phytools and some helpful code provided by Liam Revell on the phytools blog (http://blog.phytools.org).

For character 67 (describing the morphology of the autopalatine), we also performed reconstructions using alternative codings for the outgroup taxa. The outgroup species have varied autopalatine morphologies that led Sidlauskas & Vari (2008: 126) to refrain from proposing an a priori hypothesis of homology with either condition observed within the Anostomidae. Nevertheless, none of the outgroups possess a distinct process similar to that encoded in state 1 of this character. In one reconstruction we followed Sidlauskas & Vari (2008) in coding the outgroups as having missing data. In the other, we coded them as having state zero: 'palatine without distinct process extending away from main, rounded portion of bone cradled by dorsal portion of ectopterygoid' (Sidlauskas & Vari, 2008). The alternative reconstructions herein therefore explore the effect of homologizing a priori the conditions in the outgroups with that in the anostomid species that lack a distinct autopalatine process. The script used to perform the ancestral state reconstructions is available as part of the Dryad data package (Sidlauskas *et al.*, 2021), and also in the MorphoBank website (project number 3894; http://morphobank.org/permalink/?P3894).

RESULTS

Notable morphological codings

Although specimens of both nominal species of *Anostomoides* were examined and recoded for all morphological characters, we report below only on those characters for which the two species differ, on characters for which the coding decision for *A. nattereri* was non-trivial, or the single instance in which the coding for *A. atrianalis* changed as a result of re-examination.

Character 1. Presence or absence of horizontal flange of antorbital: Although both nominal species of *Anostomoides* possess a horizontal flange of the antorbital that runs ventral to the nares (and thus receive a coding of state 1 for this character), the relative size of the two ossifications differs substantially between the species. In *A. atrianalis*, the antorbital is a large, robust bone comparable in size to the first infraorbital and similar to the condition of *Rhytiodus* (Sidlauskas & Vari, 2008: fig. 10). In *A. nattereri*, the antorbital is smaller and more gracile (Fig. 3), only slightly larger than the antorbital of *Leporellus* (Sidlauskas & Vari, 2008: fig. 8), which lacks the horizontal flange of the antorbital and thus receives a coding of 0 for this character. Despite being coded as similar to *A. atrianalis* given the current state definitions, *A. nattereri* has an intermediate condition arguably more similar in size and shape to *Leporellus*.

Character 4. Orientation of sensory canal of first infraorbital: In both nominal species of *Anostomoides*, the dorsal opening of the sensory canal of the first infraorbital is anterior of the ventral opening (Fig. 3), and thus both receive a coding of state 0 for this character given the state definitions given by Sidlauskas & Vari (2008). However, the two species differ substantially in the overall canal morphology. In *A. nattereri*, the canal spans more vertical than horizontal distance, similar to the morphology demonstrated for *Leporellus* (Sidlauskas & Vari, 2008: fig. 8). In *A. atrianalis*, the canal runs primarily horizontally, similar to the condition in *Laemolyta* and *Rhytiodus* (Sidlauskas & Vari, 2008: figs 10–11).

Character 5. Number of intermediate pores along ossified portion of sensory canal of first infraorbital

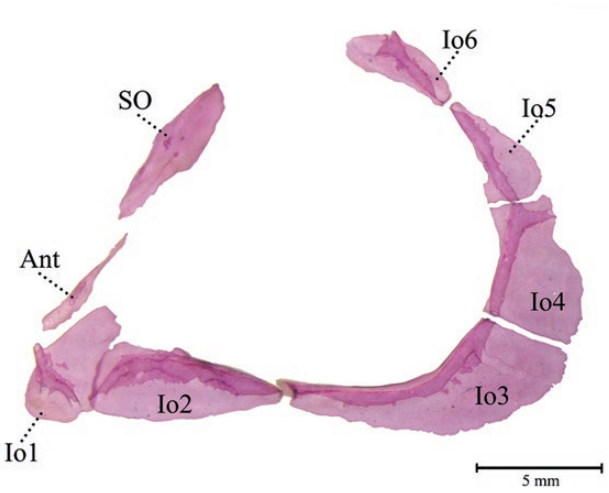

Figure 3. Infraorbital bones and associated elements of *Anostomoides nattereri*, MZUSP 5429, 138.7 mm SL. Ant: antorbital, Io1-6: infraorbital, SO: supraorbital.

between area of contact of first and second infraorbitals and anterior terminus of sensory canal proximate to antorbital: Most specimens of *Anostomoides nattereri* have a single intermediate pore of the sensory canal of the first infraorbital positioned at the bend of the canal (Fig. 3). An additional anteroventral branch of the sensory canal departs from the main channel near where it approaches the second infraorbital, typically joining in the incompletely ossified portion of the canal system and thus not forming a distinct intermediate pore. On one side of one specimen (MZUSP 110595) the ossified portion of the sensory canal extends slightly more posteriorly, and thus the anteroventrally directed branch of the canal system in that region creates a second intermediate pore. Despite the polymorphism in that specimen, the typical condition for the species appears to be possession of a single intermediate pore in this region. Following Sidlauskas & Vari's (2008) decision to code rare polymorphisms as monomorphic for the typical character state, *A. nattereri* received a coding of 1 for this character.

Character 8. Number of intermediate pores along ossified portion of sensory canal of second infraorbital: Although both specimens of *Anostomoides atrianalis* examined by Sidlauskas & Vari (2008) have two intermediate pores of this canal, one of the cs specimens examined herein has a single intermediate pore on infraorbital 2 (MZUEL 20017), whereas the other has two (INPA 15193). Even though two pores may be the more common condition, given that apparently 25% of specimens differ we elected to code *A. atrianalis* as polymorphic for this character. The same polymorphism was observed herein in specimens of *A. nattereri* and Sidlauskas & Vari (2008) noted polymorphism in the number of pores of the sensory canal of the second infraorbital among members of *Rhytiodus* and *Schizodon*. Examination of larger specimen series may demonstrate such polymorphism to be even more widespread than currently recognized.

Character 10. Relative height of fourth and fifth infraorbitals: In *Anostomoides nattereri*, the fourth and fifth infraorbitals are approximately equivalent in height (Fig. 3), while in *A. atrianalis*, the fifth infraorbital is much shorter than the fourth. Accordingly, the species received different codings for this character.

Character 11. Degree of development of flange of fifth infraorbital posterior of sensory canal: In *Anostomoides nattereri*, the flange is wide ventrally and narrows at the dorsal extreme, almost but not completely disappearing dorsally (Fig. 3), somewhat similar to the condition present in *Leporinus fasciatus* [as illustrated in Sidlauskas & Vari (2008: fig. 9)]. Based on the coding convention given in Sidlauskas & Vari (2008), we coded the species as possessing state 0 (flange present along entire margin of bone), but this is a close call, and the state in *A. nattereri* differs non-trivially from many other taxa receiving the same coding [see for example, conditions in *Petulanos plicatus* or *Gnathodolus bidens* (Sidlauskas & Vari, 2008: figs 12, 13)]. Given the intermediate condition in *A. nattereri* (and a few other taxa, including *Leporinus fasciatus*) the state definitions for this character may merit re-evaluation in a future study.

Character 15. Form and orientation of anterior portion of mesethmoid: The mesethmoid anatomy of the two nominal species of *Anostomoides* differs substantially. *Anostomoides nattereri* has a distinctly hooked anterior process of the mesethmoid (Fig. 4), a condition similar to that in *Leporellus* (Sidlauskas & Vari, 2008: fig. 16), whereas *A. atrianalis* lacks such a hook entirely and resembles the condition in *Leporinus fasciatus* (Sidlauskas & Vari, 2008: fig. 18). As such, the species differ in their coding for this character.

Character 19. Width of mesethmoid: Anostomoides nattereri has a narrow mesethmoid (Fig. 5), similar to the condition in *Leporellus* and *Hypomasticus* although not as narrow as in members of the Anostominae. *Anostomoides atrianalis* conversely has a wide mesethmoid (Sidlauskas & Vari, 2008: fig. 19). Indeed, the overall shape of the neurocranium differs substantially between the two nominal species of *Anostomoides*, with that of *A. nattereri* being markedly more laterally compressed.

Character 22. Form of articulation of vomer with autopalatine: Anostomoides nattereri possesses the angled articular facets of the vomer (Fig. 5B) that Sidlauskas & Vari (2008) encoded under state 0 and is thus similar to species of *Leporellus* and *Leporinus*, whereas *A. atrianalis* has parallel, widely separated, articular facets of the vomer similar to the condition in *Rhytiodus* and *Schizodon* (state 1).

Character 26. Presence or absence of fenestra on portion of lateral wing of lateral ethmoid situated dorsal to lateral ethmoid-ectopterygoid ligament: Sidlauskas & Vari (2008) discussed the presence of such a fenestra as convergence between *Leporellus* and *Anostomoides atrianalis*, although noting that the fenestra is larger in *Anostomoides* than in *Leporellus*. Examination of the skeletal material herein confirmed the presence of the large fenestra in all specimens of *A. atrianalis*. In most specimens of *Anostomoides nattereri* the fenestra is absent, but there is a small

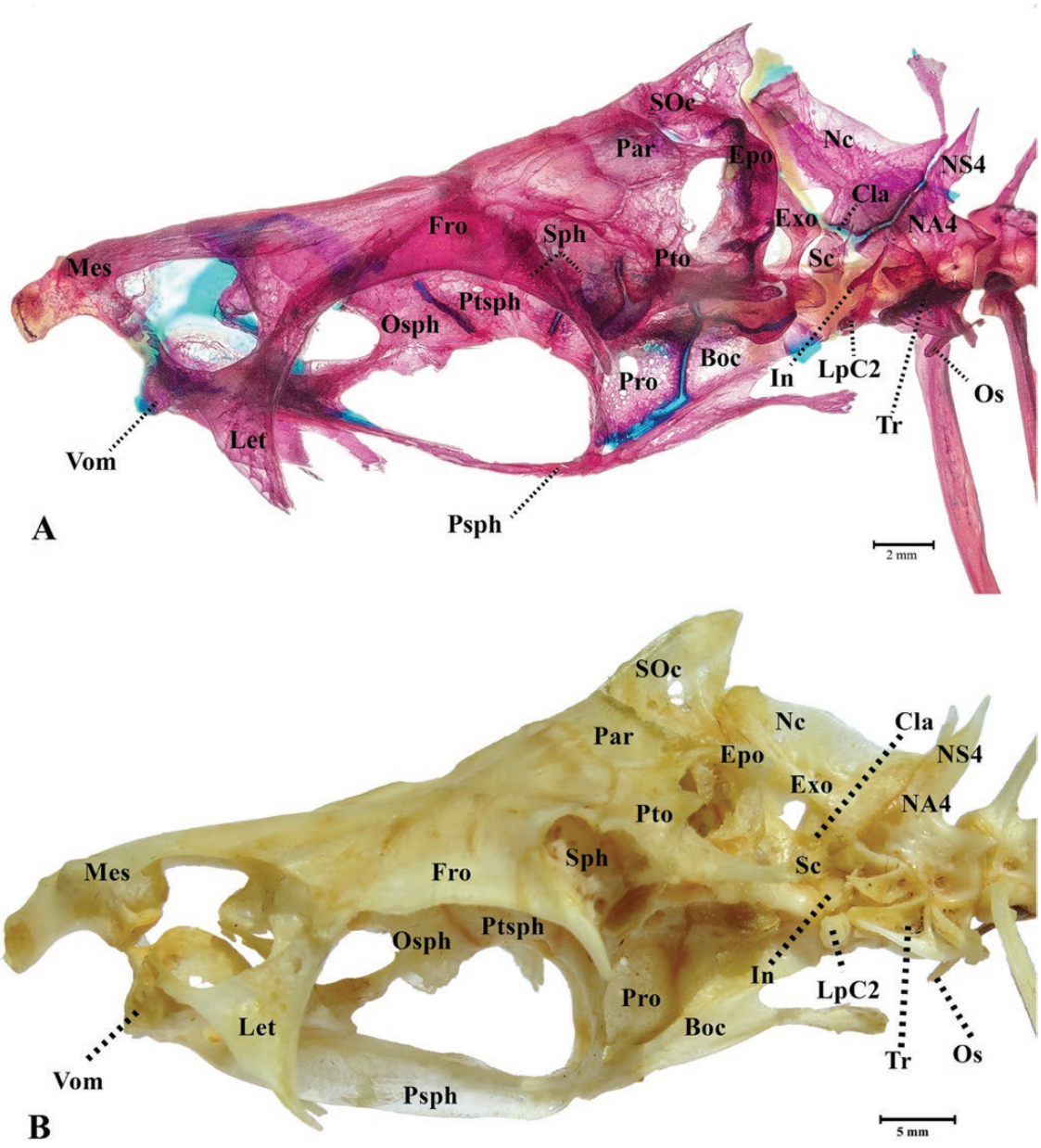

Figure 4. Cranium of *Anostomoides nattereri* in lateral view. A, MZUSP 5429, 138.7 mm SL. B, MZUSP 110595, 232 mm SL. Boc: basioccipital, Cla: claustrum, Epo: epiotic, Exo: exoccipital, Fro: frontal, In: intercalar, Let: lateral ethmoid, LpC2: lateral process of centrum 2, Mes: mesethmoid, NA4: neural arch of centrum 4, Nc: neural complex, NS4: neural spine of centrum 4, Os: os suspensorium, Osph: orbitosphenoid, Par: parietal, Pro: prootic, Pto: pterotic, Psph: parasphenoid, Ptsph, pterosphenoid, Sc: scaphium, SOc: supraoccipital, Sph: sphenotic, Tr: tripus, Vom: vomer.

fenestra present in one of the three large skeletal specimens (MZUSP 110595). The fenestra is either absent or tiny in all cleared and stained specimens of *A. nattereri*, and in all cases much smaller than the large fenestra possessed by *Anostomoides atrianalis*. This variation poses something of a coding challenge, as all specimens of *A. nattereri* differ from *A. atrianalis*, but one approaches the condition in *Leporellus*, which Sidlauskas & Vari (2008) coded as equivalent to *A. atrianalis*. Given that most specimens of *A. nattereri* lack the fenestra entirely or have a version of it smaller than the condition in *Leporellus*, we elected to code the fenestra as absent in *A. nattereri*. Future studies may wish to more rigorously define a size threshold separating these character states, or to reconsider the homologization

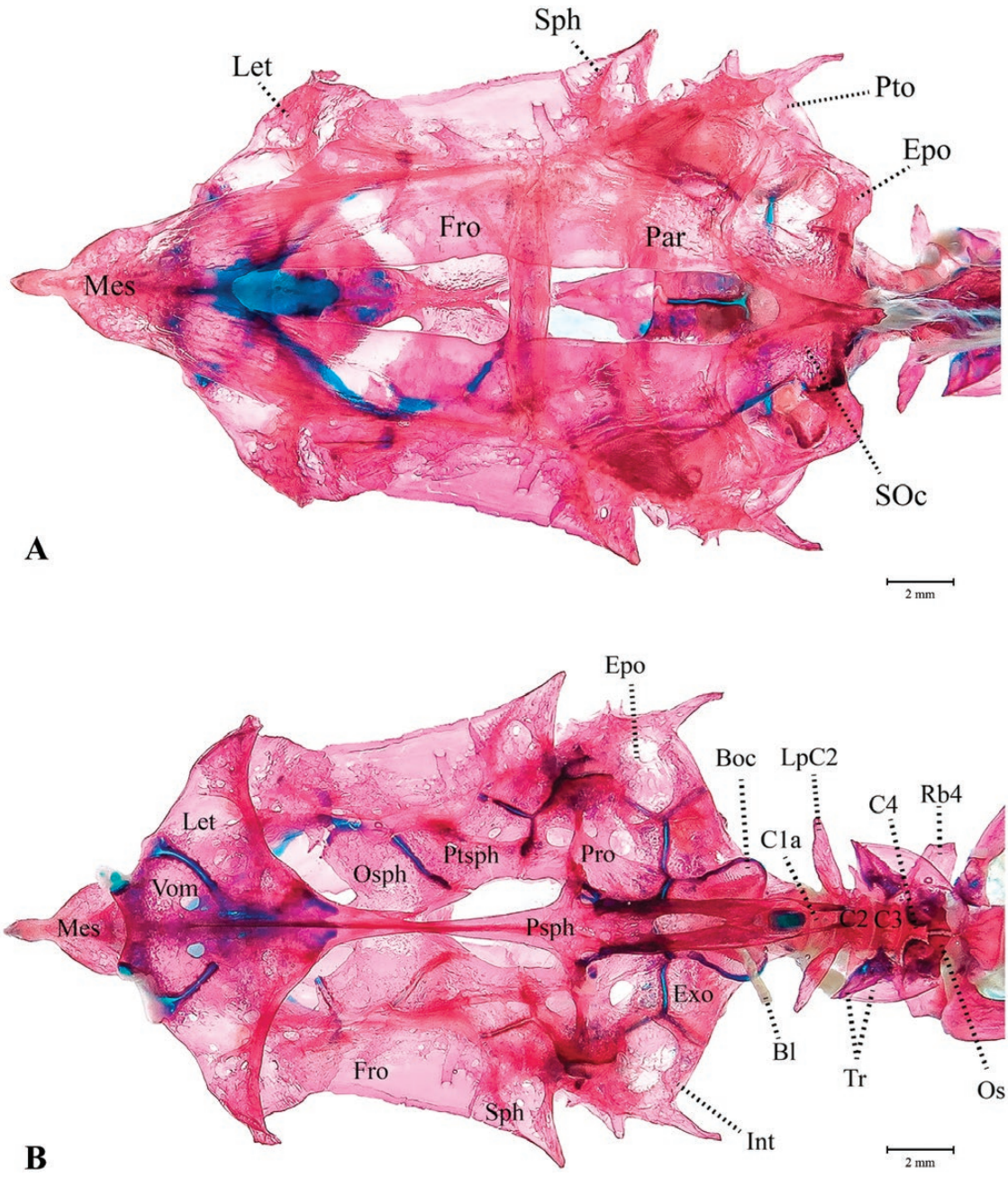

Figure 5. Cranium of *Anostomoides nattereri* in (A) dorsal and (B) ventral views, MZUSP 5429, 138.7 mm SL. Bl: Baudelot ligament, Boc: basioccipital, C1-4: centra 1–4, CLA: claustrum, Epo: epiotic, Exo: exoccipital, Fro: frontal, In: intercalar, Let: lateral ethmoid, LpC2: lateral process of centrum 2, Mes: mesethmoid, Os: os suspensorium, Osph: orbitosphenoid, Par: parietal, Pro: prootic, Pto: pterotic, Psph: parasphenoid, Ptsph: pterosphenoid, Rb4: rib of vertebra 4, SOc: supraoccipital, Sph: sphenotic, Tr: tripus, Vom: vomer.

of the fenestra in *Leporellus* with that in *Anostomoides atrianalis*.

Character 27. Presence or absence of process of lateral ethmoid directed towards posterolateral corner of mesethmoid: Anostomoides nattereri lacks the small process of the lateral ethmoid (state 0) that is present in *A. atrianalis* [state 1, see lower right section of Sidlauskas & Vari (2008: fig. 19)]. Examination of larger specimens of *A. atrianalis* in this study (e.g. MZUSP 67269) confirmed that this process falls short of a complete connection to the mesethmoid even in adults,

unlike the condition in *Rhytiodus* and *Schizodon*, in which the process forms a complete bridge linking the two bones [see Sidlauskas & Vari (2008: fig. 20) for condition in *Schizodon fasciatus*].

Character 32. Number of cusps on symphyseal tooth of premaxilla: The symphyseal premaxillary teeth in *Anostomoides atrianalis* have a distinct distal notch and thus two cusps in specimens of all sizes. The symphyseal tooth of the premaxilla in small specimens of *A. nattereri* (MZUSP 5429, 89 mm SL) also possesses two cusps (Fig. 6D) and is thus similar to *A. atrianalis* (see Assega & Birindelli, 2019: fig. 3B). However, the symphyseal tooth of the premaxilla in large specimens of *A. nattereri* (e.g. MZUSP 110595, 242 mm SL) has a blunt distal margin (Fig. 6C). This difference likely reflects an ontogenetic change similar to those described for other species of the Anostomidae (Birindelli & Britski, 2013; Machado-Evangelista *et al.*, 2015; Birindelli *et al.*, 2016). This character was coded as state 1 (tooth unicuspid) in *A. nattereri*, as that coding reflects the adult morphology.

Character 34. Structure of medial surface of second and third teeth of premaxilla: The examined specimens of *A. nattereri* differ in the presence or absence of a ridge on the medial surface of the premaxillary teeth. One large specimen with teeth that appear to have

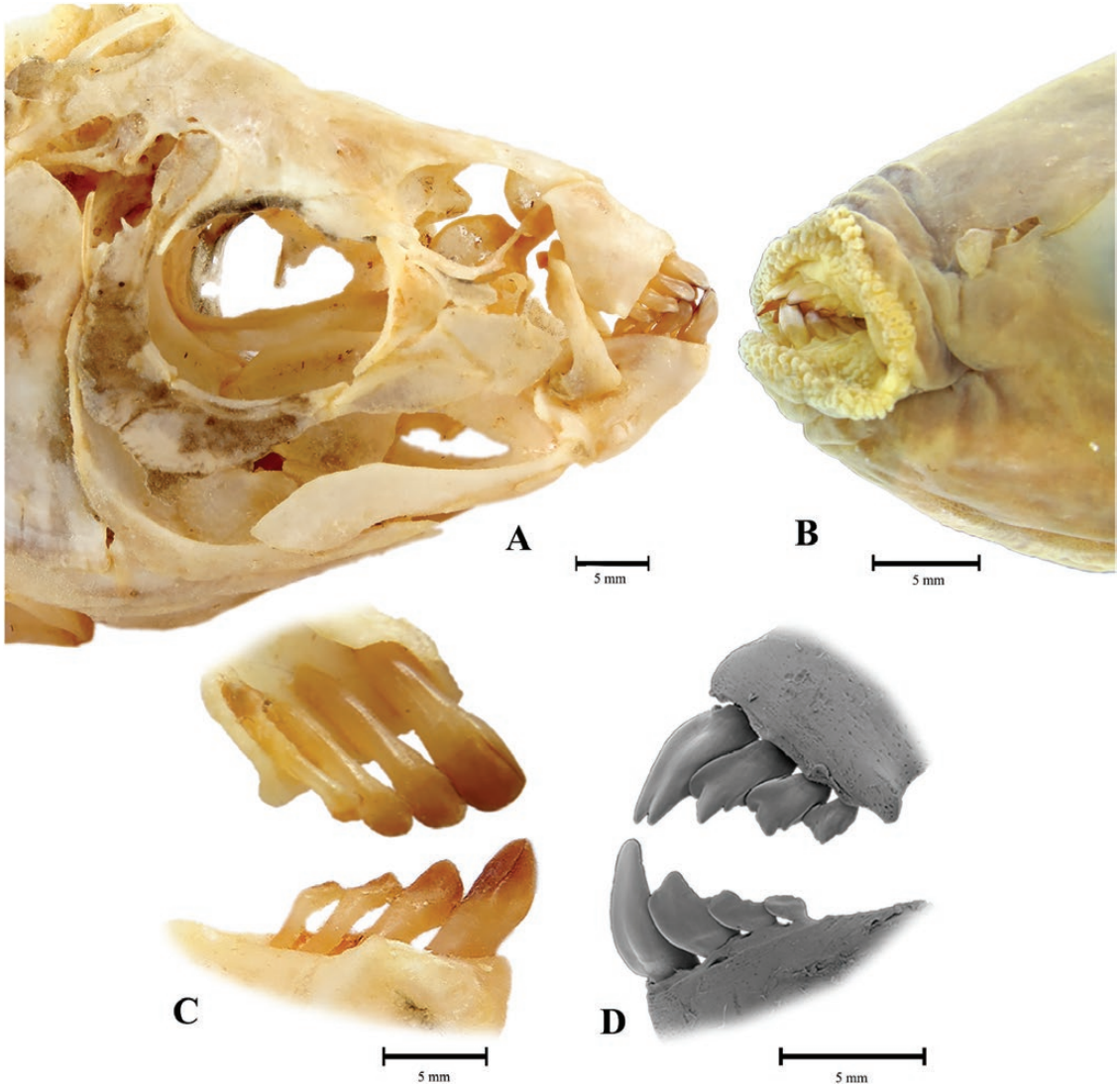

Figure 6. Details of the teeth, lips and bones of the head in *Anostomoides nattereri*. Lateral view of head (A) and medial view of teeth (C) of a specimen prepared as a dry skeleton (MZUSP 110595, 242 mm SL); details of lips (B) of an alcohol-preserved specimen (FMNH 103451, 141.8 mm SL); and scanning electron microscope image of teeth in lateral view (D) of a cleared and stained specimen (MZUSP 5429, 89.0 mm SL.

been recently replaced has prominent medial ridges, while two others lack any hint of the ridge (Fig. 6C), including one individual with distinctly worn teeth. Based on the variability at hand, we coded the species as polymorphic for this character. Perhaps more importantly, these observations suggest that the ridge erodes with use in this species, and perhaps in other members of the family. If so, future studies should re-evaluate the encoding of this character for all anostomid species on larger specimen series, with particular attention to whether the ridge is present in newly formed teeth.

Character 38. Form of posterior lamina of dentary teeth: Despite the many skeletal differences between *Anostomoides nattereri* and *A. atrianalis*, here the similarity between them is striking [Fig. 6; see also Assega & Birindelli (2019: fig. 3)]. In both species, there is no obvious posterior lamina on the symphyseal tooth, but there is a clear lamina on the third, and the second has arguably a small lamina. Both of the species are thus polymorphic for this character.

Character 52. Width of ventral portion of maxilla: In *Anostomoides nattereri*, the ventral portion of the maxilla is wide (Fig. 6A), with a distinct posterior projection at its ventral extreme (state 1). The ventral portion of the maxilla in *Anostomoides atrianalis* is narrow and lacks a prominent posterior projection (state 0).

Character 58. Form of anterior margin of dentary and angle of the teeth: The overall form of the dentary in *Anostomoides nattereri* clearly matches the triangular morphology typically encoded as state 0 of this category (Fig. 6A). However, the symphyseal teeth have a strongly vertical orientation that causes a line drawn through the teeth to pass anterior of the retroarticular, thus also fulfilling part of the original description of state 1. Given that the shape of the dentary resembles the triangular condition seen in *Abramites*, *Anostomoides atrianalis*, *Hypomasticus*, *Leporellus* and *Leporinus* much more closely than the block-like dentary found in *Laemolyta*, *Rhytiodus*, *Schizodon* and the members of the Anostominae, we coded *A. nattereri* as possessing state 0 for this character. Future work may consider redefining the conditions for this character or breaking it into two characters, since the morphology of *A. nattereri* fulfils part of both state descriptions as currently written.

Character 65. Relative positioning of retroarticular and dentary: In *Anostomoides nattereri*, as in *Abramites* Fowler, 1906, *Hypomasticus*, *Leporellus* and *Leporinus*, the retroarticular is placed laterally in the lower jaw (state 0), whereas *A. atrianalis* shows an alternative morphology similar to the condition typical of *Schizodon* in which the retroarticular sits more ventrally (state 1).

Character 66. Presence or absence of dermal papillae on lips: The presence of abundant rounded dermal papillae on the lips has been long recognized as a distinctive feature of the three anostomid genera with the most strongly upturned mouths: *Gnathodolus* G. S. Myers, 1927, *Sartor* G. S. Myers & A. L. de Carvalho, 1959 and *Synaptolaemus* G. S. Myers & Fernández-Yépez, 1950 (Myers & Carvalho, 1959; Winterbottom, 1980; see also Santos & Jégu, 1987: fig. 10). *Anostomoides atrianalis*, like most other anostomids, lacks such papillae. Therefore, we were surprised to find abundant rounded lip papillae present in *A. nattereri* (Fig. 6B), which has an overall morphology dissimilar from the three aforementioned genera. The presence of the abundant rounded papillae in *A. nattereri* calls the status of the character as a non-homoplastic synapomorphy of *Gnathodolus*, *Sartor* and *Synaptolaemus* into question, and prompted us to re-examine the condition in the other anostomine genera. *Anostomus*, *Petulanos* Sidlauskas & Vari, 2008 and *Pseudanos* all have small rounded dermal papillae on the lips in addition to ridge-like papillae (see Birindelli *et al.*, 2012: fig. 2). However, these papillae are shorter and less abundant than in *A. nattereri*, *Gnathodolus*, *Sartor* or *Synaptolaemus* (see Assega & Birindelli, 2019: fig. 4). Future work should consider altering the current character coding so that it spans three states, or breaking the current character into two, one of which would encode the presence or absence of the papillae while the other would describe their length and abundance.

Characters 67 and 68. Presence or absence and orientation of distinct process of autopalatine: Autopalatine morphology varies considerably across the Anostomoidea (Figs 7–9; Sidlauskas & Vari, 2008), with the most common condition involving the presence of a distinct process extending laterally, ventrolaterally or anteroventrolaterally from the compact main body of the bone (Figs 7G–H, 8C–H). Members of the subfamily Anostominae lack an autopalatine process entirely [Fig. 7E–F; see also Sidlauskas & Santos (2005: fig. 5) illustrating the condition in *Pseudanos gracilis* (Kner, 1858) and *Pseudanos winterbottomi* Sidlauskas & dos Santos, 2005], and that absence was proposed as one of the most important synapomorphies uniting that subfamily (Sidlauskas & Vari, 2008). Members of *Leporellus* possess an anteroposteriorly elongate autopalatine without substantial deviation from the parasagittal plane that nevertheless extends markedly anteriorly away from the ectopterygoid

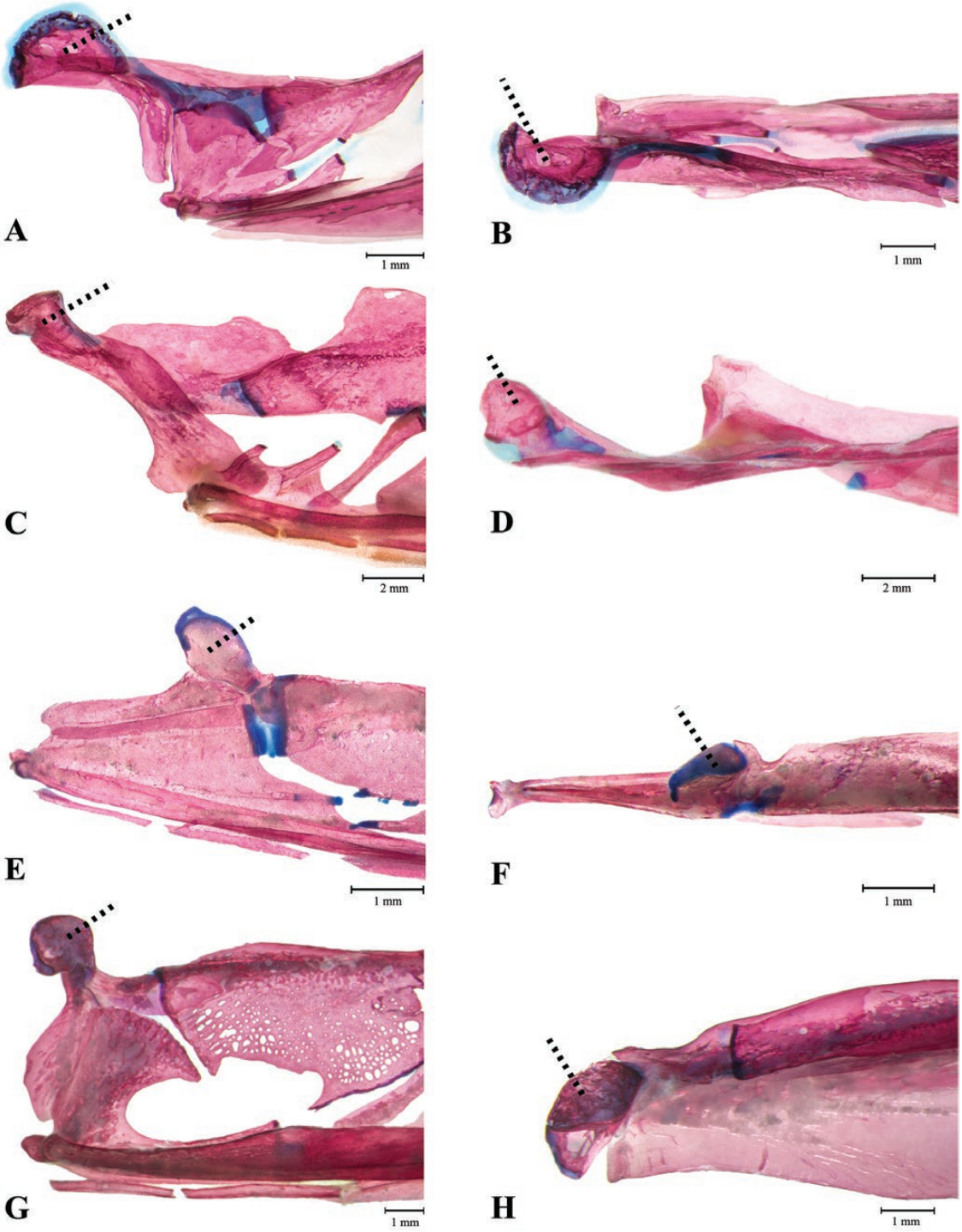

Figure 7. Detail of autopalatine in lateral (left) and dorsal (right) views of: (A, B) *Caenotropus labyrinthicus*, MZUSP 29351, 68.9 mm SL; (C, D) *Prochilodus nigricans*, MZUSP 95799, 112.5 mm SL; (E, F) *Petulanos intermedius*, MZUSP 97330, 59.6 mm SL; (G, H) *Anostomoides atrianalis*, ANSP 159599, 159.6 mm SL. The dotted lines indicate the autopalatine.

(Fig. 8C, D). Sidlauskas & Vari (2008) homologized the anteriorly-directed process in *Leporellus* with the laterally directed process in their character 67 and recognized the two distinctive morphologies in the dependent character 68, which encodes the direction of the process.

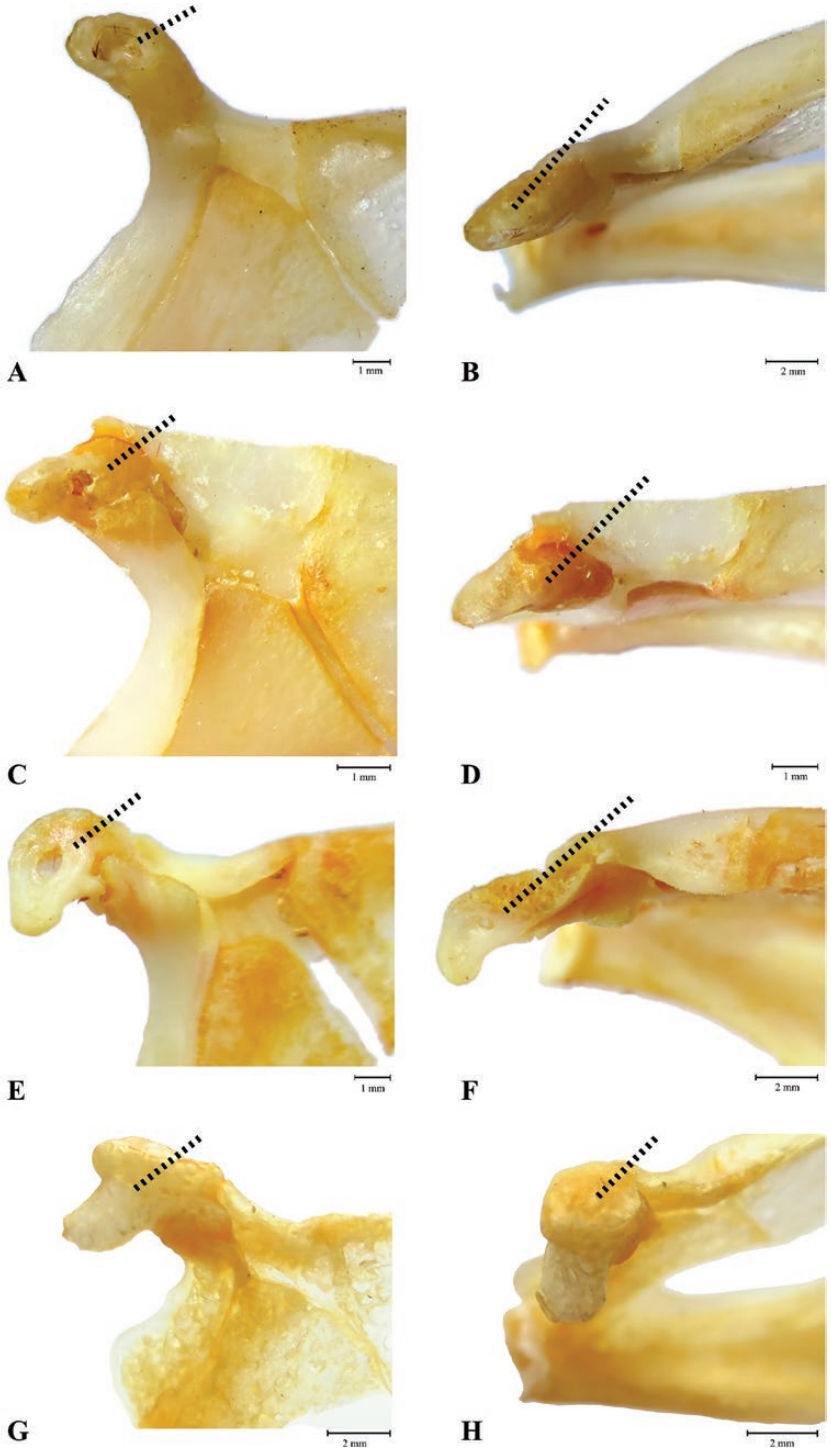

Figure 8. Detail of autopalatine in lateral (left) and dorsal (right) views in skeleton of: (A, B) *Anostomoides nattereri*, MZUSP110595, 232.0 mm SL; (C, D) *Leporellus vittatus*, MZUSP 106332, 155.0 mm SL; (E, F) *Leporinus obtusidens,* MZUEL 16470, 260.0 mm SL; (G, H) *Anostomoides atrianalis*, MZUSP 67269, 218.0 mm SL.

Anostomoides nattereri (Figs 8A, B, 9) unexpectedly possesses an autopalatine almost indistinguishable from the condition in most members of the Anostominae, such as *Anostomus* and *Pseudanos*. The bone is small and compact, extending only slightly anteriorly past the anterior extreme of the ectopterygoid, and lacking any hint of a laterally directed process. The overall morphology of the bone also bears some resemblance

to the condition in *Leporellus*, but does not extend so far anteriorly. It differs greatly from the condition in *Anostomoides atrianalis* (Figs 7G–H, 8G–H), which possesses a prominent lateral process in all specimens examined. We accordingly coded *Anostomoides nattereri* as lacking any process of the autopalatine (state 0 for character 67) making it the only non-anostomine species within the Anostomidae to lack such a process. Character 68 received a coding of 'inapplicable' for this species, since the orientation of a non-existent process is undefined.

Character 75. Association of quadrate with entopterygoid: The two species of *Anostomoides* differ substantially in the state of this character. In *A. atrianalis*, the entopterygoid does not contact the quadrate, whereas *A. nattereri* possesses a distinct ventral triangular extension that overlaps the medial surface of the quadrate. Although the ventral process of the ectopterygoid of *A. nattereri* (Fig. 9) is smaller than in some species of *Leporinus* and much smaller than the condition in *Schizodon* (see Sidlauskas & Vari, 2008: fig. 42), it is well within the range of morphologies previously encoded under state 0 of this character, and thus *A. nattereri* received that coding.

Character 76. Form of association of posterodorsal and posterior processes of quadrate: In most anostomid species, including *Anostomoides atrianalis*, an extensive plate of bone fills a gap that separates the quadrate into distinctive posterodorsal and posterior processes in most members of Characiformes. *Leporellus* possesses the plesiomorphic condition, making the reduction in the gap between the quadrate processes (or alternatively, the presence of bone in this region) a synapomorphy for all anostomids exclusive of *Leporellus*. In *Anostomoides nattereri,* the gap between the processes is present (Fig. 9A), but much less extensive than in *Leporellus*, with the length of the free portion of the posterodorsal process approximating its width. The condition in *A. nattereri* is close to several species of *Hypomasticus* and *Leporinus* (Sidlauskas & Vari, 2008: fig. 41), and dissimilar to the condition in *A. atrianalis*, *Schizodon*, members of Anostominae and various other anostomids [see discussion in Sidlauskas & Vari (2008: 131)]. Exclusive of the distinctive plesiomorphy in *Leporellus*, the variation in

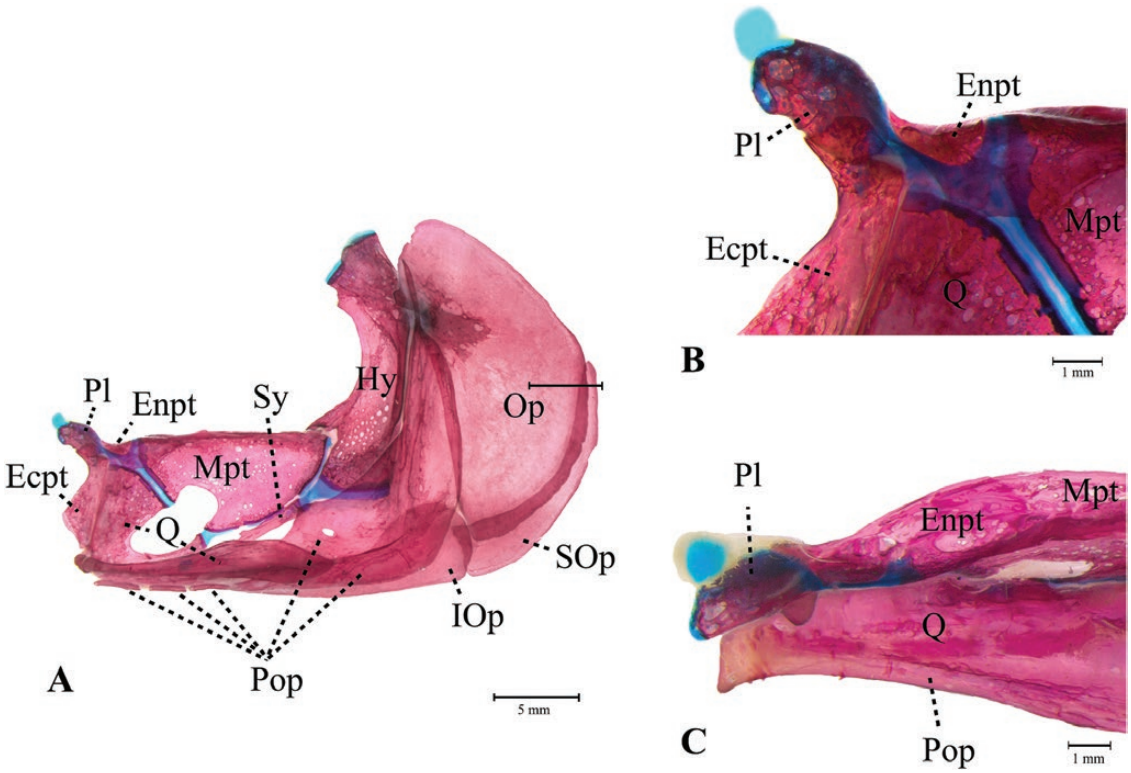

Figure 9. Suspensorium and jaws of *Anostomoides nattereri*, MZUSP 5429, 138.7 mm SL. Suspensorium of *Anostomoides nattereri*, MZUSP 5429, 138.7 mm SL, in lateral view (A), with detail of autopalatine in lateral (B) and dorsal (C) views. Ecpt: ectopterygoid, Enpt: entopterygoid, Hy: hyomandibular, IOp: interopercle, Mpt: metapterygoid, Op: opercle, Pl: autopalatine, Pop: preopercle, Q: quadrate, SOp: subopercle, Sy: symplectic.

the degree of reduction of the gap region is continuous within the Anostomidae, and Sidlauskas & Vari (2008) were not able to break this character further into distinctive character states. Although both nominal species of *Anostomoides* receive the same coding for this character, the fact that *A. nattereri* possesses an apparently intermediate condition between the large gap in *Leporellus* and the completely filled gap of *A. atrianalis* and most other anostomids, suggests that it may demonstate a transitional morphology for this character.

Character 80. Length of cartilage body spanning ventral section of metapterygoid-quadrate fenestra: In *Anostomoides atrianalis*, an elongate cartilage forms the ventral border of the metapterygoid-quadrate fenestra and connects to the posterodorsal process of the quadrate dorsal to the symplectic. This morphology resembles that possessed by most members of *Laemolyta*, *Schizodon*, *Rhytiodus* and the anostomine genera [e.g. *Synaptolaemus*, see Sidlauskas & Vari (2008: fig. 44)]. In *Anostomoides nattereri*, that cartilage is much shorter (Fig. 9A), and demonstrates a plug-like morphology similar to the condition in *Abramites*, *Hypomasticus*, *Leporellus* (Sidlauskas & Vari, 2008: fig. 40) and some members of *Leporinus* and *Schizodon* [e.g. *Leporinus fasciatus* (Sidlauskas & Vari, 2008: fig. 41)].

Character 90. Form of posterodorsal margin of opercle: Anostomoides atrianalis has a fully convex posterodorsal margin of the opercle, much like the morphology seen in *Laemolyta*, *Rhytiodus* and *Schizodon*. *Anostomoides nattereri* has a subtle concavity in that margin immediately dorsal to the dorsal limit of the subopercle (Fig. 9A), with that concavity more apparent in larger specimens. The morphology of *A. nattereri* more closely approximates that seen in *Abramites*, *Hypomasticus*, *Leporellus* and *Leporinus* than it does *Anostomoides atrianalis*, and the two nominal species of *Anostomoides* thus received different encodings for this character.

Character 92. Presence or absence of ossified first basibranchial: Some anostomid species possess a small, nub-like first basibranchial [e.g. *Leporellus* (Sidlauskas & Vari, 2008: fig. 46)] whereas others lack the bone entirely (e.g. *Rhytiodus*). *Anostomoides nattereri* possesses a well-developed, rod-like first basibranchial (Fig. 10B), larger than observed in other members of the family, but similar to the morphology possessed by members of the outgroup families Chilodontidae and Bryconidae. Conversely, *Anostomoides atrianalis* lacks an ossified first basibranchial.

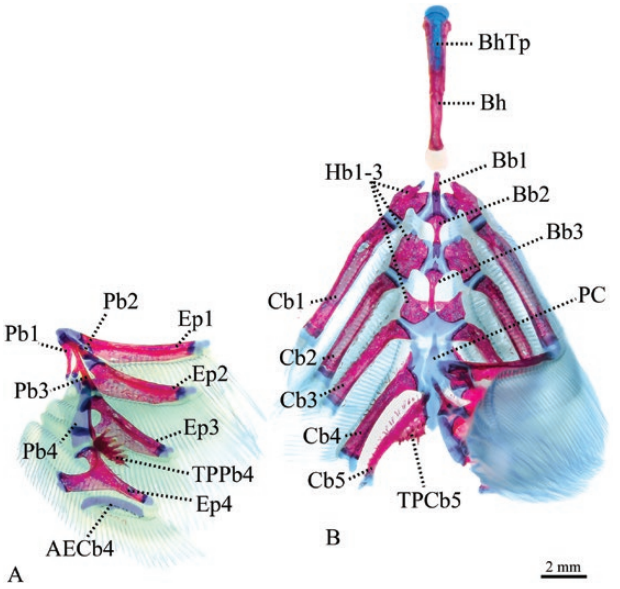

Figure 10. Branchial apparatus of *Anostomoides nattereri* MZUSP 5429, 138.7 mm SL. AECb4: accessory element of ceratobranchial 4, Bb1–3: basibranchial 1–3, Bh: basihyal, BhTp: basihyal toothplate, Cb1–5: ceratobranchial 1-5, Ep1–4: epibranchial 1–4, Hb1-3: hypobranchial 1-3, Pb1–4: pharyngobranchial 1–4, PC: posterior copula, TPPb4: tooth plate of fourth pharyngobranchial, TPCb5: tooth plate of fifth ceratobranchial.

Character 100: Number of branchiostegal rays: Anostomoides nattereri possesses four branchiostegal rays (Fig. 11A, B), which is the most common condition for the family. Conversely, *Anostomoides atrianalis* possesses only three, a condition otherwise known only in *Abramites* and *Pseudanos* (Sidlauskas & Vari, 2008), and as a rare polymorphism in *Anostomus anostomus* (Linnaeus, 1758) (Winterbottom, 1980).

Character 106. Presence or absence of supraneural dorsal to Weberian apparatus: Many anostomid species possess an ossified supraneural dorsal to the neural spine of the fourth vertebra of the Weberian apparatus [e.g. *Leporellus* (Sidlauskas & Vari, 2008: fig. 50)], with the presence of such an element being the plesiomorphic condition of the family. *Anostomoides nattereri* has such a supraneural (Fig. 4), interestingly with its ventral tip resting in a small pocket on the dorsal surface of the neural spine of the fourth vertebra. *Anostomoides atrianalis* lacks this element, a condition that it shares with *Abramites*, *Laemolyta*, *Leporinus striatus* Kner, 1858, *Rhytiodus*, *Sartor* and *Schizodon* (Sidlauskas & Vari, 2008).

Characters 117 and 118. Presence or absence of dark vertical blotches / lateral line spots on body: Anostomoides atrianalis possesses a series of faint

vertical blotches on the body similar to Character 117, also observed in many species of *Laemolyta*, *Rhytiodus* and *Schizodon*. *Anostomoides nattereri* lacks such blotches and instead has a pair of dark spots situated along the lateral line scale region [Fig. 1; see also Assega & Birindelli (2019: fig. 7)].

Character 120. Presence or absence of complete dark stripe along lateral-line scale row: Anostomoides atrianalis possesses a faint midlateral stripe which *Anostomoides nattereri* lacks entirely [Fig. 1; see also Assega & Birindelli (2019: fig. 7)]. The two nominal species of *Anostomoides* thus receive different codings for this character.

Molecular data set

The molecular matrix contained in total 5321 bp, with 81% of its cells complete. The amount of missing data varied from 10% to 38% among genes, with *CytB* showing the lowest value and 16S the largest (Table 3). Guanine-cytosine (GC) content was higher in the nuclear genes *RAG1* (53.1%) and *RAG2* (54.6%) than in *Myh6* (45.6%) or any of the mitochondrial genes (44.0% to 46.7%). The number of variable sites varied from 218 to 531 and parsimony-informative sites varied from 140 to 470 (Table 3).

Unfortunately, some of the six markers proved difficult to amplify in our samples of *Anostomoides* (Table 2), particularly for *Anostomoides nattereri*. The *COI* locus performed well for both nominal species of *Anostomoides* and amplified for all specimens except for one *A. atrianalis* (FMNH 123875). All of the other loci amplified for at least one individual of *A. atrianalis* (usually two or three); however, none of those loci amplified for any of the four *A. nattereri* specimens available to us, despite multiple PCR attempts. It is not clear whether all four tissues were degraded, or

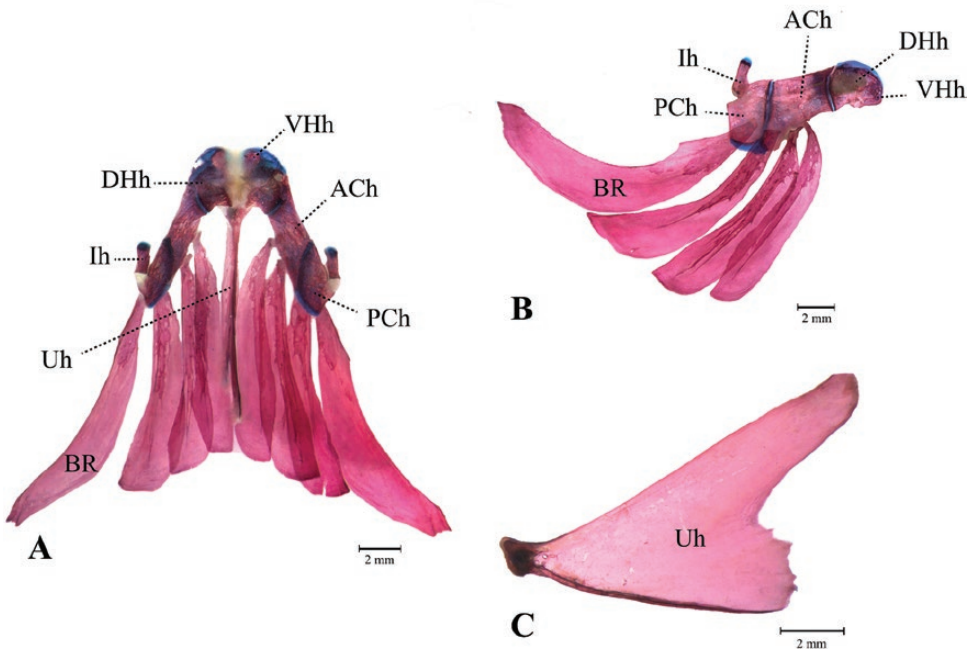

Figure 11. Hyoid arch of *Anostomoides nattereri*, MZUSP 5429, 138.7 mm SL, in ventral (A) and dorsal (B) views, with detail of the uruhyal in lateral view (C). ACh: anterior ceratohyal, BR: branchiostegal rays, DHh: dorsal hypohyal, Ih: interhyal, PCh: posterior ceratohyal, Uh: urohyal, VHh: ventral hypohyal.

Table 3. Summary statistics for each gene partition

Locus	Length (bp)	Number of variable sites	Number of parsimony-informative sites	Missing data (%)
COI	630	262	243	17
Cytb	1005	531	470	10
Myh6	750	218	140	16
RAG1	1317	470	297	19
RAG2	1020	370	254	18
16S	599	253	193	38

whether the standard primers simply do not work on this species. As a result of these failed amplifications, it is important to note that position of *A. nattereri* in the molecular-only analysis (see Supporting Information) is based on only the *COI* locus of three specimens yielding similar but not identical sequences (pairwise distance within this species of 0.35% to 0.48%). Its position in the total evidence analysis of course also relies on extensive morphological examination.

At the *COI* locus, *Anostomoides nattereri* and *A. atrianalis* differ massively, with only 83.7% to 83.8% sequence similarity. These values are far lower than typical for congeners in other anostomid genera. For example, *Schizodon fasciatus* is 91.4% to 97.0% similar to the other three sequenced congeners, the three sequenced species of *Laemolyta* are 95.6% to 97.1% similar and the two species of *Leporellus* are 93.9% similar. Even members of the species-rich but paraphyletic genus *Leporinus* tend to be more similar to each other than are the two nominal *Anostomoides* species, with similarities ranging from 85.1% for the comparison between *Leporinus striatus* and *Leporinus jatuncochi* Ovchynnyk, 1971 to 98.6% for the distance between *Leporinus friderici* (Bloch, 1794) and *Leporinus agassizii* Steindachner, 1876.

Anostomoides nattereri fails to match any other sequenced species closely for *COI*. The closest matches are *Leporinus tigrinus* Borodin, 1929 (86% similarity) and *Megaleporinus elongatus* (Valenciennes, 1850) (85% similarity). Some outgroup species are nearly as close (e.g. 84.0% similarity to *Prochilodus nigricans* Spix & Agassiz, 1829). Nevertheless, the three COI sequences of *A. nattereri* are similar to each other but not identical, making it unlikely that they represent contamination from an outgroup taxon.

Phylogenetic reconstruction

The time-calibrated analysis converged well, achieving stationarity at the log likelihood value of -46489, and all parameters converge. After removal of a 10% burn-in, and all parameters converged achieved ESS values exceeding 200, with many exceeding 1000 with the lowest ESS observed for variable BMT_proportionInvariable.3 (ESS = 881).

The phylogenetic analysis reconstructed a wide separation between *Anostomoides nattereri* and *A. atrianalis* (Fig. 12), indicating polyphyly of the genus as currently defined (Assega & Birindelli, 2019). Although separate analyses of the morphological and molecular data sets infer different overall topologies, they agree entirely on the wide separation of the two nominal species of *Anostomoides* (Supporting Information, Figs S2 –S3), with *Anostomoides nattereri* diverging from all other anostomid species early in the history of the clade, and *A. atrianalis* appearing in a much more nested position.

As previously hypothesized (Sidlauskas & Vari, 2008; Burns & Sidlauskas 2019), *Anostomoides atrianalis* is closely related and sister to a clade containing *Laemolyta*, *Rhytiodus* and *Schizodon* (Fig. 12), with the most recent common ancestor of those four genera existing in the Early Miocene at approximately 19 Mya [12.7–26.8 Mya, 95% highest posterior density (HPD)] and that unit receiving a posterior probability of 99.93%. That result is consistent with the non-time-calibrated total evidence analysis including all three specimens that placed *Anostomoides atrianalis* as a monophyletic unit sister to a clade composed of *Laemolyta*, *Rhytiodus* and *Schizodon*.

We reconstruct *Anostomoides nattereri* in a position distant from *A. atrianalis*, as the sister lineage to a clade containing all other anostomids except for *Leporellus* and the subfamily Anostominae and in a position matching that recovered by Betancur-R *et al.* (2018) in their phylogenomic analysis. The posterior probablility at that node is low (86.06%), likely due to the large amount of missing data for this species in the molecular matrix, and alternative placements are possible. *Anostomoides nattereri* forms the sister to a clade containing *Leporellus* and the Anostominae in 939 of the 9001 trees in the post-burn-in posterior distribution (10.4%). There are also 316 trees in the posterior distribution (3.5%) in which *Anostomoides nattereri* is sister to all other living anostomids, and 22 cases (0.24%) in which it is sister to the Anostominae.

No matter which of these placements is correct, *Anostomoides nattereri* clearly represents a previously unrecognized clade that diverged from the remainder of the Anostomidae early in its evolutionary history. All of the trees in the posterior distribution indicate that *Anostomoides* originated at one of the first three splits within the anostomid crown clade. Assuming the total evidence maximum clade credibility tree to reflect the best reconstruction, this lineage has been evolving independently since the Eocene-Oligocene transition, for approximately 37 Myr (24.1–51.6 Mya 95% HPD) and diverged about 5 Myr after the first cladogenetic event within the crown of the family, which separated the clade leading to the Anostominae plus *Leporellus* from that leading to all other anostomids (42 Mya; 29.2–57.8 Mya, 95% HPD).

Ancestral state reconstructions

We selected six morphological characters for ancestral state reconstruction, presentation and discussion: character 15 (form and orientation of the anterior portion of the mesethmoid), character 19 (mesethmoid width), character 52 (width of the ventral portion of the maxilla), character 65 (relative position of retroarticular and dentary in the lower jaw), character

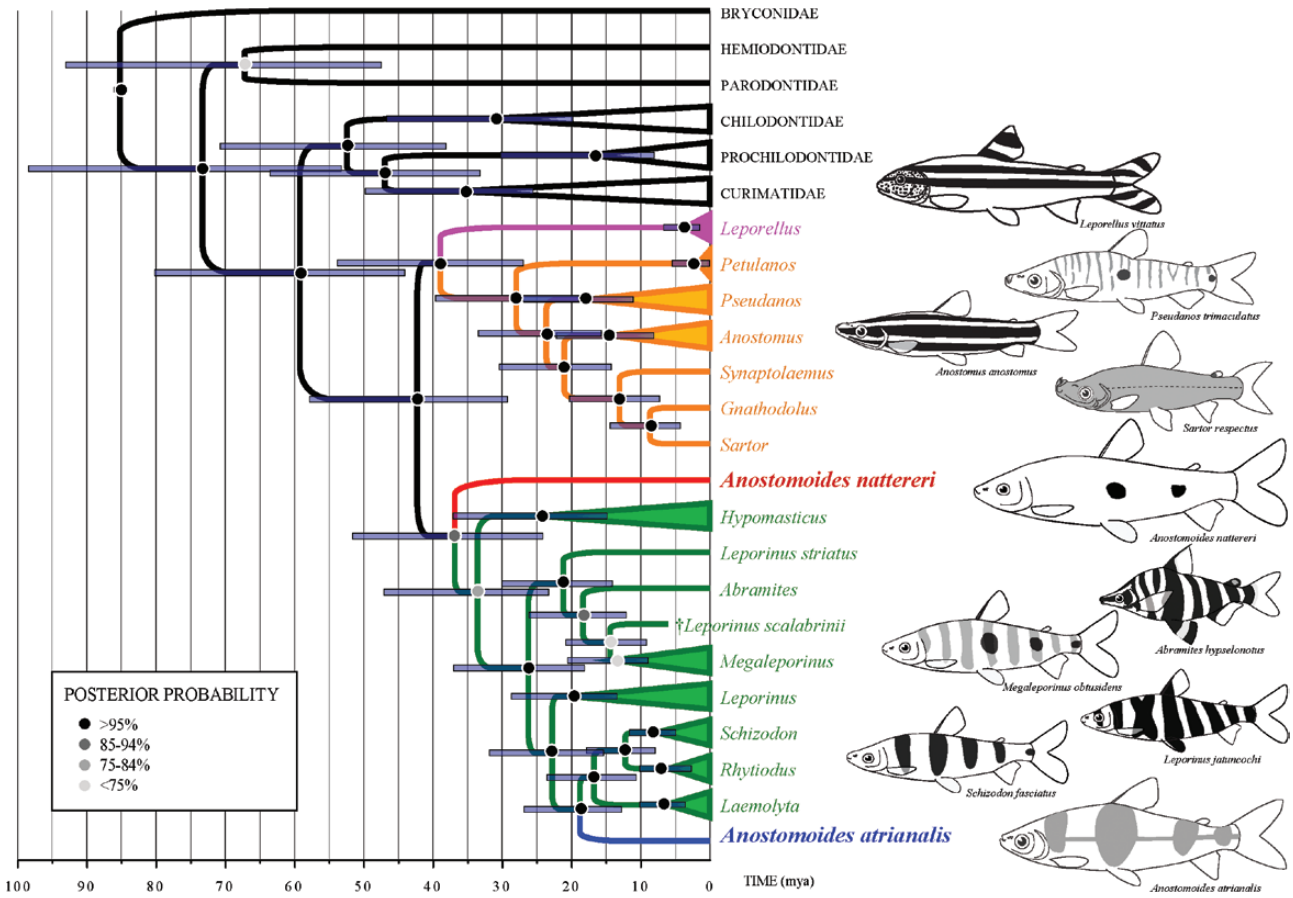

Figure 12. Summarized phylogenetic relationships of the Anostomidae and selected outgroup Characiformes, based on a node and tip calibrated Bayesian Inference analysis of combined data from morphology (158 characters) and six gene sequences (*COI*, *Cytb*, *Myh6*, *Rag1*, *Rag2*, 16S). See Supporting Information (Fig. S1) for the cladogram including the complete set of terminals.

66 (presence or absence of dermal papillae on the lips) and character 67 (presence or absence of a distinct process of the autopalatine). Each of these characters has a different distribution of tip states, and the two nominal species of *Anostomoides* differ in coding for all six. The AIC approach selected the equal rates (ER) model for characters 15, 19, 65, 66, 67 and the all rates different (ARD) model for character 52. In four cases the preference for the ER model over ARD was decisive. For character 52 (maxilla width), the AIC scores were 2.27 units apart, favouring ARD but with a barely significant p-value (0.039). For character 65 (relative position of the retroarticular), the AIC value for the ARD model was 1.3 units lower than for the ER, yielding a p-value (0.070) just short of significance at the $p < 0.05$ level). While we visualize reconstructions of the best-fitting model for all six characters, the reconstructions for characters 52 and 65 should be interpreted with the understanding that alternative models fit the data nearly as well.

The alternative placements of *Anostomoides nattereri* as sister to *Leporellus* plus the Anostominae or as sister to the rest of the family had negligible effects on all six character reconstructions. Inclusion vs. exclusion of *Anostomoides nattereri* affected substantially the reconstruction of the state of the MRCA of the Anostomidae for characters 65 and 67 (Figs 13, 14). For character 65, inclusion of *A. nattereri* increases the ambiguity in the ancestral states at most internal nodes and increases the likelihood that the most recent common ancestor of the Anostomidae possessed a laterally placed retroarticular (Fig. 13). For character 67 (autopalatine morphology), inclusion of that species also affected the reconstruction, as did recoding the outgroup taxa as possessing state 0 (process absent), rather than as possessing missing data (Fig. 14). The change in outgroup coding has the biggest effect, with the original coding yielding the inference that the MRCA of the Anostomidae most likely possessed a process of the autopalatine,

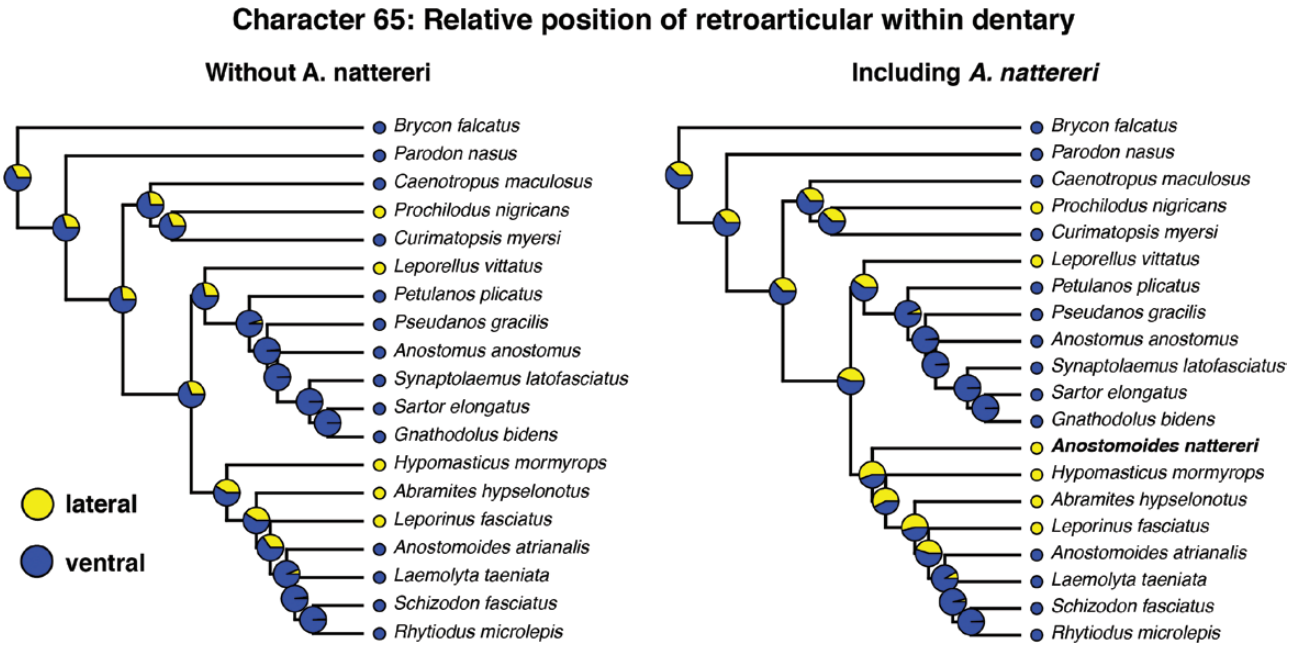

Figure 13. Maximum likelihood reconstructions of retroarticular placement performed on a pruned version of the maximum clade credibility tree with and without the inclusion of *Anostomoides naterreri*. Reconstructions used an equal rates transition model as selected using the Akaike information criterion.

and the analysis with recoded outgroups suggesting the opposite. However, in both cases, inclusion of *Anostomoides nattereri* in the analysis increases substantially the likelihood that the MRCA of the Anostomidae lacked a process on the palatine.

Reconstructions for the other four characters were robust to inclusion vs. exclusion of *Anostomoides nattereri*, and thus Figure 15 shows only a single reconstruction for each character on the pruned maximum clade credibility tree under its preferred model of character state change. Each of those characters shows a distinctive pattern of evolution, such as the apparently convergent evolution of lip papillae in *A. nattereri* and the lineage leading to the most recent common ancestor of *Gnathodolus*, *Sartor* and *Synaptolaemus*. Despite describing aspects of the morphology of the same bone, characters 15 and 19 show remarkably differed histories. Side-by-side comparison (Fig. 15) suggests that the similar mesethmoids possessed by *Anostomoides nattereri*, *Hypomasticus* and *Leporellus* result from a combination of plesiomorphy (the narrow width) and convergence (the hook in the anterior portion). It is also notable that character 15 represents a case in which likelihood-based reconstruction gives a more informative answer than parsimony. Maximum likelihood reconstructs the straight form of the mesethmoid as ancestral, with four separate transitions to the hooked form (all along long branches). Maximum parsimony admits that solution as one of two possible ones, with the other involving evolution of the hooked form in the common ancestor of the Anostomidae, Chilodontidae, Curimatidae and Prochilodontidae, followed by three separate reversions to the straight mesethmoid also seen in the distant outgroups Bryconidae and Parodontidae.

Justification for designation of a new genus

Overall, the molecular and morphological data separately and in combination indicate massive differences between *Anostomoides atrianalis* and *A. nattereri*. These two species differ for 24 (20%) of the 118 morphological characters that Sidlauskas & Vari (2008) identified as variable within the Anostomidae and differ by more than 16% at the *COI* molecular locus. Total evidence phylogenetic results demonstrate conclusively that *Anostomoides* as currently defined is polyphyletic, as do separate analyses of molecular and morphological data using varied analytical paradigms. Therefore, we restrict *Anostomoides* to a monotypic genus including only the type species *A. atrianalis* and allocate *A. nattereri* to the new genus described below.

TAXONOMY

INSPERANOS ASSEGA, SIDLAUSKAS & BIRINDELLI, **GEN. NOV.**

Type species: Leporinus nattereri Steindachner 1876

Zoobank registration: urn:lsid:zoobank.org:pub:A7A88AB9-DF88-49AE-8678-681A5F21CE27

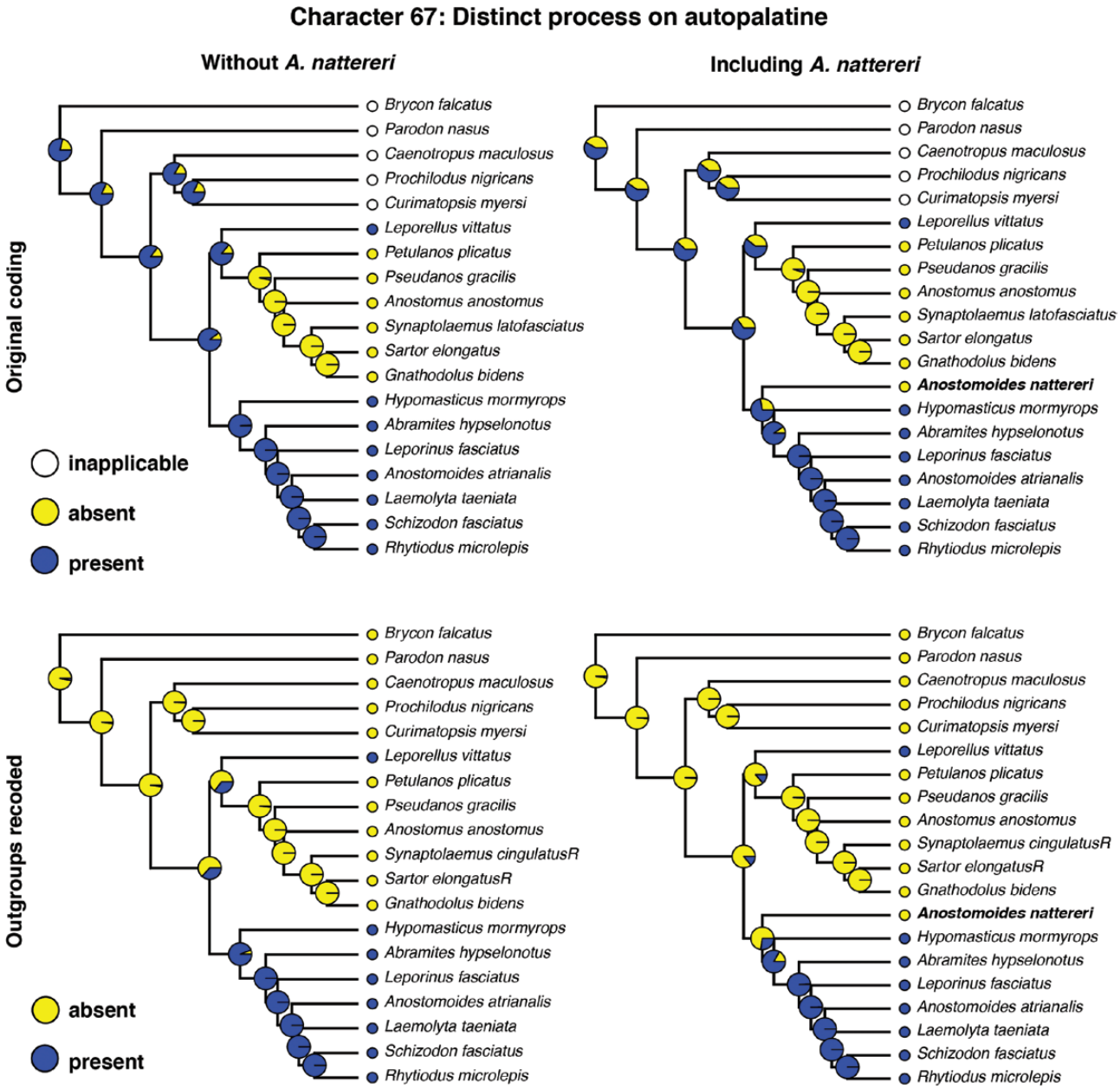

Figure 14. Maximum likelihood reconstructions of autopalatine evolution with and without the inclusion of *Anostomoides naterreri* and under alternative outgroup codings. Reconstructions were performed on a pruned version of the maximum clade credibility tree using equal transition rates between the character states as selected using the Akaike information criterion.

Diagnosis: *Insperanos* can be distinguished from all other members of the Anostomidae except for species of *Leporellus* and the subfamily Anostominae (*Anostomus*, *Gnathodolus*, *Petulanos*, *Pseudanos*, *Sartor* and *Synaptolaemus*) by lacking a laterally, ventrolaterally or anteroventrolaterally directed process of the autopalatine (vs. possessing such a process). *Insperanos* is diagnosed from *Leporellus* by having a slightly upturned mouth (vs. a subterminal or inferior mouth), scale-less caudal-fin rays (vs. squamation of the medial third of the caudal-fin rays) and a uniformly hyaline caudal fin (vs. a caudal fin with three to seven dark longitudinal stripes). *Insperanos* can be distinguished from all other anostomids except *Gnathodolus*, *Sartor* and *Synaptolaemus* by possessing abundant rounded papillae on the upper and lower lips (vs. lips smooth or with ridge-like papillae). It can be easily separated from those three genera, and from

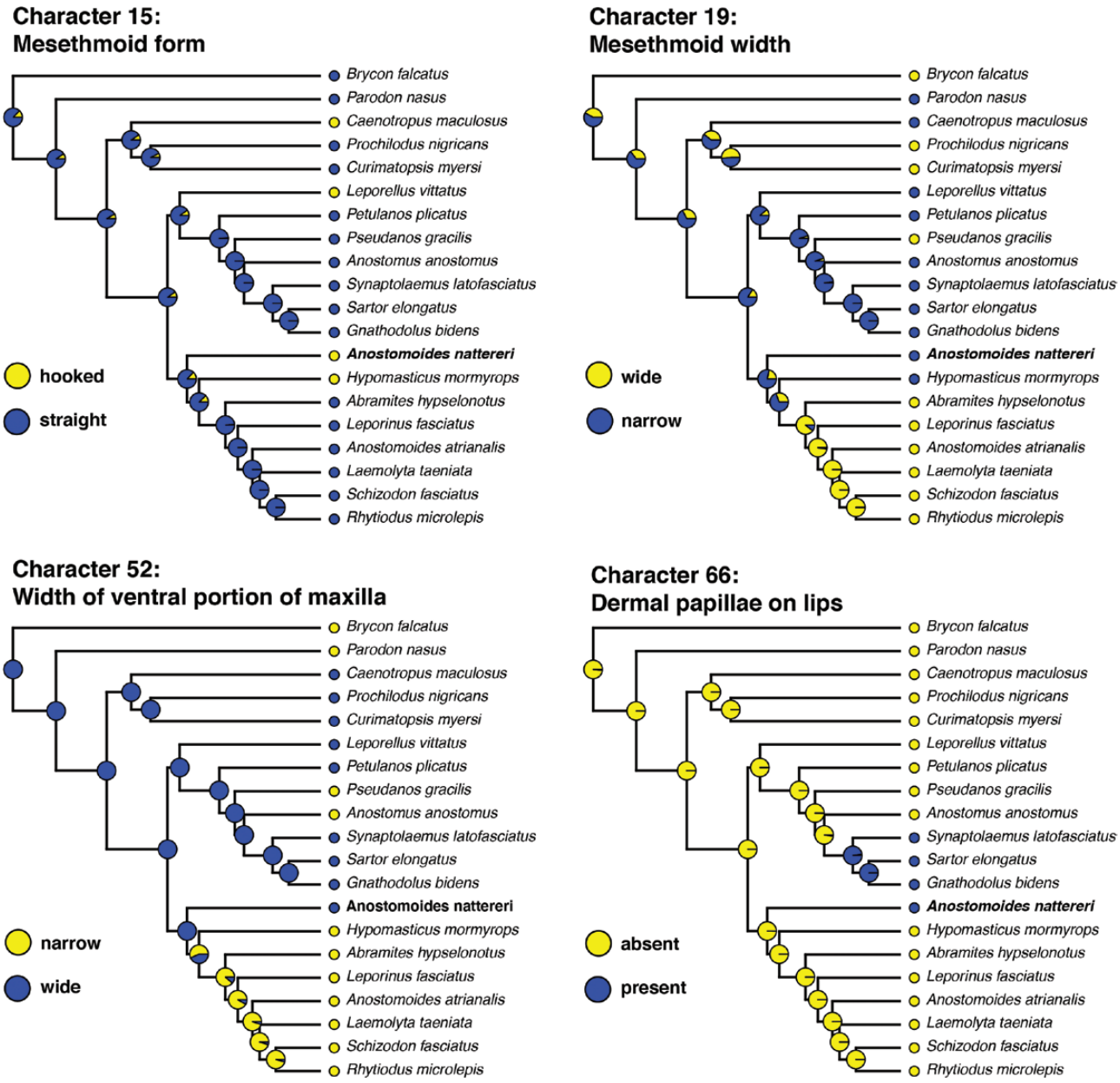

Figure 15. Maximum likelihood reconstructions of mesethmoid, maxilla and papilla evolution performed on a pruned version of the maximum clade credibility tree. Reconstructions for maxilla width (character 52) were conducted under an all-rates different transition model, while other reconstructions used an equal rates models of evolution. All models were selected using the Akaike information criterion.

Anostomus, *Petulanos* and *Pseudanos* by possession of a slightly upturned mouth in specimens larger than 100 mm SL (vs. a superior mouth in specimens of all sizes).

Insperanos can be distinguished externally from *Abramites* and *Megaleporinus* by having four teeth on the premaxillary and dentary bones (vs. three); from *Laemolyta* and *Schizodon* by having one or two cusps on the two medial premaxillary teeth (vs. premaxillary teeth with four or five cusps); from *Rhytiodus* by having a strongly compressed body (vs. an elongate fusiform body) and 37 to 39 lateral line scales (vs. 48 to 92); from *Hypomasticus* and *Leporinus* by having a slightly upturned mouth in specimens larger than 100 mm SL (vs. mouth terminal, subterminal or inferior in specimens larger than 100 mm SL) and from *Anostomoides* by having four branchiostegal rays (vs. three) and 37 to 39 lateral line scales (vs. 41 to 44).

Numerous internal features not listed in this diagnosis also separate *Insperanos* from *Anostomoides* (see section on *Notable morphological codings* above), and indeed, from all other members of the Anostomidae. Perhaps the best example is the presence of a well-developed, rod-like first basibranchial in *Insperanos* (vs. first basibranchial small and knob-like or absent in all other members of the Anostomidae).

Description: Assega & Birindelli (2019) provided an extended description of the external morphology of *Insperanos nattereri*, including body shape, pigmentation, morphometrics and counts of rays, scales and teeth. We refer to the reader to that publication for detail on those characteristics and focus herein on internal anatomy.

Osteology

Infraorbital bones and associated elements: As typical for members of the Anostomidae (Sidlauskas & Vari, 2008), infraorbital series composed of six primary bones plus associated nasal, antorbital and supraorbital (Fig. 3). Margins of all bones wavy or irregular. Depth of first infraborbital approximately twice length. Sensory canal of first infraorabital typically tripartite, with dorsal branch opening immediately anterior to antorbital, anterior branch directed towards snout and posteroventral branch connecting to canal system of second infraorbital. Overall orientation of canal system almost perfectly vertical, with dorsal opening and ventral opening aligned. One smaller specimen (MZUSP 5429) with anterior branch reduced to single intermediate pore at obtuse bend in canal. Additional intermediate pore sometimes presents along posteroventral branch, leading to additional anteriorly directed sensory canal running through soft tissue. Anterior of second infraorbital lateral to posterior portion of first infraorbital. Second infraorbital elongate, with irregular ventral lamina along mid to anterior margin, height of overall bone contained approximately 2.5 times in length. Sensory canal of second infraorbital curved and running dorsally along margin of contact with first infraorbital and then posteriorly along dorsal margin of second infraorbtial. One or two intermediate pores on sensory canal of second infraorbital, sometimes with single specimen dimorphic on contralateral sides. Area of contact between second and third infraorbitals narrow, just slightly greater than height of ossified tube of sensory canal. Third infraorbital elongate with maximum height contained three times in length. Anterior portion of sensory canal of third infraorbital incompletely ossified and open for about third of total length. One intermediate pore at posterior extent of canal, near connection to canal of fourth infraorbital. Third and fourth infraorbitals in close contact along straight margins. Fourth infraorbital deep, about twice as high as long. Canal system of fourth infraorbital tripartite or quadripartite with main canal running near anterior margin of bone and one or two accessory branches directed posteriorly towards preopercle. Fifth infraorbital similar in dorsoventral extent to fourth, dorsoventrally elongate, height approximately twice longest anteroposterior measurement and with bone narrowing dorsally to just slightly greater than width of ossified sensory canal. Sensory canal of fifth infraorbital straight and without intermediate pores. Sixth infraorbital ovoid with longest axis of oval 2.5 length of perpendicular axis. Canal system of sixth infraorbital forks at dorsal extreme with one branch directed anteriorly and the other directed dorsally in a morphology common to most members of the Anostomidae and indeed most characiforms (Sidlauskas & Vari, 2008: 88).

Antorbital composed of small ventral plate with thinner posteriodorsally ascending process, with bone overall forming ventral margin of nasal chamber. Nasal broad and plate-like, two median pores evenly spaced along length of single unbranched sensory canal. Supraorbital ovoid and flat, curved slightly ventrally along lateral margin to form part of border of orbit.

Suspensorium and jaws: Quadrate with dorsal, posterodorsal and posterior processes, plus prominent lateral shelf (Fig. 9). Triangular dorsal process of quadrate and smaller posterodorsal process frame large fenestra matching corresponding fenestra in anteroventral portion of metapterygoid. Condyle for articulation with articular at anteroventral limit of quadrate. Quadrate with prominent horizontal shelf of bone forming floor of adductor mandibulae chamber. Shelf begins at condyle with articular and continues posteriorly to vertical through anterior limit of hyomandibular. Shelf continues posteriorly from that point as part of preopercle. Anterodorsal region of quadrate forms long, straight margin of contact with ectopterygoid. Posterodorsal region of quadrate closely bound to entopterygoid and metapterygoid by narrow bands of cartilage. Entopterygoid situated posterior to ectopterygoid, dorsal to quadrate and anterior of metapterygoid, embracing cartilage with long medial portion projecting ventrally and partially overlapping medial face of quadrate and short lateral portion not reaching quadrate (Fig. 9A, B). Posterior half of entopterygoid medial to anterior region of metapterygoid (Fig. 9C). Ectopterygoid in shape of inverted L, lying along anterodorsal margin of quadrate. Ventral portion of ectopterygoid large and dorsal portion short. Dorsal portion cradling posteroventral surface of small ovoid autopalatine. Long axis of

autopalatine with anterolateral orientation, with no distinct process projecting from main body of bone in any direction (Figs 8A, B, 9B, C). Autopalatine articulates dorsolaterally with vomer, posteromedially with entopterygoid and ventrally with ectopterygoid.

Metapterygoid large, upper part inclined medially to form sloping shelf under orbit and nearly contacting wing of lateral ethmoid, anteroventral region with large invagination mirroring similar invagination on quadrate to form large fenestra, posteroventral region adjacent to symplectic and hyomandibular gently concave. Sympletic small, rod-like and located ventral to metapterygoid. Symplectic articulated anteriorly to medial face of quadrate and posteriorly to ventral corner of hyomandibular proximate to interhyal. Hyomandibular a large, vertically oriented and curved plate of bone lying medial to preopercle and opercle, thickened greatly at dorsal extreme forming articulation with ventral face of neurocranium. Hyomandibular articulating anteroventrally with metapterygoid and symplectic, ventrally with preopercle, dorsally with pterotic and sphenotic, and posteriorly with opercle.

Opercle large, sheet-like and roughly ovoid with slightly concave posterodorsal margin (nearly straight in cleared and stained specimen MZUSP 5429, but larger dry specimens with more pronounced concavity, e.g. MZUSP 110595). Lateral surface of opercle slightly convex. Medial surface with small anterodorsal ridge along which dilatator operculi muscle inserts extending posteriorly from articulation with hyomandibular. Anteroventral margin of opercle slightly concave at region of contact with interopercle. Interopercle anteroposteriorly elongate with rounded posterior margin and positioned medial to preopercle. Interopercle deepest posteriorly, tapering anteriorly in region where interopercular-mandibular ligament originates. Subopercle a narrow and flat bone closely associated with convex posteroventral margin of opercle and lying medial to that bone, and lateral to branchiostegal series. Preopercle a large bone with anterior and anterodorsal extensions and a prominent ascending arm. Preopercle with posterolateral ridge continuous with lateral shelf of quadrate. Anterior extension of preopercle passing ventral to lateral shelf of quadrate. Anterodorsal process of preopercle a thin rhomboidal sheet of bone lying ventral to symplectic and articulating with posterior process of quadrate. Ascending arm of preopercle lying immediately lateral to posterior margin of hyomandibular, lacking distinct triangular process overlapping joint between interhyal, hyomandibular, metapterygoid and symplectic in lateral view [see Sidlauskas & Vari (2008: fig. 44) for illustration of such a process in *Synaptolaemus latofasciatus* (Steindachner, 1910)]. Three tubular ossifications around sensory canal anterior to tip of anterior process of preopercle, and one such tubular ossification dorsal to ascending arm of preopercle. These tubular ossifications typically considered homologous with, and thus part of, preopercle (Vari, 1983).

Dentary large, triangular and thick, forming major part of lower jaw (Fig. 6A). Dentary bearing four robust teeth with symphyseal teeth largest and lateral smallest. Symphyseal tooth of dentary directed dorsally, with broad, rounded distal margin tapering slightly to a medial cusp. Each of three remaining teeth with a single prominent dorsal cusp, a concave dorsomedial margin and peg-like base. Third dentary tooth with well-developed dorsal lamina. Four replacement teeth developing freely in medial crypt ventral to functional teeth. Dentary articulating tightly with anguloarticular along sigmoid suture. Anguloarticular T-shaped, with anterior portion (angular) fitting into notch of dentary, and posterior portion (articular) consisting of thin ascending process lying lateral to posterodorsal flange of dentary and thicker ventral condyle with which quadrate articulates. Retroarticular a small, cup-shaped bone lying in recessed socket along ventrolateral face of dentary, forming anterior insertion point for interopercular-mandibular ligament. Meckel's cartilage small, T-shaped and located along medial surface of lower jaw dorsal to anguloarticular. Coronomeckelian bone small and rounded, located dorsally to Meckel's cartilage along medial face of dentary.

Maxilla L-shaped, dorsoventrally elongate, edentulate (Fig. 9A). Dorsal portion curved anteromedially to cradle posteroventral margin of premaxilla. Ventral extreme of maxilla attached by flexible ligaments to dorsolateral face of dentary [the paramaxilar preangular ligaments, following Datovo & Vari (2013)]. Widest dorsal portion of maxilla lying in transverse plane and widest ventral portion of maxilla lying in parasagittal plane, forming morphology termed 'torsion of the anterolateral flange of maxilla' by Sidlauskas & Vari (2008: 118, character 51). Supralabial ligament uniting maxilla and premaxilla and tendon of the pars endorictalis muscle insert on medial face of maxilla ventral to region of torsion in morphology typical for members of the Anostomidae exclusive of *Leporellus* (Sidlauskas & Vari, 2008: 117, character 49, therein termed primordial ligament).

Premaxilla triangular, formed by anterodorsal union of prominent lateral and medial sheets that partially enclose cavity in which replacement teeth develop (Fig. 4A, C, D). Cavity partially open on medial surface of premaxilla. Four thick, robust functional premaxillary teeth angled anteroventrally and decreasing gradually in size, with symphyseal tooth largest and lateral tooth smallest. Symphyseal tooth with broad, chisel-like cutting margins and scoop-like medial surface

(Fig. 4C). Symphyseal tooth with two similar-sized cusps (Fig. 4D) in small specimens (e.g. MZUSP 5429, 89 mm SL). Second and third teeth with a large median cusp on distal margin accompanied by smaller anteromedial and posterolateral cusps. Medial surface of second and third teeth with medial ridge (except in some large specimens prepared as dry skeletons, perhaps eroded due to wear). Fourth tooth with one median cusp or two indistinct cusps, and no medial ridge. Four replacement teeth insert freely in connective tissue within cavity of premaxilla. Premaxilla articulates posteriorly with mesethmoid.

Hyoid arch: Dorsal hypohyal compact and block-like, situated at anterodorsal extreme of hyoid arch and with cartilaginous dorsal margin (Fig. 11A, B). Ventral hypohyal roughly triangular, forming anterior margin of hyoid arch and articulating with dorsal hypohyal along angled suture. Anterior ceratohyal largest element of hyoid arch exclusive of branchiostegal rays, approximately rectangular with slight posteroventral expansion. Posterior ceratohyal small and rectangular, with dorsoventral axis approximately twice length of anteroposterior axis, and articulated to posterior margin of anterior ceratohyal. Small cartilaginous cap along ventral margin of posterior ceratohyal. Interhyal small and rod-like with cartilaginous dorsal cap, articulating ventrally with shallow pocket in dorsal margin of posterior ceratohyal, and dorsally on medial face of cartilaginous joint between hyomandibular and symplectic. Urohyal positioned along sagittal plane, prominent and roughly triangular with distinct posterior V-shaped notch (Fig. 11C). Dorsal branch of V longer than ventral. Small ventrolateral ridge on each side of urohyal.

Four branchiostegal rays, each slender and spathiform (Fig. 11A, B). Anterior three articulate with anterior ceratohyal, fourth with posterior ceratohyal. Anterior two rays nearly straight, posterior two distinctly curved, with posteriormost notably longer and more strongly curved than remaining three.

Branchial arches: Basihyal elongate, rod-like, with slight lateral expansion towards cartilaginous anterior extreme (Fig. 10B). Edentulous toothplate affixed to anterodorsal face. Basihyal articulates posteriorly with first of three basibranchials that lie along midline of body and join ventral extremes of contralateral branchial arches along with cartilaginous posterior copula. First basibranchial rod-like, slightly ventrally curved, posteriorly articulated to second basibranchial by triangular cartilage. Second and third basibranchials rod-like and thin with anterior lateral expansions providing attachment surfaces for cartilaginous connections to first and second hypobranchials. Posterior copula elongate, cartilaginous. Central section of posterior copula ovoid, situated medial to contralateral fourth ceratobranchials. Posterior portion of posterior copula rod-like, articulating medially with contralateral fifth ceratobranchials. Small rod-like anterior process of posterior copula articulates with third basibranchial.

Hypobranchials compact and irregularly shaped, each with cartilaginous articulations to two elements of basibranchial series medially, and to equivalently numbered ceratobranchial laterally (Fig. 10B). Thus, first hypobranchial attaches medially to first and second basibranchials and laterally to first ceratobranchial. Third hypobranchial with additional cartilaginous connection to cartilage joining second hypobranchial and second ceratobranchial. Ventral margin of third hypobranchial with hooked process passing ventral to third basibranchial and approaching matching process of contralateral third hypobranchial.

Ceratobranchials rod-like and elongate, articulating anteriorly with hypobranchials and/or with posterior copula and posterodorsally with epibranchial series (Fig. 10B). Series of minute gill rakers extend along anterior margins of all ceratobranchials and posterior margins of all but fifth. Gill rakers not attached directly to ceratobranchial and epibranchials, but floating in soft tissue immediately adjacent to bones. Dorsal surface of fifth ceratobranchial modified into flat plate, with two rows of teeth on dorsal surface. One specimen (MZUSP 5429) with only one row of teeth on left fifth ceratobranchial.

Epibranchials rod-like, articulating dorsomedially with pharyngobranchials and lateroventrally with ceratobranchial series (Fig. 10A). Minute gill rakers associated with both long margins of epibranchials as described for ceratobranchials above. Third and fourth epibranchials with well-developed dorsally directed uncinate processes causing bones to resemble the letter Y. Dorsal process of epibranchial three passes dorsal and medial to fourth pharyngobranchial demonstrating classic synapomorphic morphology for the Anostomidae (Vari, 1983: fig. 18). Fourth epibranchial articulated loosely to ventral-facing toothplate with two rows of teeth. Anterior row with four or five teeth, posterior row with six to eight. Accessory element of fourth ceratobranchial elongate, rod-like running parallel to fourth epibranchial.

First, second and third pharyngobranchials ossified; fourth pharyngobranchial mostly a cartilaginous plate but with small rod-like portion ossified along lateral margin of element (Fig. 10A). First pharyngobranchial rod-shaped, narrow, articulating ventrally with first epibrachial and dorsally with ventral face of neurocranium via small posterodorsal process. Second pharyngobranchial articulates anteriorly with first pharyngobranchial, anteromedially to second epibranchial and posteriorly with anterior margin of

third pharyngobranchial. Third pharyngobranchial articulates posterolaterally with third epibranchial and posteriorly with fourth pharyngobranchial. Second and third pharyngobranchials with dorsolateral processes ending in cartilaginous tips. Fourth pharyngobranchial articulates anteriorly with third pharyngobranchial, anterolaterally to third epibranchial, posteroventrally to fourth epibranchial and its associated toothplate.

Neurocranium: Neurocranium laterally compressed and narrow (Fig. 5) relative to condition in other anostomids [see also discussion of overall compressiform body plan in Assega & Birindelli (2019)]. Mesethmoid located at anterodorsal extreme of neurocranium, triangular in dorsal view and with prominent anteroventrally curving process along which contralateral premaxillae articulate (Fig. 6). Mesthmoid also articulates posteriorly with frontals and posteroventrally with vomer.

Vomer located at anteroventral extreme of neurocranium, with prominent rounded dorsal projection along sagittal plane, easily visible in lateral view, medial to lateral ethmoid. A prominent foramen present on each side of ventral face of vomer near midline. Vomer pentagonal in ventral view with two anterior projections with cartilaginous caps which articulate with contralateral autopalatines and plate-like ventral ridge along sagittal plane which articulates posteriorly with matching ridge of parasphenoid. Vomer also articulates posterolaterally with lateral ethmoid.

Lateral ethmoid with well-developed ventrolateral wings, posterior margin of which forms anterior wall of orbit; anterodorsal face of which forms the floor of nasal cavity. Additional thin plate forms posterior wall of nasal cavity. Lateral ethmoid-ectopterygoid ligament inserts on ventral surface of lateral ethmoid. No deep notch on anterior margin of lateral ethmoid or fenestra on anterodorsal face [see characters 25 and 26 of Sidlauskas & Vari (2008)]. No process of dorsal face of lateral ethmoid directed at posterolateral corner of mesthmoid [see character 27 of Sidlauskas & Vari (2008)]. Lateral ethmoid articulates anterodorsomedially with mesethmoid, anteriorly with vomer, posteromedialy with orbitosphenoid and posterodorsally with frontal.

Frontal largest element of neurocranium forming substantial portion of dorsal roof of neurocranium. Frontal rectangular, elongate along anteroposterior axis, and with irregular anterior margin lying dorsal to mesethmoid. Contralateral frontals separated by cranial fontanelle along most of length but connected by epiphyseal bar anterior to suture with parietal. On ventral surface of neurocranium, frontal articulates with orbitosphenoid and forms olfactory nerve foramen. Frontal also articulates ventrally with pterosphenoid, ventrolaterally with sphenotic and posterolaterally with pterotic.

Parasphenoid long and thin, forming portion of ventral margin of neurocranium. Prominent dorsolateral lateral processes on each side of parasphenoid articulate with prootics to form anterior margin of carotid foramen. Parasphenoid also articulates anteriorly with vomer and lateral ethmoid and posterodorsally with basioccipital. Additional pair of flat processes extend posteriorly from parasphenoid, ventral to basioccipital and running close to carotid artery.

Orbitosphenoid complex, lying medial to eyes and forming ventral floor of brain case. In lateral view, orbitospheniod forms obvious bridge of bone connecting lateral ethmoid to frontal. Posteroventral margin concave, with distinct ventral processes separating contralateral optic chambers. Orbitosphenoid articulates posteriodorsally with pterosphenoid along long, nearly straight suture.

Pterosphenoid forming substantial portion of ventral floor of braincase, roughly hexagonal in lateral view, laminar, thin and gently concave. Pterosphenoid articulates anteriorly with orbitosphenoid, dorsally with frontal, posterodorsally with sphenotic and posteroventrally with prootic.

Sphenotic situated at posterodorsal margin of orbit, with prominent ventrolateral laminar process forming border between orbit and dilatator operculi muscle fossa. Sixth infraorbital situated lateral to sphenotic, covering the dilatator operculi muscle fossa in lateral view. Sphenotic articulates anteroventromedially with pterosphenoid, posteroventrally with prootic, posteriorly with pterotic and dorsomedially with frontal.

Prootic with typical morphology for characiforms, closely approximating that in *Brycon* (Weitzman, 1962). Prootic situated at posterior of orbit immediately dorsal to inflection point of parasphenoid and forming part of floor of braincase. Well-developed ventromedial process of prootic forms lateral wall of posterior myodome, and medially directed shelf joins contralateral prootic to form dorsal wall of that cavity. Auditory, trigemino-facial and facial foramina visible in ventral view (Fig. 5B). Prootic articulates anterodorsomedially with pterosphenoid, anterodorsolateraly with sphenotic, posterodorsolateraly with pterotic, posterodorsally with exoccipital, posteroventrally with basioccipital and ventrally with parasphenoid.

Pterotic situated at posterodorsal corner of neurocranium. Well-developed ventrolateral spine-like process of pterotic forms posterior border of dilatator operculi muscle fossa, and anterior border of levator operculi muscle fossa. Ventral face of pterotic with recessed fossa into which dorsal condyle of hyomandibular inserts. Extrascapular rests against

posterodorsal margin of pterotic at suture with parietal. Pterotic forms lateral border of posttemporal fossa. Pterotic also articulates anterodorsally with frontal, posterodorsally with parietal, ventrally with prootic and posteroventrally with exoccipital and epoccipital.

Parietal approximally rectangular, situated along posteriodorsal surface of neurocranium, posterior to frontals and anterior of supraoccipital. Contralateral parietals separated medially by prominent cranial fontanel (Fig. 5A). Parietal articulates anteriorly with frontal, anterolaterally with pterotic, posterolaterally with epioccipital and posteriorly with supraoccipital.

Supraoccipital forms prominent crest at posterodorsal extreme of neurocranium. Supraoccipital anteriorly notched by posterior extent of cranial fontanelle at articulation with parietal. Anterolateral extreme of supraoccipital forms small portion of medial margin of posttemporal fossa. Supraoccipitial articulates posterolaterally with epiotic, ventrally with exoccipital, and posteriorly with neural complex of Weberian apparatus.

Epiotic T-shaped, situated on posterior surface of neurocranium to form dorsal face of posttemporal fossa. Well-developed process of epiotic runs from posterolateral margin of parietal near suture with pterotic posteroventrally towards exoccipital. That process thereby subdivides postemporal fossa immediately ventral to postemporal bone. Epiotic also articulates dorsomedially with supraocciptal, anterolaterally with pterotic and posteroventromedialy with exoccipital.

Intercalar a small L-shaped ossification positioned medial to prominent lateral process of pterotic, and most easily seen in ventral view. Intercalar articulates medially with prootic at extreme of small ridge, anteriorly and laterally with pterotic, and posteromedially with exoccipital.

Exoccipital situated along posteroventral surface of neurocranium, forming dorsal margin of lagenar capsule and part of attachment for vertebral column. Exoccipital pierced by several prominent foramina. Vagus foramen clearly visible in ventral view, lying anterolateral to lagenar capsule. Lateral occipital foramen located dorsal to lagenar capsule, clearly visible in posterior view. Ventral margin of exoccipital also forms dorsal margin of foramen magnum through which spinal cord passes, visible only when neurocranium is separated from vertebral column.

Basioccipital positioned near posteroventral extreme of neurocranium, ventral to exoccipital and forming ventral portion of lagenar capsule. Baudelot's ligament originates on ventromedial surface of basioccipital ventral to lagenar capsule. Small cartilaginous area visible along posteroventral margin of basioccipital in cs specimens. Basioccipital articulates anteriorly with prootic, dorsally with exoccipital and ventrally with paraphenoid.

Weberian apparatus: Weberian apparatus includes centra and associated elements of four anterior abdominal vertebrae (labelled centrum 1 through 4 in Figures 4 and 5B). Neural complex laminar and roughly triangular, projecting dorsally from vertebral column in sagittal plane. Dorsal margin of neural complex abuts ventral margin of supraoccipital crest, then runs posteroventrally. Ventral portion of neural complex with slight lateral expansion, anteroventral margin with small invagination creating fossa between neural complex and exoccipital. Small posterodorsal projection of neural complex joins neural arch and spine of fourth vertebrae to form small pocket in which anterior supraneural rests. Neural complex otherwise articulates anteroventrally with basioccipital and posteroventrally with neural arch pedicle and transverse process of third vertebra.

Claustrum small, rod-like and slightly curved, long axis of rod oriented along anteroposterior axis of fish. Claustrum positioned at junction between exoccipital and neural complex, posteroventral to fenestra formed by invagination in anteroventral margin of neural complex. Claustrum closely associated with posterodorsal surface of scaphium.

Scaphium small and shell-shaped, with curved anterior margin fitting into pocket of exoccipital, thin posterodorsal process passing lateral to neural complex and pin-like process ventrally articulated with first centrum. Scaphium articulates anteriorly with exoccipital, posterodorsally with neural complex and posteroventrally with neural arch of third vertebra.

Intercalarium small and L-shaped, positioned in pocket along dorsolateral margin of second vertebra posteroventral to scaphium and posterodorsal to lateral process of second vertebral centrum. Intercalarium articulates with scaphium via small anterolateral process (manubrium intercalarii) and posteroventrally with tripus by means of strong fibrous ligament. Posterodorsally, intercalarium articulates with anteroventral margin of neural arch of third vertebra.

Tripus roughly triangular, with posterior point of tripus elongate and gracile, passing ventral to fourth rib and curving medially to form hooked projection that articulates with os suspensorium via connective tissue. Anteriorly tripus expands laterally to parallel lateral process of second vertebral central and connects to intercalarium via ligamentous connection. Large triangular pocket on dorsolateral surface of tripus lies lateral to third vertebral centrum.

First centrum anteroposteriorly abbreviated relative to other three Weberian centra. First centrum with deep, narrow pit on either side of dorsal margin, into which ventral process of scaphium fits. Dorsal margin

of second centrum shorter than ventral margin along anteroposterior axis. Elongate contralateral processes extend anterolaterally from anteroventral margin of second centrum. Third centrum slightly larger than second. Third centrum with prominent anterolateral process extending from dorsolateral margin ventral to the plate-like and broad third neural arch, which articulates posteriorly with neural arch of fourth vertebra along long angled suture. Third neural arch with a small anterodorsally directed process, which runs lateral to ventral portion of neural complex and creates sigmoid suture in larger specimens. Fourth centrum largest within Weberian apparatus, bearing broad neural arch and posterodorsally directed neural spine. Anterior supraneural fits into pocket on anterodorsal margin of neural spine of fourth vertebra.

Fourth rib robust, triangular and projecting laterally from ventrolateral margin of fourth vertebral centrum. Fourth rib curves ventrally after passing lateral to posterior process of tripus.

Os supensorium arising from ventral margin of fourth rib and then curving medially to connect to contralateral partner via thin band of connective tissue along sagittal plane. Hooked posterior process of tripus connects to posterior margin of os suspensorium via fan-like sheet of connective tissue.

Six supraneurals lie along dorsal midline, each closely associated with anterodorsal margin of neural spine of fourth to ninth vertebrae. Each supraneural a dorsoventrally elongate rod that expands dorsally into laminar plate in sagittal plane. Ventral tip of supraneural with cartilaginous cap. Anterior (first) supraneural shortest and displaced ventrally relative to other five. Anterior supraneural closely associated with Weberian apparatus, with ventral extreme inserting into pocket between contralateral faces of neural spine of fourth vertebra immediately posterior to articulation of neural complex with neural spine of fourth vertebral centrum. Second supraneural with small anterior projection. Sixth supraneural with most attenuate dorsal lamina.

Pectoral girdle : Extrascapular small and roughly ovoid, with irregular anterodorsal margin (Fig. 16A). Extrascapular rests lateral to posttemporal fossa formed by epioccipital and posteroventral process of pterotic. Extrascapular articulates medially and posteroventrally with postemporal. Quadripartite sensory canal of extrascapular approximates shape of angled letter H. Dorsal branch confluent with sensory canal of parietal. Ventral branch leads to sensory canal of posttemporal. Anterior branch opens medially to connect with sensory canal system of pterotic. Posterior branch leads to soft tissue posterior to posttemporal.

Posttemporal laminar with two spine-like processes. Anterodorsomedial process of postemporal slightly curved and passing lateral to horizontal process of epiotic that subdivides posttemporal fossa. Tip of anterodorsomedial process of posttemporal rests in small cavity on posterior surface of parietal. Medial process of postemporal smaller, finger-like, and articulating with tip of posteroventral process of pterotic. Ventral margin of posttemporal with dorsoventrally oriented sensory canal confluent with ventral branch of sensory canal of extrascapular and with sensory canal of supracleithrum.

Supracleithrum laminar and dorsoventrally elongate, posterior margin convex and following curve of opercle, to which supracleithrum lies medial. Sensory canal of supracleithrum connects with canal of postemporal on lateral face of dorsal extreme of supracleithrum. Canal exits supracleithrum on lateral surface of bone near posterior margin at horizontal line through dorsal tip of cleithrum. Canal continues posterior from that point to form externally visible lateral line.

Cleithrum large and triangular, with long tapering dorsal process and medially directed lamina that forms posterior wall of branchial chamber. Cleithrum situated posteromedially to opercle. Dorsal portion of cleithrum lies medial to supracleithrum. Cleithum articulates posteriorly with postcleithra one and two, which lie immediately medially. Mesocoracoid articulates along medial extreme of medial lamina of cleithrum (Fig. 16B, C). Scapula and coracoid articulate along ventromedial surface of cleithrum, with coracoid lying anterior to scapula.

Coracoid roughly triangular with large central foramen. Lamina of coracoid dorsal to central foramen articulates with medial surface of cleithrum along extensive suture oriented in anterolateral direction. Lamina of coracoid ventral to central foramen highly fenestrated and articulating along medial surface of cleithrum at anteroventral extreme. Prominent dorsomedial process of coracoid articulates with mesocoracoid and scapula along Y-shaped suture. Posteroventrally, coracoid articulates with ventralmost proximal radial.

Mesocoracoid columnar, forming a dorsoventrally oriented strut on medial side of pectoral girdle, bridging ventromedial face of cleithrum to scapula and coracoid. Dorsal portion of mesocoracoid expanded into a broad triangular lamina tightly bound to cleithrum. Ventral portion of mesocoracoid expands in anteroposterior axis to form dorsal portion of Y-shaped suture with scapula along ventromedial margin and cleithrum along dorsomedial margin.

Scapula columnar and situated ventromedially within pectoral girdle. Dorsal portion of scapula expands to articulate with medial surface of cleithrum along anteroposteriorly elongate suture. Posteroventral margin of scapula provides attachment surface for

three proximal radials of pectoral fin. Ventromedial margin of scapula contacts mesocoracoid dorsally and coracoid ventrally. Scapular foramen prominent and circular, circumscribed by anterodorsal margin of scapula and posterior margin of dorsal lamina of coracoid.

Four proximal radials present. Dorsalmost proximal radial narrow anteriorly and expanded posteriorly to form separate articular facets with three distal radials in morphology similar to that described for *Brycon* (Weitzman, 1962). Remaining three proximal radials elongate, rod-like bones with cartilaginous caps, each articulating with one distal radial. Dorsalmost four distal radials ossified and ventralmost two entirely cartilaginous in examined specimens (Fig. 16C), similar to condition of 'four distal radials partially ossified distally' reported for *Moenkhausia lepidura* (Kner, 1858) (Darlim & Marinho, 2018). Pectoral fin with one unbranched ray and fifteen or sixteen branched rays.

Three postcleithra present along posteromedial margin of pectoral girdle. First postcleithrum dorsalmost, small and ovoid, located medial to ventral extreme of supracleithrum and posterior to ascending arm of cleithrum. Second postcleithrum largest, forming broad lamina located medial to posteroventral margin of cleithrum in parasagittal plane. Second postcleithrum wider at ventral limit than at dorsal limit, and with thicker anteroventral margin along and dorsal to region of contact with third postcleithrum. Third postcleithrum an elongate rod-like element oriented along dorsoventral axis of fish. Third postcleithrum articulates dorsally with second postcleithrum and passes medially by base of pectoral-fin rays.

Pelvic girdle: Pelvic bone (basipterygium) elongate, paralleling its counterpart. Anterior portion of pelvic bone trough-like and triangular, tapering to anterior point. Middle portion of pelvic bone joins mirrored contralateral element along L-shaped suture. Prominent ischial process extends posterolaterally from central suture, forming forked morphology with contralateral process (Fig. 17).

Pelvic fin possesses one unbranched ray, eight branched rays and supporting elements (radials). Radial closest to midline of the fish largest, ossified and L shaped, resembling ischial process in morphology and orientation, although smaller in size. Lateral radial small and cartilaginous, inset between base of unbranched ray and first branched ray. Three additional radials inset between third and seventh branched rays, as typical for the Characiformes (Weitzman, 1962).

Dorsal fin: Two unbranched and ten branched rays, plus tiny unbranched rudiment anterior to base of first unbranched ray and not typically included in meristic counts (Fig. 19). Anterior unbranched ray approximately half the length of posterior.

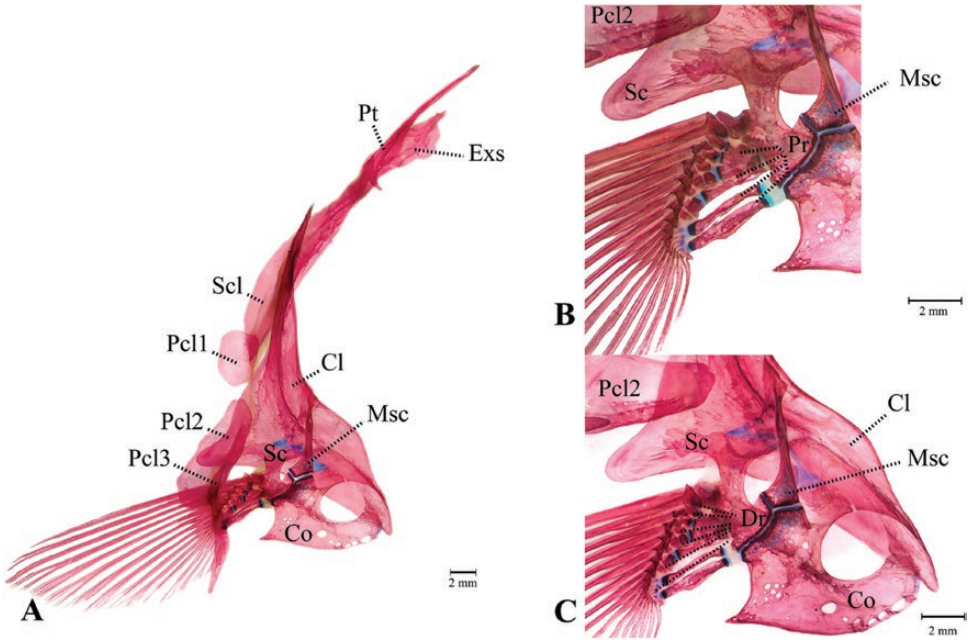

Figure 16. Pectoral fin of *Anostomoides nattereri*, MZUSP 5429, 138.7 mm SL, in lateral view (A) and in detail in medial view (B, C). Co: coracoid, Cl: cleithrum, Dr: distal radial, Exs: extrascapular, Msc: mesocoracoid, Pcl 1-3: postcleithra 1-3, Pr: proximal radials, Pt: posttemporal, Scl: supracleithrum.

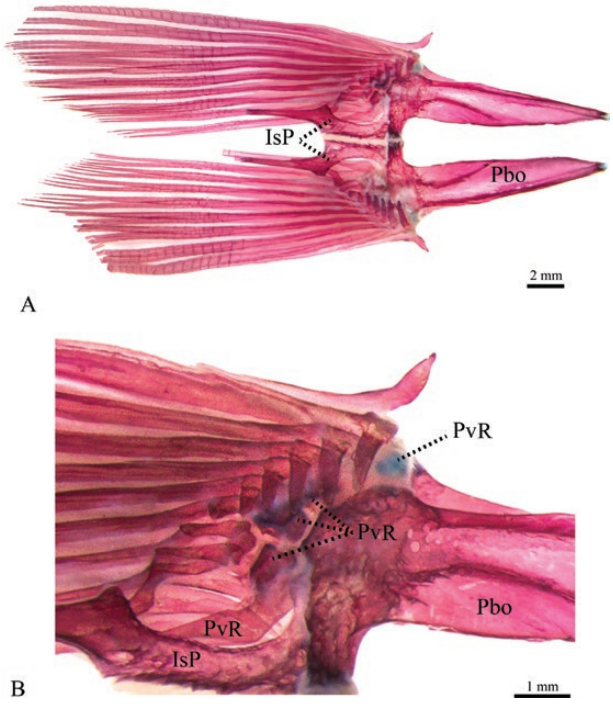

Figure 17. Pelvic fin of *Insperanos nattereri*, MZUSP 5429, 138.7 mm SL. IsP: isquiatic process, Pbo: pelvic bone, PvR: pelvic-fin radials.

Posterior three branched rays substantially shorter than those anterior, with posterior one divided to its base. Eleven pterygiophores present. Anterior pterygiophore largest, situated between the neural spines of vertebrae eight and nine, and supporting two unbranched dorsal-fin rays plus anterior rudiment. Remaining pterygiophores each support one branched dorsal-fin ray.

Anterior three pterygiophores divided into larger proximal (ventral) and smaller distal (dorsal) radials. Remaining eight pterygiophores divided into proximal, medial and radials, with medial radial of fourth pterygiophore partially fused to proximal radial. Posterior to last proximal pterygiophore, hook-shaped cartilage with ossified dorsal portion present [the end piece or dorsal fin stay of Weitzman (1962)].

Anal fin: Two unbranched and eight branched anal-fin rays, plus two tiny anterior unbranched rudiments not typically included in meristic counts (Fig. 18). Anterior branched ray about half length of posterior. Posterior branched ray much shorter than others and divided to its base. Anterior (first) pterygiophore largest, with plate-like morphology ventrally and positioned between haemal spines of vertebrae 23–24. First pterygiophore supports unbranched rays and both

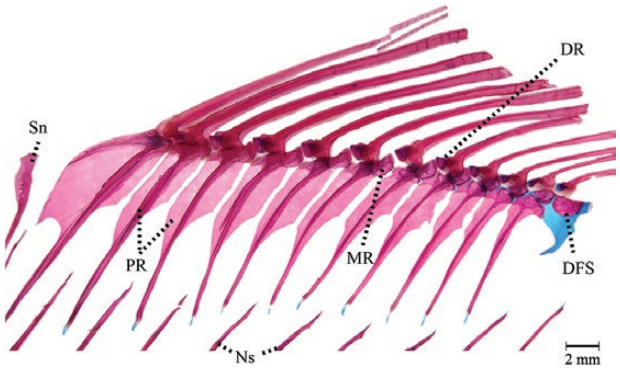

Figure 18. Dorsal fin of *Insperanos nattereri*, MZUSP 5429, 138.7 mm SL. DFS: dorsal fin stay, DR: distal radial, MR: medial radial, Ns: neural spine, PR: proximal radial, Sn: supraneural.

anterior rudiments. Eight posterior pterygiophores each support one branched anal-fin ray.

First to fourth pterygiophores divided into proximal (dorsal) and distal (ventral) radials. Remaining pterygiophores also include medial element. Hook-shaped cartilaginous end-piece (stay) with ossified ventral portion present posterior to ninth pterygiophore.

Caudal skeleton: Elements of caudal skeleton include one parhypural, six hypurals, three epurals, a paired unfused uroneural, a pleurostyle and a compound centrum formed by the first preural plus the first ural (Fig. 20). Ventral portion of hypural plate includes parhypural and first and second hypurals, with parhypural and second hypural fused to terminal compound centrum of vertebral column. First hypural large, separated from compound centrum by gap, with distal tip cartilaginous. Second hypural rod-like with distal tip cartilaginous. Ventral lobe of caudal fin with nine principal caudal fin-rays and five procurrent rays. First and second hypurals and parhypural support ventral principal rays and tips of haemal spines of second and third pre-ural centra support ventral procurrent rays. Dorsal and ventral lobes of caudal fin separated by diastema.

Dorsal portion of hypural plate includes four hypurals, of which ventral (third hypural) largest and dorsal (sixth hypural) smallest, scarcely visible medial to base of principal caudal-fin rays. Third hypural with proximal tip small, contacting compound centrum; with distal margin large and cartilaginous. Fourth, fifth and sixth hypurals smaller, separated from compound centrum by gap and with cartilaginous distal tips. Anterior portion of divided uroneural substantially larger and contacting urostyle. Posterior uroneural thin and rod-like, positioned between

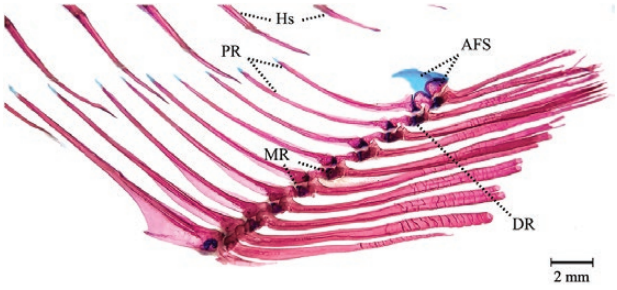

Figure 19. Anal fin of *Insperanos nattereri*, MZUSP 5429, 138.7 mm SL. AFS: anal fin stay, DR: distal radial, Hs: haemal spine, MR: medial radial, PR: proximal radial.

anterior uroneural and opisthural cartilage, which caps posterior tip of notochord. Three epurals present dorsal to uroneurals and posterodorsal to modified, plate-like neural spine of terminal compound centrum. Dorsal lobe of caudal fin with ten principal caudal-fin rays and six procurrent rays. Third through sixth hypurals support principal rays of dorsal lobe of caudal fin, and distal tips of epurals, uroneural and neural spine of pre-ural centrum two support dorsal procurrent rays.

Distribution

Insperanos nattereri occurs throughout the Orinoco and Amazon basins, including the Araguaia, Negro, Tapajós, Tocantins and Xingú rivers in Brazil and possibly Bolivia and Colombia [see more details in Assega & Birindelli (2019)].

Etymology

Insperanos from the Latin *īnspērāns*, unexpected, alluding to the surprising discovery of an ancient lineage of Anostomidae represented today by *I. nattereri*, plus the four first letters of *Anostomus*, in reference to the type genus of the family, following the practice of previous authors who described genera in the Anostomidae (e.g. *Pseudanos* Winterbottom, 1980; *Petulanos* Sidlauskas & Vari, 2008).

DISCUSSION

Polyphyly of *Anostomoides*

Given that *Insperanos nattereri* and *Anostomoides atrianalis* have been known to science for more than a century, it seems remarkable that previous studies overlooked their extensive osteological and genetic differences and considered them to be congeners until the lack of an exclusive synapomorphy led Assega & Birindelli (2019) to doubt the monophyly

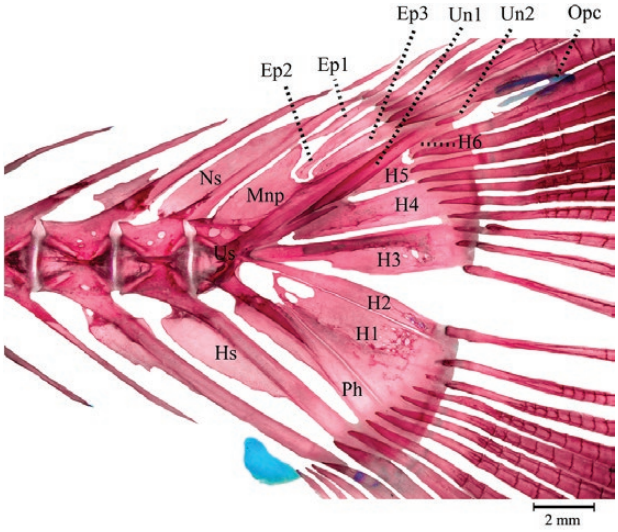

Figure 20. Caudal fin of *Insperanos nattereri*, MZUSP 5429, 138.7 mm SL. Ep1–3: epural s1–3; H1-6: hipurals 1–6; Hs: haemal spine; Mnp: modified neural process, Ns: neural spine, Opc: opisthural cartilage, Ph: parhypural, Un1–2: uroneurals 1–2, Us: urostyle.

of *Anostomoides*. The source of the error likely lies in over-reliance on external characters such as tooth morphology and mouth position in framing genus-level diagnoses, as such characters relate to dietary niche and are thus prone to convergence. For example, Kolmann *et al.* (2020) recently demonstrated polyphyly of several serrasalmid genera traditionally united by tooth morphology, and many studies have documented convergence of mouth shape, oral dentition and pharyngeal dentition among disparate non-characiform taxa such as cichlids (Ruber & Adams, 2001; Hulsey *et al.*, 2008), cyprinids (Qi *et al.*, 2012) and terapontoids (Davis & Betancur-R, 2017).

Among anostomids, molecular (Ramirez *et al.*, 2017) and morphological (Sidlauskas & Vari, 2008) phylogenetic investigation has revealed several instances of morphological convergence in mouth morphology. For example, molecular results (Ramirez *et al.*, 2017) indicate that strongly upturned mouths in adult individuals have clearly evolved at least twice (in *Laemolyta* and the subfamily Anostominae), despite the close relationship between those taxa hypothesized by Sidlauskas & Vari (2008) on osteological grounds. The Ramirez *et al.* (2017) phylogeny also recovered examples of closely related species with different mouth orientations [e.g. *Megaleporinus garmani* (Borodin, 1929) and *M. reinhardti* (Lütken, 1875), with downturned and terminal mouths, respectively] and others with similar mouth orientation but distant phylogenetic position [e.g. *Hypomasticus mormyrops* (Steindachner, 1875) and *H. pachycheilus* (Britski,

1976), both with strongly inferior mouths]. Sidlauskas & Vari (2008) also reconstructed and discussed convergent evolution of an inferior mouth in *Schizodon nasutus* and *Hypomasticus*. These results clearly indicate that trophically-relevant similarity poorly reflects the degree of shared evolutionary history within the Anostomidae.

Anostomoides, like many characiform genera, was until recently diagnosed primarily by trophically-relevant characteristics. That diagnosis included an upturned or slightly upturned mouth, unicuspid or bicuspid sympheseal premaxillary teeth (character 32 of Sidlauskas & Vari, 2008) and compressed symphyseal dentary teeth without posterior laminae [character 38 of Sidlauskas & Vari (2008), see also Santos & Zuanon (2006); Assega & Birindelli (2019)], and no other members of the Anostomidae share the combination of tooth character states present in these two species. Although bicuspid premaxillary teeth are somewhat rare in the Anostomidae (Sidlauskas & Vari, 2008: 103; Birindelli *et al.*, 2013), that condition can be observed in small specimens of *Insperanos nattereri* (around 100 mm SL; Fig. 6D), and in *Anostomoides atrianalis* individuals of all sizes (Assega & Birindelli, 2019: fig. 3). The dentary sympheseal tooth is perhaps the most strikingly similar and convergent feature present in *Insperanos nattereri* and *Anostomoides atrianalis*. That tooth is large, compressed anteroposteriorly and bears no posterior lamina (Fig. 6C, D).

Some differences in tooth and mouth morphology do exist between these species. For example, the symphyseal premaxillary tooth becomes unicuspid in *Insperanos nattereri* specimens larger than 200 mm SL (Fig. 6C), while adult specimens of *Anostomoides atrianalis* retain a bicuspid morphology. Whereas the mouth of *A. atrianalis* is notably upturned and approaches the condition in *Laemolyta* and most members of *Schizodon*, the mouth of *Insperanos* is only slightly upturned, a condition more similar to some species of *Leporinus*. Even so, these differences are well within the scope of the variation observed among species in other anostomid genera.

Considered alone, these tooth and mouth characteristics give no indication of the remarkable differences hidden beneath the skin or encoded within the mitochondrion. These two species differ for 24 of the 118 (20%) morphological characters that Sidlauskas & Vari (2008) identified as variable within the Anostomidae and by more than 16% at the *COI* molecular locus. That molecular difference far exceeds the divergence typical of other congeneric anostomid species. For example, congeneric specimens of *Laemolyta*, *Leporellus*, *Leporinus* and *Schizodon* studied herein all differ by less than 10% at *COI*. Although in retrospect the historical reasons for grouping these two species seem clear, the total evidence analysis of molecules and morphology, as well as separate analyses of those data sets leave no doubt about the polyphyly of *Anostomoides* as defined by Santos & Zuanon (2006) and Assega & Birindelli (2019).

On the importance of osteology in characiform taxonomy

The surprising discovery of the polyphyly of *Anostomoides* demonstrates the importance of examining internal and external morphology when describing a species, and also of combining molecular and morphological data when investigating phylogenetic relationships. Some other genera of the Anostomidae were defined and diagnosed based almost exclusively on mouth orientation and teeth morphology (Myers, 1950; Géry, 1977) as is the case for genera of other freshwater fish families. Perhaps the best example is the megadiverse Characidae, within which Eigenmann (1917, 1918, 1921, 1927) diagnosed many genera (e.g. *Hyphessobrycon* Durbin, 1908) based on a combination of features that have been since proven to be highly homoplastic (Weitzman & Palmer, 1997; Oliveira *et al.*, 2011; Mirande, 2018). Combined analysis of morphological and molecular data provides the best way to recognize such homoplasies, to identify strongly supported clades and diagnose them with morphological characters [see Arce *et al.* (2016), Mirande (2018), Calegari *et al.* (2019) for excellent examples]. Researchers should also make such molecular and morphological data available freely so that future researchers can augment and re-analyse the data sets. Such an approach facilitates future studies and allows the field to advance more swiftly towards a comprehensive classification of ichthyological diversity.

Phylogenetic position of *Insperanos*

Our phylogenetic results (Fig. 12) corroborate previous hypotheses that placed *Anostomoides atrianalis* close to *Laemolyta*, *Rhytiodus* and *Schizodon* (Sidlauskas & Vari, 2008; Burns & Sidlauskas, 2019), while generally confirming Betancur-R *et al.*'s (2018) unexpected placement of *Insperanos nattereri* as sister to a large clade containing *Abramites*, *Leporinus*, *Schizodon* and other related genera. The expanded taxon sampling and dated total evidence approach herein refines Betancur-R *et al.*'s (2018) result to reveal that *I. nattereri* is the sole surviving representative of an ancient lineage that diverged from all other Anostomidae approximately 37 Mya.

Although the ancient origins of *Insperanos* are clear, its exact phylogenetic placement is not. Our maximum clade credibility tree places the taxon as sister to a

clade containing the majority of the other anostomid genera (*Abramites*, *Anostomoides*, *Hypomasticus*, *Megaleporinus*, *Laemolyta*, *Leporinus*, *Rhytiodus* and *Schizodon*). Nevertheless, the statistical support for that clade is weak (86% posterior probability; Fig. 12). Two other positions for *Insperanos* receive moderate support in the posterior distribution of possible phylogenies. About 10% of those trees place *Insperanos* as sister to a clade containing *Leporellus* and the anostomine genera (*Anostomus*, *Gnathodolus*, *Petulanos*, *Pseudanos*, *Sartor* and *Synaptolaemus*), and 3.5% of the posterior trees suggest provocatively that *Insperanos* might be the sister to a clade containing all of the other living species in the family. Thus, the exact pattern of relationship among the earliest diverging lineages within the Anostomidae is an open question that begs further investigation.

It is important to acknowledge that the low support for the phylogenetic placement of *Insperanos* stems at least in part from the fact that all three available tissues from this genus amplified only for the *COI* locus (see *Results* for more details). A richer molecular data set with more complete data for *Insperanos* and denser taxon sampling throughout the tree will likely help to refine future reconstructions. However, the phylogenomic data set of approximately 280 000 base pairs (Betancur-R *et al.*, 2018) places *Insperanos* in an identical position, albeit in a phylogeny containing only sixteen anostomid species and with a bootstrap value below 50%. The low support value in the Betancur-R *et al.* (2018) phylogeny and the presence of several possible placements in the Bayesian posterior recovered herein suggest that the long branch and early divergence of *Insperanos* may present a difficult inferential challenge for any study attempting to pinpoint its exact relationships, even with access to an extensive molecular data set.

Nevertheless, all analyses (including parsimony analysis of the rich morphological data set alone, see Supporting Information) reconstruct *Insperanos* as one of the earliest diverging anostomid genera. That concordance illustrates that the most important conclusion from the total evidence analysis is not an artefact of missing molecular data. Similarly, the unique combination of ancestral and derived morphological characteristics of *Insperanos* (Figs 13–15) render it difficult to pinpoint its exact relationships with other anostomids on morphological grounds. No matter which of the possible placements of *Insperanos* is correct, the four major anostomid lineages diverged rapidly during the first few million years of the evolution of the family, leaving little time to accumulate morphological or molecular changes on the internodes separating the first split from the second and third. An expanded total evidence approach may provide the best chance to resolve those crucial early divergences separating *Insperanos* from the lineages leading to *Leporellus*, the Anostominae and the remainder of the family.

Evolutionary implications of *Insperanos*' morphology

As *Insperanos* diverged from all other anostomids early in the evolutionary history of the family, it likely shares some morphological features with the most recent common ancestor of the Anostomidae. However, the species has been evolving for as long as any other living anostomid species, and its long subtending branch means that it has had ample time to evolve autapomorphies or to converge on morphologies that also arose elsewhere within the Anostomidae. In such cases, ancestral state reconstruction can help reveal which morphologies of a species are primitive and which are derived. Such analysis reveals that *Insperanos* shares numerous morphologies with *Leporellus* and various non-anostomid species. Many such characteristics were likely also possessed by the most recent common ancestor of the Anostomidae, such as the narrow mesethmoid (character 19, Fig. 15), the wide ventral portion of the maxilla (character 52, Fig. 15), the narrow form of the mesethmoid (character 19, Fig. 15) and others not formally illustrated herein. In the case of the large first basibranchial, *Insperanos* possesses a primitive morphology shared only with outgroup taxa like *Brycon*, *Caenotropus* Günther, 1864 and *Chilodus* J. P. Müller & Troschel, 1844 (Sidlauskas & Vari, 2008: 139), which provides a tantalizing piece of evidence that might support an eventual placement of the genus as sister to all other anostomids, even though that placement currently appears in fewer than 4% of the posterior distribution of trees. The prevalence of such primitive morphologies certainly corroborates an early divergence for the genus, or perhaps more accurately, supports exclusion of *Insperanos* from anostomid clades supported by numerous derived characteristics, such the subfamily Anostominae, or the clade formed by *Anostomoides*, *Laemolyta*, *Rhytiodus* and *Schizodon*.

At the same time, it is important to recognize that *Insperanos* itself is not inherently primitive, even if it possesses numerous character states also possessed by ancestral anostomids. Some of the morphologies that *Insperanos* shares with *Leporellus*, *Hypomasticus* and other early diverging lineages, appear to be derived homoplasies, such as the hooked form of the mesethmoid (character 15, Fig. 15). Similarly, we reconstruct the shared presence of rounded dermal papillae on the lips (character 66, Fig. 15) as evolving independently in *Insperanos* and on the lineage leading to the small clade containing the anostomine genera *Gnathodolus*, *Sartor* and *Synaptolaemus* for which such papillae have been long

considered diagnostic (Myers & Carvalho, 1959) or synapomorphic (Sidlauskas & Vari, 2008). This latter conclusion must be viewed with some uncertainty, as some other anostomine species not included in the reconstruction (e.g. *Pseudanos varii* Birindelli, F. C. T. Lima & Britski, 2012) possess lip papillae, albeit not as large or numerous. A more thorough examination of lip morphology may reveal a broader taxonomic distribution that could change this character reconstruction. Nevertheless, the conclusion that *Insperanos* has a unique combination of primitive and derived characteristics is unescapable.

This exceptional combination of character states, in conjunction with its early divergence, grants *Insperanos* the potential to clarify patterns of evolution during the initial stages of the diversification of the Anostomidae. The two characters illustrated in Figures 13 and 14 demonstrate that potential. For the ambiguously-reconstructed character 65, the inclusion of *Insperanos* substantially increases the likelihood that the most recent common ancestor of the Anostomidae had a laterally-placed retroarticular and causes the most likely character state to reverse at several internal nodes (Fig. 13). For character 67 (which describes the presence or absence of a distinct process on the palatine), including *Insperanos* increases substantially the likelihood of that process being absent ancestrally (Fig. 14). Alternative placements of *Insperanos* do not alter the reconstruction further, meaning that the effect on the reconstruction stems from its morphology, not the choice of one of the possible placements.

Of course, the accuracy of the reconstruction depends on the degree to which the chosen model of character change reflects the true generating evolutionary process. If the model is wrong, then so might be the reconstruction. There is always room for error and the discovery of new data can alter our views. However, the critical point is not that the ancestral anostomid definitely had a wide maxilla, a laterally placed retroarticular or any other specific morphology. The crucial point is that the discovery of the remarkable morphology of *Insperanos* and early divergence allows deeper and more accurate investigations into those ancestral morphologies than were previously possible.

Characters in need of further investigation

Examination of the broader sample of specimens and species herein suggests that several of the morphological characters proposed by Sidlauskas & Vari (2008) merit reformulation or reconsideration. For example, the current coding for the derived state of their character 58 (‘dentary rhomboidal with its anterior margin inflected such that a line drawn through the long axis of the sympheseal tooth of the dentary passes distinctly anterior of joint of quadrate and anguloarticular’) encompasses a wide range of dentary morphologies, and also yields an ambiguous coding for *Insperanos nattereri,* which possesses a triangular dentary despite having inflected symphyseal teeth (see *Results* for further detail). Thus, the current coding obscures major variation in tooth morphology and dentary shape.

This character was one of several that Sidlauskas & Vari (2008) used to support the monophyly of a large clade of species with upturned mouths (*Anostomoides*, *Laemolyta*, *Rhytiodus*, *Schizodon* and Anostominae) that is not supported in analyses of molecular data, including the results herein. The Anostominae appears in a phylogenetically distant position from the clade containing the other four genera. Does that separation provide an example of truly convergent morphology, or would a more granular encoding of the variation in two distinct characters or a three-state character reveal the presence of distinct derived morphologies in the two distantly related clades? Only critical re-evaluation of the morphology can reveal the answer.

In other cases, new data call into question the hypotheses of homology implicit in Sidlauskas & Vari’s (2008) original coding. Characters 67 and 68, which describe the morphology of the autopalatine, provide the best example. The authors reconstructed the absence of a distinct process of the autopalatine as a synapomorphy of the Anostominae, and thus the absence of that process in *Insperanos* seems to signal either a close relationship with the anostomine genera, or a convergent loss of the process. However, Sidlauskas & Vari (2008) reconstructed the Anostominae in a deeply nested placement within the family, while molecular results (Ramirez *et al.*, 2017; Betancur-R *et al.*, 2018) or the total evidence reconstruction herein place the divergence of the Anostominae near the base of the anostomid phylogeny. That relocation calls the polarity and homology of the characters describing the evolution of the autopalatine process into question. Did the ancestral anostomid possess such a process? Is the anteriorly directed process of *Leporellus* homologous with the lateral process of *Anostomoides*, *Leporinus*, *Schizodon* and other genera, or do these represent independent elaborations of a plesiomorphically compact and unadorned autopalatine still possessed by *Insperanos* and members of the Anostominae?

With *Insperanos* included, reconstructions of character 67 using Sidlauskas & Vari’s (2008) original encoding yield ambiguous results (Fig. 14, top right). Although the ancestral anostomid appears to possess such a process, there is less than 75% confidence in that statement, and the morphology possessed by older ancestors is also deeply ambiguous. That ambiguity stems from the original decision to refrain from coding the outgroups, citing the fact that ‘proximate outgroups

to the Anostomidae all have significant modifications of the form of the palatine relative to the condition present in many groups within the Characiformes' (Sidlauskas & Vari, 2008: 127). However, it is also clear that none of the outgroups possess the distinct laterally directed process of the autopalatine obviously present in members of *Leporinus*, *Schizodon* and related genera, and obviously absent in *Insperanos* and the anostomine genera. As such, a strong argument can be formed that Sidlauskas & Vari (2008) were too conservative in this instance and should have coded all of the outgroups as possessing state zero for this character.

Such a change in coding, in combination with the inclusion of *Insperanos*, radically changes the reconstruction of autopalatine evolution (Fig. 14, bottom right) and reverses the polarity of character 67. Now, the ancestral anostomid is inferred to have most likely lacked such a process. If that reconstruction is correct, then it would imply non-homology of the anteriorly directed process of *Leporellus* and the lateral or ventrolaterally directed process of *Leporinus*, *Schizodon* and other genera. It would also imply that possession of a laterally or ventrally directed process is an unreversed synapomorphy for a major anostomid subclade, as one of two possible optimizations of Sidlauskas & Vari's (2008) character 68 hinted in its original formulation.

Similar to our discussion of the evolutionary history of the retroarticular above, our point is not to argue that the ancestral anostomid definitely did or did not possess a prominent process of the autopalatine. We use this character to illustrate how decisions made during character coding can have major cascading effects on evolutionary reconstructions, as can the addition of even a single taxon. Future studies should critically revisit the coding of characters 67 and 68, with particular attention to the morphology of *Leporellus*, which Sidlauskas & Vari (2008) originally noted as demonstrating certain similarities to members of the outgroup families Chilodontidae and Curimatidae, and to members of *Abramites* and *Hypomasticus*, which possess anterolaterally directed processes. What are the true homologies among these character states? Which morphologies are ancestral, and which derived? Only by revisiting such characters and their coding with fresh eyes and richer taxon sampling will we be able to clarify the most plausible scenario of evolution and reveal the morphologies possessed by ancestral anostomids. In the meantime, the recognition of the ancient origin and distinctive mosaic of plesiomorphic and derived morphologies of *Insperanos* illustrates how careful anatomical study combined with molecular phylogenetics can illuminate the evolutionary origins of exceptional modern diversity.

Comparative material

For a complete list of specimens of *Anostomoides* and *Insperanos* see Assega & Birindelli (2019). *Abramites hypselonotus* (Günther, 1868): MZUSP 48123, 1 cs, 63.5 mm SL, Solimões River, Amazonas, Brazil. *Anostomus anostomus*: MZUSP 85153, 2 cs, 89.5 to 90.4 mm SL, Tiquié River, downstream of Caruru waterfall, Amazonas, Brazil. *Laemolyta fernandezi* G. S. Myers, 1950: MZUSP 91837, 1 cs, 94.0 mm SL, stream at Lício farm, tributary of Culuene River, Mato Grosso, Brazil. *Laemolyta proxima* (Garman, 1890): MZUSP 22105, 1 cs, 109.0 mm SL, Tapajós River, Pará, Brazil. *Leporellus vittatus*: MZUSP 106332, 1 sk, 155.0 mm SL, Ribeirão do Pântano, at the confluence of the Mogi Guaçú River, São Paulo, Brazil. *Pseudanos trimaculatus*: MZUSP 101646, 1 cs, 92.9 mm SL, Jari River, upstream of Santo Antônio waterfall, Amapá, Brazil. *Pseudanos trimaculatus*: MZUSP 103509, 1 cs, 105.7 mm SL, Jari River, upstream of Santo Antônio waterfall, Amapá, Brazil. *Petulanos intermedius* (R. Winterbottom, 1980): MZUSP 97330, 1 cs, 59.6 mm SL, Jamanxim River, Pará, Brazil. *Rhytiodus microlepis* Kner, 1858: INPA 16180, 1 cs, 99.7 mm SL, Solimões River, Amazonas, Brazil. *Sartor respectus* G. S. Myers & A. L. de Carvalho, 1959: MZUSP 94867, 1 cs, 80.9 mm SL, Culuene River, Mato Grosso, Brazil.

ACKNOWLEDGEMENTS

We thank Coordenação de Aperfeiçoamento de Pessoal de Nível Superior (CAPES) for the fellowship grant to the Programa de Pós-Graduação em Ciências Biológicas of Universidade Estadual de Londrina that supported F.M.A.; and an US-Brazil Fulbright Fellowship that sponsored B.L.S.' participation as a visiting professor at Universidade Estadual de Londrina. We thank O.A. Shibatta and F.C. Jerep (UEL) for discussions and various suggestions. For loans and exchanges of specimens we thank: A. Datovo, O.T. Oyakawa, M.D. Gianeti (MZUSP), C.S. Pavanelli (NUPELIA), H. Ortega (MUSM), L. Rapp Py-Daniel (INPA), L. Sousa (LIA-UFPA), M.R.M. Fernandes (UFRO-ICT), M. Sabaj (ANSP), J. Armbruster and D. Werneke (AUM), M. Britto (MNRJ) and W.B. Wosiacki (MPEG). We thank A. Datovo (MZUSP), C. Ribas (INPA), M.H. Sabaj (ANSP-Projeto iXingu), T. Hrbek and I. Farias (UFAM-Projeto Conselho Nacional de Desenvolvimento Científico e Tecnológico (CNPq)/SISBIOTA-BioPHAM) for loan of tissues and voucher specimens, and B.F. Dorini (LBP) for molecular assistance. Assistance was provided during museum visits by A. Datovo, O.T. Oyakawa, M.D. Gianeti (MZUSP) and L. Rapp Py-Daniel (INPA). Crucial logistical and travel support was provided by

C. Nagayassu, L.C. Silva and M. Rosa. We are grateful to M. Tatineni, who worked after hours to fix a bug in the job submission scripts at CIPRES and thereby allowed us to finish the analyses reported herein, and to M. Matschiner, who answered our queries regarding the analysis using the CladeAge package in Beast2. Special thanks go to R. and F. Sidlauskas for their perseverance while quarantined in a foreign country during a global pandemic, without which we could not have completed this contribution. B.F.M. was supported by Fundação de Amparo à Pesquisa do Estado de São Paulo (FAPESP) #16/11313–8, #18/24040–5 and CNPq #404991/2018-1; C.O. was supported by FAPESP #18/20610–1, #16/09204-6, #14/26508-3 and CNPq #306054/2006-0; J.L.B. was supported by research grants from CNPq #203489/2018-7 and #302872-2018-3.

REFERENCES

Abe KT, **Mariguela TC**, **Avelino GS**, **Castro RCM**, **Olviera C. 2013.** Multilocus molecular phylogeny of Gasteropelecidae (Ostariophysi: Characiformes) reveals the existence of an unsuspected diversity. *Molecular Phylogenetics and Evolution* **69:** 1209–1214.

Antoine PO, **Abello MA**, **Adnet S**, **Sierra AAJ**, **Baby P**, **Billet G**, **Boivin M**, **Calderón Y**, **Candela A**, **Chabain J**, **Corfu F**, **Croft DA**, **Ganerød M**, **Jaramillo C**, **Klaus S**, **Marivaux L**, **Navarrete RE**, **Orliac MJ**, **Parra F**, **Pérez ME**, **Pujos F**, **Rage JC**, **Ravel A**, **Robinet C**, **Roddaz M**, **Tejada-Lara JV**, **Vélez-Juarbe J**, **Wesselingh FP**, **Salas-Gismondi R. 2016.** A 60-million-year Cenozoic history of western Amazonian ecosystems in Contamana, eastern Peru. *Gondwana Research* **31:** 30–59.

Arce HM, **Lundberg JG**, **O'Leary MA. 2017.** Phylogeny of the North American catfish family Ictaluridae (Teleostei: Siluriformes) combining morphology, genes and fossils. *Cladistics* **33:** 406–428.

Assega FM, **Birindelli JLO. 2019.** Taxonomic revision of the genus *Anostomoides* (Characiformes: Anostomidae). *Zootaxa* **4646:** 124–144.

Barido-Sottani J, **Bošková V**, **Plessis L**, **Kühnert D**, **Magnus C**, **Mitov V**, **Müller NF**, **Pečerska J**, **Rasmussen DA**, **Zhang C**, **Drummond AJ**, **Heath TA**, **Pybus OG**, **Vaughan TG**, **Stadler T. 2018.** Taming the BEAST – a community teaching material resource for BEAST 2. *Systematic Biology* **67:** 170–174.

Bemis WE, **Hilton EJ**, **Brown B**, **Arrindell R**, **Richmond AM**, **Little CD**, **Grande L**, **Forey PL**, **Nelson GJ. 2004.** Methods for preparing dry, partially articulated skeletons of osteichthyans, with notes on making Ridewood dissections of the cranial skeleton. *Copeia* **3:** 603–609.

Betancur-R R, **Arcila D**, **Vari RP**, **Hughes L**, **Oliveira C**, **Sabaj MH**, **Ortí G. 2018.** Phylogenomic incongruence, hypothesis testing, and taxonomic sampling: the monophyly of characiform fishes. *Evolution* **73:** 329–345.

Birindelli JLO, **Britski HA. 2009.** New species of the genus *Leporinus* Agassiz (Characiformes: Anostomidae) from the Rio Curuá, Rio Xingu basin, Serra do Cachimbo, Brazil, with comments on *Leporinus reticulatus*. *Neotropical Ichthyology* **7:** 1–10.

Birindelli JLO, **Britski HA. 2013.** Two new species of *Leporinus* (Characiformes: Anostomidae) from the Brazilian Amazon, and redescription of *Leporinus striatus* Kner 1858. *Journal of Fish Biology* **83:** 1128–1160.

Birindelli JLO, **Lima FCT**, **Britski HA. 2012.** New species of *Pseudanos Winterbottom*, 1980 (Characiformes: Anostomidae). *Zootaxa* **3425:** 55–68.

Birindelli JLO, **Melo BF**, **Ribeiro-Silva LR**, **Diniz D**, **Oliveira C. 2020.** A new species of *Hypomasticus* from eastern Brazil based on morphological and molecular data (Characiformes, Anostomidae). *Copeia* **108:** 416–425.

Birindelli JLO, **Teixeira TF**, **Britski HA. 2016.** Two new species of *Leporinus* Agassiz, 1929 (Characiformes: Anostomidae) from tributaries of the lower Amazon basin in Brazil. *Zootaxa* **4178:** 97–115.

Bloch ME. 1794. Naturgeschichte der ausländischen Fische. *Berlin* **8:** 1–174.

Bogan S, **Sidlauskas BL**, **Vari RP**, **Agnolin F. 2012.** *Arrhinolemur scalabrinii* Ameghino, 1898, of the late Miocene - a taxonomic journey from the Mammalia to the Anostomidae (Ostariophysi: Characiformes). *Neotropical Ichthyology* **10:** 555–560.

Bollback JP. 2006. SIMMAP: stochastic character mapping of discrete traits on phylogenies. *BMC Bioinformatics* **7:** 88.

Borodin NA. 1929. Notes on some species and subspecies of the genus *Leporinus* Spix. *Memoirs of the Museum of Comparative Zoology* **50:** 269–290.

Borodin NA. 1931. On the genus *Anostomus* (Family Characinidae). *Bulletin of the Museum of Comparative Zoology* **72:** 37–52.

Bouckaert R, **Heled J**, **Kühnert D**, **Vaughan T**, **Wu C-H**, **Xie D**, **Suchard MA**, **Rambaut A**, **Drummond AJ. 2014.** BEAST 2: a software platform for Bayesian evolutionary analysis. *PLoS Computational Biology* **10:** e1003537.

Bouckaert RR, **Drummond AJ. 2017.** bModelTest: Bayesian phylogenetic site model averaging and model comparison. *BMC Evolutionary Biology* **17:** 42.

Britski HA. 1997. Descrição de duas espécies novas de *Leporinus* dos rios Araguaia e Tocantins, e comentários sobre as demais espécies do gênero assinaladas na bacia (Ostariophysi, Characiformes, Anostomidae). *Communicações do Museu de Ciêcias da PUCRS* **10:** 27–43.

Burns MD, **Chatfield M**, **Birindelli JLO**, **Sidlauskas BL. 2017.** Systematic assessment of the *Leporinus desmotes* species complex, with a description of two new species. *Neotropical Ichthyology* **15:** 1–23.

Burns MD, **Sidlauskas BL. 2019.** Ancient and contingent body shape diversification in a hyperdiverse continental fish radiation. *Evolution* **73:** 569–587.

Caldas IV, **Schrago CG. 2019.** Data partitioning and correction for ascertainment bias reduce the uncertainty of placental mammal divergence times inferred from the morphological clock. *Ecology and Evolution* **9:** 2255–2262.

Calegari BB, **Vari RP**, **Reis RE. 2019.** Phylogenetic systematics of the driftwood catfishes (Siluriformes: Auchenipteridae): a combined morphological and molecular analysis. *Zoological Journal of the Linnean Society* **187:** 661–773.

Chakrabarty P, **Faircloth BC**, **Alda F**, **Ludt WB**, **McMahan CD**, **Near TJ**, **Dornburg A**, **Albert JS**, **Arroyave J**, **Stiassny MJ**, **Sorenson L**, **Alfaro ME. 2017.** Phylogenomic systematics of ostariophysan fishes: ultraconserved elements support the surprising non-monophyly of characiformes. *Systematic Biology* **66:** 881–895.

Cuvier G, **Valenciennes A. 1850.** Histoire naturelle des poissons. Tome vingt-deuxième. Suite du livre vingt-deuxième. Suite de la famille des Salmonoïdes. *Table générale de l'Histoire Naturelle des Poissons* **22:** 1–91.

Dahdul WM. 2010. Review of the phylogenetic relationships and fossil records of Characiformes. In: Grande T, Poyato-Ariza F, Diogo R, eds. *Gonorynchiformes and ostariophysan relationships: a comprehensive review.* Enfield: Science Publisher, 441–464.

Dahdul WM, **Lundberg JG**, **Midford PE**, **Balhoof JP**, **Lapp H**, **Vision TJ**, **Haendel MA**, **Westerfield M**, **Mabee PM. 2010.** The Teleostei anatomy ontology: anatomical represention for genomics age. *Systematic Biology* **59:** 369–383.

Darlim G, **Marinho MMF. 2018.** *Moenkhausia lepidura* (Kner, 1858) (Characiformes, Characidae): osteology and relationships. *Biota Neotropica* **8:** e20180546.

Datovo A, **Vari RP. 2013.** The jaw adductor muscle complex in teleostean fishes: evolution, homologies and revised nomenclature (Osteichthyes: Actinopterygii). *PLoS One* **8:** e60846.

Davis AM, **Betancur-R R. 2017.** Widespread ecomorphological convergence in multiple fish families spanning the marine–freshwater interface. *Bulletin of the Royal Society B, Biological Sciences* **284:** 201705065.

Eigenmann C. 1912. The freshwater fishes of British Guiana, including a study of the ecological grouping of the species and the relation of fauna of the plateau to that of the lowland. *Memoirs of the Carnegie Museum* **5:** 1–578.

Eigenmann C. 1917. The American Characidae [Part 1]. *Memoirs of the Museum of Comparative Zoology* **43:** 1–102.

Eigenmann C. 1918. The American Characidae [Part 2]. *Memoirs of the Museum of Comparative Zoology* **43:** 103–208.

Eigenmann C. 1921. The American Characidae. *Memoirs of the Museum of Comparative Zoology* **43:** 209–310.

Eigenmann C. 1927. The American Characidae. *Memoirs of the Museum of Comparative Zoology* **43:** 311–428.

Faircloth BC, **Alda F**, **Hoekzema K**, **Burns MD**, **Oliveira C**, **Albert JS**, **Melo BF**, **Ochoa LE**, **Roxo FF**, **Chakrabarty P**, **Sidlauskas BL**, **Alfaro ME. 2020.** A target enrichment bait set for studying relationships among ostariophysan fishes. *Copeia* **108:** 47–60.

Felsenstein J. 1978. Cases in which parsimony or compatibility methods will be positively misleading. *Systematic Zoology* **27:** 401–410.

Foote M, **Miller AI. 2007.** *Principles of paleontology*, *3rd edn*. New York: W.H. Freeman.

Fricke R, **Eschmeyer WN**, **Van der Laan R. 2020.** *Eschmeyer's catalog of fishes*. Available at: http:// researcharchive.calacademy.org/research/ichthyology/ catalog/fishcatmain.asp (date last accessed May 2020).

Garamszegi LZ, **ed. 2014.** *Modern phylogenetic comparative methods and their application in evolutionary biology: concepts and practice*. Berlin: Springer.

Garavello JC. 1990. A new species of the anostomid genus *Leporinus* Spix from Suriname, with redescriptions of two related species (Pisces, Characiformes, Anostomidae). *Bulletin Zoölogisch Museum, Universiteit van Amsterdam* **12:** 161–170.

Garavello JC, **Britski HA. 2003.** Family Anostomidae. In: Reis RE, Kullander SO, Ferraris CJ, eds. *Check list of the freshwater fishes of South and Central America.* Porto Alegre: EDIPUCRS, 71–84.

Gayet M, **Marshall LG**, **Sempere T. 1991.** The Mesozoic and Paleocene Vertebrates of Bolivia and their stratigraphic context: a review. *Revista Técnica de YPFB*, **12**(3–4): 393–433.

Gayet M, **Jégu M**, **Bomcquentin J**, **Negri FR. 2003.** New characoids from the Upper Cretaceous and Paleocene of Bolivia and the Mio-Pliocene of Brazil: phylogenetic position and paleobiogeographic implications. *Journal of Vertebrate Paleontology* **2003:** 28–43.

Géry J. 1974. Notes sur quelques Anostomidae (Pisces, Characoidei) du basin Amazonien. *Vie Milieu 1972–1973* **23:** 143–175.

Géry J. 1977. *Characoids of the world.* New Jersey: TFH Publications.

Géry J, **Planquette P**, **Le Bail PY. 1988.** Nomenclature des espèces du groupe *Leporinus maculates* et forms affines des Guyanes (Pisces, Characoidei, Anostomidae). *Revue suísse Zoologie* **95:** 699–713.

Goloboff PA, **Catalano SA. 2016.** TNT version 1.5, including a full implementation of phylogenetic morphometrics. *Cladistics* **32:** 1–16.

Goloboff PA, **Pittman M**, **Pol D**, **Xu X. 2019.** Morphological data sets fit a common mechanism much more poorly than DNA sequences and call into question the Mkv model. *Systematic Biology* **68:** 494–504.

Goloboff PA, **Torres A**, **Arias JS. 2018.** Weighted parsimony outperforms other methods of phylogenetic inference under models appropriate for morphology. *Cladistics* **34:** 407–437.

Harmon LJ. 2018. *Phylogenetic comparative methods: learning from trees. Self published under a CC-BY-4.0 license.* Available at: https://lukejharmon.github.io/pcm/

Hulsey CD, **Roberts RJ**, **Lin ASP**, **Guldberg R**, **Streelman JT. 2008.** Convergence in a mechanically complex phenotype: detecting structural adaptations for crushing in cichlid fish. *Evolution* **62:** 1587–1599.

Jordan DS. 1920. The genera of fishes, part IV, from 1881 to 1920, thirty-nine years, with the accepted type of each. A contribution to the stability of scientific nomenclature. Leland Stanford Jr. *University Publications, University Series* **43:** 411–576.

Kealy S, **Beck R. 2017.** Total evidence phylogeny and evolutionary timescale for Australian faunivorous

marsupials (Dasyuromorphia). *BMC Evolutionary Biology* **17:** 240.

Kearse M, **Moir R**, **Wilson A**, **Stones-Havas S**, **Cheung M**, **Sturrock S**, **Buxton S**, **Drummond A. 2012.** Geneious Basic: an integrated and extendable desktop software platform for the organization and analysis of sequence data. *Bioinformatics* **28:** 1647–1649.

Kolmann MA, **Hughes LC**, **Hernandez LP**, **Arcila D**, **Betancur-R R**, **Sabaj MH**, **López-Fernández H**, **Ortí G. 2020.** Phylogenomics of piranhas and pacus (Serrasalmidae) uncovers how convergent diets obfuscate traditional morphological taxonomy. *Systematic Biology* syaa065. Available at: https://doi.org/10.1093/sysbio/syaa065.

Lanfear R, **Calcott B**, **Ho SYW**, **Guindon S. 2012.** PartitionFinder: combined selection of partitioning schemes and substitution models for phylogenetic analyses. *Molecular Biology and Evolution* **29:** 1695–1701.

Lewis PO. 2001. A likelihood approach to estimating phylogeny from discrete morphological character data. *Systematic Biology* **50:** 913–925.

Li C, **Ortí G**, **Zhang G**, **Lu G. 2007.** A practical approach to phylogenomics: the phylogeny of ray-finned fish (Actinopterygii) as a case study. *BMC Evolutionary Biology* **7:** 44.

Linnaeus C. 1758. *Systema naturae per regna tria naturae, secundum classes, ordines, genera, species, cum characteribus, differentiis, synonymis, locis. Editio decima, reformata. Tomus 1*. Stockholm: Laurentius Salvius.

Lovejoy NR, **Collette BB. 2001.** Phylogenetic relationships of New World needlefishes (Teleostei: Belonidae) and the biogeography of transitions between marine and freshwater habitats. *Copeia* **2001:** 324–338.

Machado-Evangelista M, **Esguícero ALH**, **Arcifa MS**, **Pereira TNA. 2015.** Diet and ecomorphology of *Leporinus reticulatus* (Characiformes: Anostomidae) from the upper Rio Juruena, MT, Brazil: ontogenetic shifts related to the feeding ecology. *Acta Amazonica* **45:** 383–392.

Maddison WP, **Maddison DR. 2017.** *Mesquite: a modular system for evolutionary analysis, Version 3.3*. Available at: http://www.mesquiteproject.org

Madeira F, **Park YM**, **Lee J**, **Buso N**, **Gur T**, **Madhusoodanan N**, **Basutkar P**, **Tivey ARN**, **Potter SC**, **Finn RD**, **Lopez R. 2019.** The EMBL-EBI search and sequence analysis tools APIs in 2019. *Nucleic Acids Research* **47:** W636–W641.

Malabarba MC, **Malabarba LR. 2010.** Biogeography of Characiformes: an evaluation of the available information of fossil and extant taxa. In: Nelson JS, Schultze HP, Wilson MVH, eds. *Origin and phylogenetic interrelationships of teleosts.* Munich: Dr Friedrich Pfeil, 317–336.

Marshall LG, **Hoffstetter R**, **Pascual R. 1983.** Mammals and stratigraphy: geochronology of the continental mammal-bearing Tertiary of South America. *Palaeovertebrata (Mémoire Extraordinaire)* 1–93.

Matschiner M, **Musilová Z**, **Barth JMI**, **Starostová Z**, **Salzburger W**, **Steel M**, **Bouckaert R. 2017.** Bayesian phylogenetic estimation of clade ages supports trans-Atlantic dispersal of cichlid fishes. *Systematic Biology* **66:** 3–22.

Melo BF, **Benine RC**, **Mariguela TC**, **Oliveira C. 2011.** A new species of *Tetragonopterus* Cuvier, 1816 (Characiformes: Characidae: Tetragonopterinae) from the rio Jari, Amapá, northern Brazil. *Neotropical Ichthyology* **9:** 49–56.

Melo BF, **Sidlauskas BL**, **Hoekzema K**, **Vari PR**, **Dillman CB**, **Oliveira C. 2018.** Molecular phylogenetics of Neotropical detritivorous fishes of the family Curimatidae (Teleostei: Characiformes). *Molecular Phylogenetics and Evolution* **127:** 800–812.

Mirande JM. 2018. Morphology, molecules and the phylogeny of Characidae (Teleostei, Characiformes). *Cladistics* **35:** 282–300.

Mol JHA, **Vari RP**, **Covain R**, **Willink PW**, **Fisch-Muller S. 2012.** Annotated checklist of the freshwater fishes of Suriname. *Cybium* **36:** 263–292.

Müller J, **Troschel FH. 1844.** Einige Bemerkungen über die Familie der Cyprinodonten. *Bericht über die zur Bekanntmachung geeigneten Verhandlungen der Königlichen Preussischen Akademie der Wissenschaften zu Berlin* **1844:** 35–36.

Myers GS. 1950. Studies on South American fresh-water fishes. II. The genera of Anostomine characids. *Stanford Ichthyological Bulletin* **1950:** 185–197.

Myers GS, **Carvalho AL. 1959.** A remarkable new genus of anostomin characid fishes from the Upper Rio Xingú in central Brazil. *Copeia* **1959:** 148–152.

Nelson JS, **Grande TC**, **Wilson MVH. 2016.** *Fishes of the world, 5th edn*. New Jersey: John Wiley & Sons, Inc.

Nixon KC. 2002. *WinClada version 1.00.08*. Ithaca: by the author. Available at: http://www.diversityoflife.org/winclada/

Oliveira C, **Avelino GS**, **Abe KT**, **Mariguela TC**, **Bemine RC**, **Ortí G**, **Vari RP**, **Castro RMC. 2011.** Phylogenetic relationships within the speciose family Characidae (Teleostei: Ostariophysi: Characiformes) based on multilocus analysis and extensive ingroup sampling. *BMC Evolutionay Biology* **11:** 275.

Palumbi SR. 1996. Nucleic acids II: the polymerase chain reaction. In: Hillis DM, Moritz C, Mable BK, eds. *Molecular systematics, 2nd edn*. Sunderland: Sinauer, 205–247.

Paradis E, **Schliep K. 2019.** Ape 5.0: an environment for modern phylogenetics and evolutionary analyses in R. *Bioinformatis* **35:** 526–528.

Pellegrin J. 1909. Characinidés américains nouveaux de la collection du Muséum d'Histoire naturelle. *Bulletin du Muséum National d'Histoire Naturelle (Série 1)* **14:** 342–347.

Puttick MN, **O'Reilly JE**, **Tanner AR**, **Fleming JF**, **Clark J**, **Holloway L**, **Lozano-Fernandez J**, **Parry LA**, **Tarver JE**, **Pisani D**, **Donoghue PC. 2017.** Uncertain-tree: discriminating among competing approaches to the phylogenetic analysis of phenotype data. *Proceedings of the Royal Society B: Biological Sciences* **284:** 20162290.

Qi D, **Chao Y**, **Guo S**, **Zhao L**, **Li T**, **Wei F**, **Zhao X. 2012.** Covergent, parallel and correlated evolution of trophic morphologies in the subfamily Schizothoracinae from Qinghai-Tibetan Plateau. *PLoS One* **7:** e34070.

R Core Team. 2019. *R: a language and environment for statistical computing*. Vienna: R Foundation for Statistical Computing. Available at: https://www.R-project.org/

Rambaut A, **Drummond AJ. 2016.** *TreeAnnotator v.1.8.4*. Available at: http://www.beast2.org/

Rambaut A, **Drummond AJ**, **Xie D**, **Baele G**, **Suchard MA. 2018.** Posterior summarization in Bayesian phylogenetics using Tracer 1.7. *Systematic Biology* **67:** 901–904.

Ramirez JL, **Birindelli JBL**, **Galetti Jr PM. 2017.** A new genus of Anostomidae (Ostariophysi: Characiformes): diversity, phylogeny and biogeography based on cytogenetic, molecular and morphological data. *Molecular Phylogenetics and Evolution* **107:** 308–323.

Ramirez JL, **Carvalho-Costa LF**, **Vemere PC**, **Carvalho DC**, **Troy WP**, **Galetti Jr PM. 2016.** Testing monophyly of the freshwater fish *Leporinus* (Characiformes, Anostomidae) through molecular analysis. *Journal of Fish Biology* **88:** 1204–1214.

Revell LJ. 2012. Phytools: an R package for phylogenetic comparative biology (and other things). *Methods in Ecology and Evolution* **3:** 217–223.

Ridewood WG. 1904. On the cranial osteology of the fishes of the families Elopidae and Albulidae, with remarks on the morphology of the skull in lower teleostean fishes generally. *Proceedings of the Zoological Society of London* **1904:** 35–81.

Ronquist F, **Klopfstein S**, **Vihelmsen L**, **Schulmeister S**, **Murray DL**, **Rasnisyn A. 2012.** A total-evidence approach to dating with fossils, applied to early radiation of the Hymenoptera. *Systematic Biology* **61:** 973–999.

Ronquist F, **Teslenko M**, **Van der Mark P**, **Ayres DL**, **Darling A**, **Höhna S**, **Larget B**, **Liu L**, **Suchard MA**, **Huelsenbeck JP. 2012.** MRBAYES 3.2: efficient Bayesian phylogenetic inference and model selection across a large model space. *Systematic Biology* **61:** 539–542.

Ruber L, **Adams DC. 2011.** Evolutionary convergence of body shape and trophic morphology in cichlids from Lake Tanganiyika. *Journal of Evolutionary Biology* **14:** 325–332.

Sabaj MH. 2019. *Standard symbolic codes for institutional resource collections in herpetology and ichthyology: an online reference. Version 7.1 (21 March 2019)*. Washington: American Society of Ichthyologists and Herpetologists. Available at: https://asih.org/standard-symbolic-codes

Santini F, **Harmon LJ**, **Carnevale G**, **Alfaro ME. 2009.** Did genome duplication drive the origin of teleosts? A comparative study of diversification in ray-finned fishes. *BMC Evolutionary Biology* **9:** 194.

Santos GM, **Jégu M. 1987.** Novas occorências de *Gnathodolus bidens*, *Synaptolaemus cingulatus* e descrição de duas espécies novas de *Sartor* (Characiformes, Anostomidae). *Amazoniana* **10:** 181–196.

Santos GM, **Zuanon J. 2006.** *Anostomoides passionis*, a new fish species from rio Xingu, Brasil (Characiformes: Anostomidae). *Zootaxa* **1168:** 59–68.

Scopoli JA. 1777. *Introductio ad historiam naturalem, sistens genera lapidum, plantarum et animalium hactenus detecta, caracteribus essentialibus donata, in tribus divisa, subinde ad leges naturae*. Prague: Wolfgang Gerle.

Sidlauskas B. 2007. Testing for unequal rates of morphological diversification in the absence of a detailed phylogeny: a case study from characiform fishes. *Evolution* **61:** 300–316.

Sidlauskas B, **Birindelli JLO. 2017.** Family Anostomidae - toothed headstanders. In: Van der Sleen P, Albert JS, eds. *Field guide to the fishes of the Amazon, Orinoco and Guyanas*. New Jersey: Princeton University Press, 82–89.

Sidlauskas B, **Santos GM. 2005.** *Pseudanos winterbottomi*: a new anostomine species (Teleostei: Characiformes: Anostomidae) from Venezuela and Brazil, and comments on its phylogenetic relationships. *Copeia* **2005:** 109–123.

Sidlauskas B, **Vari RP. 2008.** Phylogenetic relationships within the South American fish family Anostomidae (Teleostei, Ostariophysi, Characiformes). *Zoological Journal of the Linnean Society* **154:** 70–210.

Sidlauskas B, **Vari RP. 2012.** Diversity and distribution of anostomoid fishes (Teleostei: Characiformes) throughout the Guianas. *Cybium* **36:** 71–103.

Sidlauskas B, **Assega F**, **Melo B**, **Oliveira C**, **Birindelli J. 2021.** Data and scripts from: Total evidence phylogenetic analysis reveals polyphyly of Anostomoides and uncovers an unexpectedly ancient genus of anostomid fishes. doi:10.5061/dryad.d2547d82m

Steel M, **Penny D. 2000.** Parsimony, likelihood, and the role of models in molecular phylogenetics. *Molecular Biology and Evolution* **17:** 839–850.

Steindachner F. 1875. Die Süsswasserfische des südöstlichen Brasilien (II). Sitzungsberichte der Kaiserlichen Akademie der Wissenschaften. *Mathematisch-Naturwissenschaftliche Classe* **71:** 211–245.

Steindachner F. 1876. Ichthyologische Beiträge (V). [Subtitles i–v.]. Sitzungsberichte der Kaiserlichen Akademie der Wissenschaften. *Mathematisch-Naturwissenschaftliche Classe* **74:** 49–240.

Taylor WR, **Van Dyke GC. 1985.** Revised procedures for staining and clearing small fishes and other vertebrates for bone and cartilage study. *Cybium* **9:** 107–119.

Vari RP. 1983. Phylogenetic relationships of the families Curimatidae, Prochilodontidae, Anostomidae, and Chilodontidae (Pisces: Characiformes). *Smithsonian Contributions to Zoology* **378:** 1–60.

Weitzman SH. 1962. The osteology of *Brycon meeki*, a generalized characid fish, with an osteological definition of the family. *Stanford Ichthyogical Bulletin* **8:** 3–77.

Weitzman SH. 1974. Osteology and evolutionary relationships of the Sternoptychidae, with a new classification of stomiatoid families. *Bulletin of the American Museum of Natural History* **153:** 327–478.

Weitzman SH, **Palmer L. 1997.** A new species *Hyphessobrycon* (Teleostei: Characidae) from the Neblina region of Venezuela and Brazil, with comments on the putative 'rosy tetra clade'. *Ichthyological Explorations of Freshwaters* **7:** 209–242.

Winterbottom R. 1980. Systematics, osteology and phylogenetic relationships of fishes of the ostariophysan subfamily Anostominae (Characoidei, Anostomidae). *Life Sciences Contributions: Royal Ontario Museum* **123:** 1–112.

Wright AM, **Hillis DM. 2014.** Bayesian analysis using a simple likelihood model outperforms parsimony for estimation of phylogeny from discrete morphological data. *PLoS One* **9:** e109210.

Zhang C, **Stadler T**, **Klopfstein S**, **Heath TA**, **Ronquist F. 2015.** Total-evidence dating under the fossilized birth-death process. *Systematic Biology* **65:** 228–249.

SUPPORTING INFORMATION

Additional Supporting Information may be found in the online version of this article at the publisher's web-site:

Figure S1. Phylogenetic tree based on combined morphological and molecular data using tip- and node-based fossil calibrations. One asterisk indicates species included based exclusively on morphological data, and two asterisks indicate species included based exclusively on molecular data.
Figure S2. Phylogenetic tree based exclusively on morphological data. Tree represents the strict consensus of 152 trees with 469 steps, resulted from a Maximum Parsimony analysis of 48 species of Anostomidae plus 11 outgroup Characiformes coded for 158 morphological characters. Node values consist of Bremer support.
Figure S3. Phylogenetic tree based exclusively on sequences of 16S, *COI*, *CytB*, *Myh6*, *RAG1*, and *RAG2*. Tree represents maximum clade credibility tree of a Bayesian Inferrence analysis of 5309 bp coded for three individuals of *Anostomoides atrianalis*, three of *A. nattereri*, plus 38 other species of 13 genera of Anostomidae, and 11 outgroup species of other families of Characiformes. Node values (support) consist of posterior probability.

SHARED DATA

Data deposited in the Dryad digital repository (Sidlauskas *et al.*, 2021).